Materials Science & Engineering R 149 (2022) 100682

Contents lists available at ScienceDirect

Materials Science & Engineering R

journal homepage: www.elsevier.com/locate/mser

# A comprehensive review of template-assisted porous carbons: Modern preparation methods and advanced applications

V. Pavlenko [a,*], S. Khosravi H [b], S. Żółtowska [c], A.B. Haruna [d,1], M. Zahid [e,2], Z. Mansurov [a], Z. Supiyeva [a], A. Galal [f], K.I. Ozoemena [d], Q. Abbas [b,g,**,3], T. Jesionowski [c,*,4]

[a] Al-Farabi Kazakh National University, 71 al-Farabi Ave., 050040 Almaty, Kazakhstan
[b] Institute for Chemistry and Technology of Materials, Graz University of Technology, Stremayrgasse 9, 8010 Graz, Austria
[c] Institute of Chemical Technology and Engineering, Faculty of Chemical Technology, Poznan University of Technology, Berdychowo 4, 60965 Poznan, Poland
[d] Molecular Sciences Institute, School of Chemistry, University of the Witwatersrand, Private Bag 3, PO Wits, Johannesburg 2050, South Africa
[e] Department of Chemistry, University of Agriculture Faisalabad, Pakistan
[f] Chemistry Department, Faculty of Science, Cairo University, 12613 Giza, Egypt
[g] Institute of Chemistry and Technical Chemistry, Faculty of Chemical Technology, Poznan University of Technology, Berdychowo 4, 60965 Poznan, Poland

ARTICLE INFO

*Keywords:*
Templated carbon
Porous carbon
Carbon production
Nano-casting
Hard and soft templates
Self-template

ABSTRACT

Carbons with hierarchical pores in the range of few nanometers obtained via template-assisted methods offer a great control over structure and geometry of pores, keeping them uniformly distributed and better connected. Another advantage is the easy functionalization of templated porous carbons (TPCs) by various dopants, which makes them excellent materials for catalysis, energy storage and conversion, sensors and environmental applications. Herein, beyond zeolite-templated carbons, key methodologies based on the template material such as organic and metal oxides, silica, polymers, metal-organic framework (MOFs) and bio-originated materials used for the preparation of porous carbons possessing predetermined structure and composition, have been reviewed. The effects of precursor material on the textural and structural properties of TPCs have been described. In scope of applying novel methods such as evaporation induced self-assembling (EISA), the influence of different templates on the properties of resulting materials has been discussed. Further, advances on the template-induced synthesis of self-supporting metal-organic frameworks and their utilization as advanced templates have been described. Moreover, self-templates are especially emphasized, application of which in our opinion can provide a

*Abbreviations:* IUPAC, International Union of Pure and Applied Chemistry; PAN, Polyacrylonitrile; MONT, Montmorillonite; FA, Furfuryl alcohol; 3DNG, 3D nanoporous graphene; CVD, Chemical vapor deposition; 3D, Three-dimensional; BET, Brunauer Emmett Teller; DFT, Density functional theory; EASA, Electrochemically available surface; TCXs, Templated carbon xerogels; PSCs, Porous spheres of carbon; PTFE, Polytetrafluoroethylene; F-PAA, Fluorine-containing poly (amic acid); PS, Polystyrene; PSN, Porous silver network; TEOS, Tetraethyl orthosilicate; CTAB, Cetyltrimethylammonium bromide; BJH, Barrett-Joyner-Halenda; OMC, Ordered mesoporous carbon; HF, Hydrofluoric acid; NaOH, Sodium hydroxide; ZTCs, Zeolite templated carbons; MB, Methylene blue; CSA, Carbon surface area; XRD, X-ray diffraction; EISA, Evaporation-Induced Self-Assembly; SWCNTs, Single-wall carbon nanotubes; MWCNT, Multiwalled carbon nanotube; AC, Activated carbon; SSA, Specific surface area; TEM, Transmission electron microscopy; CMSs, Carbon microspheres; MPS, 3-methacryloxypropyl)-trimethoxysilane; SSMCs, Sewage sludge-based mesoporous carbons; DAN, Diaminonaphthalene; ORR, Oxygen reduction reaction; 3DHSC, 3D porous hard-soft composite carbon; PCNSs, Porous carbon nanosheets; NPC, Nitrogen-doped porous carbon; KISPCs, N/S co-doped hierarchical porous carbons; TNPs, Template nanoparticles; TPO, Tire derived pyrolytic oil; THF, Tetrahydrofuran; ZIF, Zeolitic imidazolate framework; FTIR, Fourier-transform infrared spectroscopy; XPS, X-ray photoelectron spectroscopy; NADH, Nicotinamide adenine dinucleotide; NPPC, Nitrogen–phosphorus co-doped porous carbon; PEMFCs, Proton exchange membrane fuel cells; GO, Graphite oxide; HQ, Hydroquinone; CC, Catechol; MIP, Molecularly imprinted polymer; NC, Nanoporous carbon; GOD, Glucose oxidase; HNC, Hierarchical nanoporous carbon; DOE, Department of Energy; $PAM^-$, Anionic polyacrylamide; HS-TENGs, Helical spring-like triboelectric nanogenerators.

* Corresponding authors.
** Corresponding author at: Institute for Chemistry and Technology of Materials, Graz University of Technology, Stremayrgasse 9, 8010 Graz, Austria.
*E-mail addresses:* vladimir.pavlenko@kaznu.kz (V. Pavlenko), soniazolaks@gmail.com (S. Żółtowska), aderemi.haruna@wits.ac.za (A.B. Haruna), Zmansurov@kaznu.kz (Z. Mansurov), zhazyra@mail.ru (Z. Supiyeva), galal@sci.cu.edu.eg (A. Galal), kenneth.ozoemena@wits.ac.za (K.I. Ozoemena), qamar.abbas@tugraz.at (Q. Abbas), teofil.jesionowski@put.poznan.pl (T. Jesionowski).
[1] https://orcid.org/0000-0001-6208-5327.
[2] https://orcid.org/0000-0001-8407-6886.
[3] https://orcid.org/0000-0002-1169-1906.
[4] https://orcid.org/0000-0002-7808-8060.

https://doi.org/10.1016/j.mser.2022.100682
Received 18 February 2022; Received in revised form 1 May 2022; Accepted 7 May 2022
Available online 18 May 2022

sustainable large-scale production of TPCs. The recent progress in the study of the diffusional processes, energy and biomedical applications as well as the confinement effects of different liquids and proteins within the porous matrices of template-derived carbons, have been reviewed.

## 1. Introduction and historical background

Nanoporous materials exist in various compositions and possess a system of regular isolated or interconnected pores. Nanopores are recognized to have maximal diameter of 100 nm, while depending on pore size, the porous structures can be divided into microporous, mesoporous and macroporous. According to classification proposed by the International Union of Pure and Applied Chemistry (IUPAC), micropores are the pores with diameters less than 2 nm, the range between 2 and 50 nm is classified as mesopore, and macropores represent pores bigger than 50 nm [1]. The presence of porous structure gives materials specific characteristics such as low density and high specific surface area (SSA). In turn, a large surface area typical for porous materials allows to use them in the wide scope of applications, such as adsorbents, catalyst carriers, gas storage, or electrode materials, etc. The $sp^2$-hybridized carbon allotropes, also known as nanocarbons possess well-defined structures at nanoscale. On the other hand, conventional carbons have disordered and complicated structures, e.g., chars, charcoals, glassy carbons, carbon blacks, carbon fibers, exfoliated graphites and activated carbons. These materials are characterized by a high level of disorder and their structural model consists of ribbons of graphene [2–4]. Overall, traditional carbons consist of randomly aggregated stacked graphene sheets with a lot of defects, edges, and/or heteroatoms.

Whether porous carbons originate from natural resources or synthesized in a lab, their structural and surface features largely depend on the physicochemical properties of the precursors and the implemented synthetic route. Advanced carbons with narrow pore size distribution are highly demanded in catalysis, energy storage systems, photovoltaics and pharmacology. Nevertheless, application of traditional processes for the production of porous carbon materials usually does not provide a precise control of the pores architecture. For instance, carbonization and activation which are widely used as technological processes lead to the production of porous carbons having polymodal pore size distribution (a broad range of sizes from few nm up to 100 nm). Therefore, manufacturing of carbons with predetermined characteristics of porous structure is challenging, that requires to use special approaches and consequently increases the cost. Among these approaches, template methods have been investigated thoroughly due to their unique versatility and functionality [5–8]. According to the concept of template-assisted synthesis, one or several precursors, or products of their interaction, act as a pattern or template that allows the synthesis of porous carbons. In the simplest case, the geometric structure of the resulting porous material represents an inverse replica of the template implemented. As a result of subsequent removal of the template used as a sacrificial material, a porous volume is formed. Therefore, the structure of resulting porous carbon will directly depend on the properties of the template utilized. Moreover, doping of carbons, that is used as a general term to chemically (via grafting) or physically (via insertion/intercalation) incorporate any element into the template structure, gives them unique activity characteristics due to electron donor or electron withdrawing ability. Overall, the template synthesis is a unique method for designing porous carbons that are more complicated to produce by conventional techniques. In the last ten years, new research methods for producing template-assisted carbons have been introduced and they have found applications in various sectors of life (Fig. 1). Majority of these methods utilize the inverse replica of the corresponding precursor materials which are used as template resulting in desired porous characteristics of microporous, mesoporous or macroporous carbons, as well as carbon nanotubes [9].

Carbons with highly ordered porous structures can be prepared by filling porous structure of an inorganic matrix with a precursor, e.g., sucrose, propylene, pitch or polymer solutions. A pioneer work on the

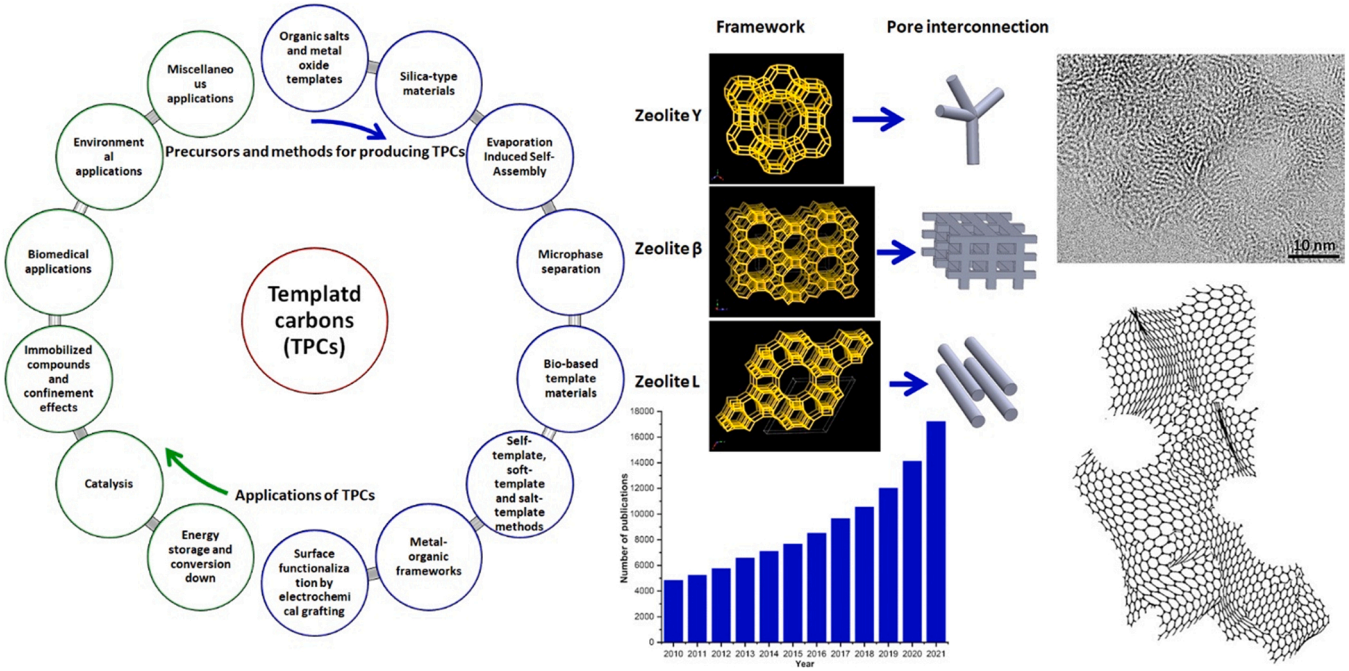


**Fig. 1.** The development of new synthesis methods for templated carbons and their applications in different sectors of science and technology. Achieving the controlled porosity of carbons by utilizing the inverse replica of the corresponding precursor materials as template framework. Number of publications between years 2010–2021 on the topic of templated carbons. The data accessed from various publishers including Elsevier, Wiley-VCH and the Royal Society of Chemistry (RSC).

templated nanocarbons was reported by Kyotani et al. in 1988 [10]. In this work, a highly-orientated graphite from polyacrylonitrile (PAN) intercalated in montmorillonite (MONT) was prepared. The filling of interlamellar openings of MONT by PAN was performed using the components mass ratio of ca. 7:1. Then the MONT-PAN intercalation compound was heat treated at 700 ºC, followed by a liberation of resulting carbon material via leaching of inorganic template. The synthesis of mesoporous carbon materials using a template-assisted approach was not developed until early 1980 s, when Knox et al. pioneered the field using spherical solid gel as template [11]. Their approach is often used for the hard-template synthesis of carbons with well-defined mesopores. This so-called 'nanocasting' approach involves several steps, (i) synthesis of pore structure controlled silica gel, (ii) infiltration of polymer precursors within the silica gel template, (iii) cross-linking reaction, (iv) pyrolysis of organic precursor, and (v) removal of the template [12]. In particular, Knox and coworkers synthesized mesoporous carbon material using a hydroxybenzen/1-aminohexane mixture as carbon source, followed by the polymerization and pyrolysis of the cross-linked polymer. After removing the silica template, a spherical mesoporous carbon was successfully produced, exhibiting a surface area of 460–600 $m^2$ $g^{-1}$. High-temperature graphitization at 2500 ºC in inert atmosphere decreased the surface area down to 150 $m^2$ $g^{-1}$ as the micropores present in the spherical mesoporous carbon completely disappeared in the process. Carbon materials prepared by the later method were commercialized, which offered fascinating retention properties in liquid chromatographic separation technique [12]. This method is suitable for controlling the pore size distribution, and the size of pores could be adjusted by the choice of the template, and is mainly limited by the thickness of the walls of the templates [13]. It is well-known that the pore diameter of an ordered carbon replicated from a hard template is originally estimated from the pore wall thickness of the corresponding template [12].

Different clays as template have been used to prepare porous carbons [14]. Thin graphite films are prepared via unique method of incorporating organic polymers in the two-dimensional lamellae of a layered clay and then processing through carbonization. Sonobe et al. [15] used polyaniline in between the interlamellar opening of montmorillonite followed by carbonization. In the work of Bandosz et al. [16], carbons possessing pores no larger in diameter than the interlayer space of the clay were produced. Similarly, polyvinyl acetate based carbons were produced between the lamellae of montmorillonite which was followed by further heat treatment for graphitization. This method is useful for the synthesis of highly oriented two-dimension-like graphite [17]. An important milestone in the development of the template-assisted method was the synthesis of macroporous carbons with core/shell and hollow structures from the submicrometer spherical silica particles used as hard template, reported by Zakhidov et al. Particularly, the uniformly-sized colloidal silica opals were used as template, and it was shown that changing the silica particle size gives a possibility to tune the pore size [18]. After carbonization under inert atmosphere of carbon precursor infiltrated in opals, followed by leaching the inorganic template, macroporous carbon with inverse opal structures was derived. It was shown that the infiltration of the carbon precursors was preceded by sintering the silica spheres to bridge them together connecting the spherical pores of the resulting macroporous carbon material [12].

From the foregoing, it is clear that a number of experimental approaches for template-assisted carbon synthesis have been developed in the past. Among them, three main directions are i.e., hard-templates, soft-templates and self-templates. Research interest in the field of ordered carbon materials have greatly modified experimental approaches which or even combined the previously known techniques to facilitate the synthesis process. Selected strategies for TPCs have been summarized in a recent work where removable inorganic particles such as NaCl, MgO, $CaCO_3$, ZnO or polymeric materials like block copolymers and surfactants were used [19]. Generally, a hard-templating approach uses pre-synthesized organic or inorganic templates, which serve as pattern for the replication of porous carbons and do not involve any significant chemical interactions with the precursors. Thereby, the morphology of the resulting carbons is pre-determined by the well-defined structure of templates. In contrast to hard template, soft-templating approache utilizes various species and block copolymers co-assembled to form materials having an ordered structure ("first templating"), which is then removed at a later stage. In addition, the resulting patterns produced through the soft-templating approach can be further used as the hard templates ("second templating"). Finally, the self-templates can be the substances of natural or synthetic origin undergoing direct pyrolysis leading to the formation of composite materials containing carbon and inorganic phases. This is followed by the removal of one particular phase giving rise to the formation of porous structure in derived carbon material. This review paper classifies template-assisted carbon preparation based primarily on the precursor materials employed while simultaneously looking into some of the well-known classical template methods. Furthermore, the advanced application of templated porous carbons in the areas of energy storage, catalysis, biomedicine and environment have been thoroughly reviewed. This comprehensive review is an up-to-date valuable compendium of knowledge for scientists and professionals from other fields involved in the fabrication, characterization and application of tempalates carbon structures.

## 2. Methods and precursors for producing TPCs

### 2.1. Organic salts and metal oxide templates

Metal oxides are useful to fabricate hierarchically network of pores achieved via migration of templates to follow the rivers formation-like mechanism. For example, Prussian blue ($Fe_4[Fe(CN)_6]_3$) cages under thermal treatment resulted in iron oxides-based nanoparticles which diffused and aggregated to grow larger in size, and eventually were pushed out of the porous carbons [20]. The iron oxides moved through carbon cages by forming channels hierarchical structure. An extension of this strategy is the use of mobile templates to prepare hierarchical pores from macropores to micropores. For example, $Fe_3O_4$ crystallites generated during thermal pyrolysis of the Prussian blue cages should be responsible for the creation of porous channels. Certainly, Prussian blue was chosen as precursor for the carbonization due to its high metal to cyanide ratio. Apart from Fe nodes acting as catalyst for graphitization of the carbons, they also reacted with the oxygen to generate iron oxides which served as mobile templates moving from the interior to the external shell. In another work, such migration pathways formed hierarchical pores when furfuryl alcohol (FA) was filled as the second carbon source and the resulting carbon possessed surface area of 699 $m^2$ $g^{-1}$ [20].

High quality nanoporous graphene with free-standing three dimensional structure were fabricated using nanoporous nickel as template and catalyst. In particular, nanoporous Ni were prepared by lengthy chemical de-alloying of $Ni_{30}Mn_{70}$ ingots in 1.0 M $(NH_4)_2SO_4$ and followed by chemical vapor deposition (CVD) with $C_2H_2$. This process is further followed by $NH_3$ annealing and treatment with $HNO_3$. However, the prepared material comprised of uniformly distributed particle-like nanopore and ligaments, which consist of few-layer graphene sheets. The presence of D-band in Raman spectra revealed the existence of defects caused by the nanoporous structure and heteroatoms doping. The resulting carbon possessed a specific surface area of ~737 $m^2$ $g^{-1}$, with a pore volume of 1.793 $cm^3$ $g^{-1}$ [21]. To avoid the use of metallic catalyst, method to produce one dimensional nitrogen-doped carbon coated $TiO_2$ nanotube arrays (NTAs) by template carbonization of polydopamine nanofilm coated onto anodized $TiO_2$ has been reported. This carbon/-$TiO_2$ composite possesses organized structure with an inner diameter for nanotubes around 80 nm and a length of about 8 μm. The carbon coating was about 10 nm in thickness and is doped by nitrogen from the polydopamine precursor [22]. A ZnO template method for the large scale

preparation of hollow carbon nanostructures has been developed where a diluted ethylbenzene stream was used to form a carbon layer on the template at a high temperature and a dilute HCl solution to etch the template. Hollow carbon nanotubes and hollow carbon nanospheres were synthesized using ZnO nanorods and nanospheres as templates. The isotherm exhibited a typical IV-type curve, suggesting the presence of mesopores. The specific surface area of the hollow carbon nanotubes and hollow carbon nanospheres were calculated to be 245 and 382 $m^2$ $g^{-1}$, respectively [23].

Certain organic molecules also act as structure defining components for producing templated porous carbons. In situ templates etching approach has been employed where citric acid serves as a carbon source and etchant (see Fig. 2) to prepare three-dimensional (3D) interconnected Fe-N doped hierarchical porous carbon materials. Here, the $Fe_2O_3$ nanoparticles not only provide the iron source by in situ etching but also act as templates to construct the hierarchical porous structure. The prepared carbons displays a high specific surface area of 1644 $m^2$ $g^{-1}$ with an interconnected hierarchical pores and homogeneous distribution of iron and nitrogen in the carbon [24].

Porous carbon nanofibers and graphite hybrid composite material was produced with a mixture of $C_2H_2$, Ar, and $H_2$ at 800 °C for 10 min. For this purpose, first the cobalt catalyst precursor, supported on copper foil, was prepared by a dip-coating technique using 0.01 mol $L^{-1}$ Co $(NO_3)_2$ 6 $H_2O$ solution. Then the carbon nanofibers were synthesized by CVD method using Co-based catalyst supported onto copper foil. The prepared carbon exhibited a typical type-IV isotherm with a distinct adsorption hysteresis loop indicating that there are large amounts of micropores and mesopores. Brunauer-Emmett-Teller (BET) and density functional theory analyses reveal that this hybrid material possesses a specific surface area of ~352 $m^2$ $g^{-1}$ and the pore sizes of 1–10 nm with pore volume around 0.539 $cm^3$ $g^{-1}$ [25]. Graphene/$MnO_2$ composites were prepared by using nanoporous copper (obtained by de-alloying $Cu_{40}Mn_{60}$ ingots) that underwent CVD with $C_2H_2$ followed by electrodeposition of $Mn(CH_3COO)_2.4\ H_2O$ and 0.2 mol $Na_2SO_4$ to prepare $MnO_2$. Consequently, $MnO_2$ product with a flower-like morphology was uniformly coated to form $MnO_2$/Graphene/$MnO_2$ composite structure [26].

High quality graphene foams possessing tunable pore size were prepared by CVD method where porous sacrificial templates obtained via sintering of nickel and copper metal powders were used. The particle size of the metal powders along with the progressive temperature treatments allowed to tune the pore size of these three-dimensional graphene-based structures. Availability of high electrochemically active surface of the fabricated foams, larger than the surface area of commercial graphene makes the proposed materials very attractive electrodes for energy storage applications. As a result, a volumetric capacitance of 165 mF $cm^{-3}$ was reached which is approximately five orders of magnitude higher than the one achieved with commercial Ni foams (5 μF $cm^{-3}$) grown under similar experimental conditions [27].

Templated carbon xerogels (TCXs) containing macropores, mesopores and micropores as the carbon electrode were prepared from resorcinol and formaldehyde via hard template based on cotton fibers. Resulting carbons possessed maximal surface area of 615 $m^2$ $g^{-1}$ and total pore volume of 1.6 $cm^3$ $g^{-1}$ [28]. Cannular congeries of $MnO_2$ (CC-$MnO_2$) have been prepared via the in situ chemical reaction where carbon tubes derived from polypyrrole act as reductive agent and sacrificial template. Porous spheres of carbon (PSCs) are prepared by a one-step calcination and template removal method, in which silica/chitosan spheres obtained by spray-drying process are carbonized and the $SiO_2$ templates have been etched by mixing Polytetrafluoroethylene powder (PTFE) as in-situ template removal agent [29]. Highly microporous carbon was synthesized through a combination of fluorine-containing poly(amic acid, F-PAA) and a mesoporous polystyrene (PS) cryogel where the former has the ability to produce a microporous carbon material with high specific surface area (~1300 $m^2$ $g^{-1}$)upon carbonization at 1000 °C. In addition, a PS cryogel template with microcellular structure was prepared by freeze-drying of PS solution in 1,4-dioxane. Scheme in Fig. 3 shows that the template was then impregnated with F-AA, followed by the carbonization at 1000 °C. Carbon material produced from such microcellular structure exhibited a high surface area of 2443 $m^2$ $g^{-1}$ and a large micropore volume of 0.90 $cm^3$ $g^{-1}$ [30].

Polymer foam materials have been used as template to prepare three-dimensional cross-linked porous silver network (PSN) via silver mirror reaction. Furthermore, the nitrogen doping of such material is carried out by chemical vapor deposition followed by ammonia gas. Nitrogen gas adsorption data clearly shows the presence of type IV isotherm with a BET surface area up to 801 $m^2$ $g^{-1}$ [31]. Cross-linked polymers were developed and used as template as well as carbon source in a recently reported study where high surface area via graphene as a

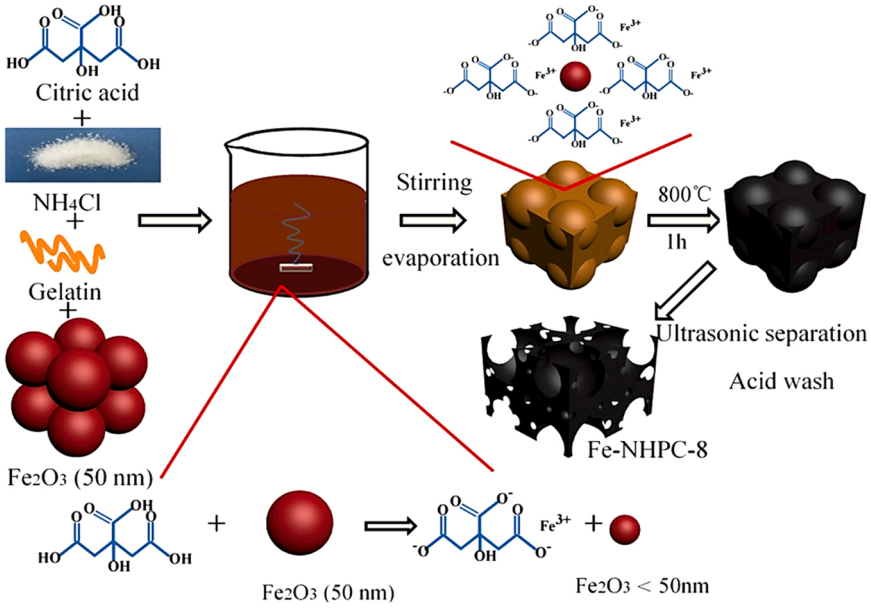


**Fig. 2.** Scheme for the preparation of porous carbon with Fe-N doping where citric acid acts as carbon precursor and $Fe_2O_3$ as template for hierarchical porous structure. Reproduced with permission [24].

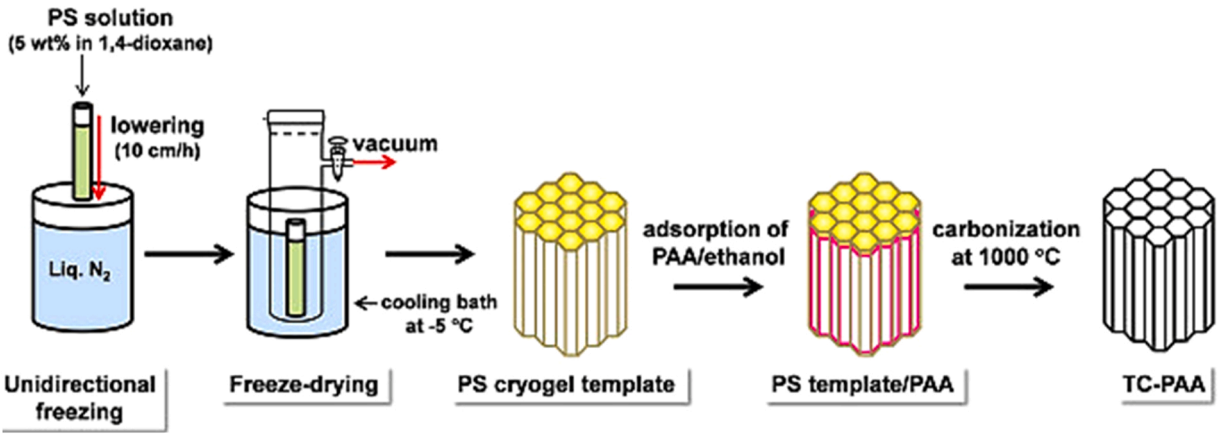


**Fig. 3.** Schematic for the preparation of polystyrene cryogel template and the hierarchical porous carbon material. Reproduced with permission [30].

structure-directing template during activation has been achieved. Excellent electrochemical performance of these graphene-based composite carbons was demonstrated in supercapacitors cells and comparable to the commercial carbons [32].

### 2.2. Silica-type materials

#### 2.2.1. Silica

Silica-type materials are used as hard template where the precursor material such as sucrose is first incorporated into the pores, followed by pyrolysis and then template is removed via treatment with acids. Silica gel has been used as template material and furfuryl alcohol as carbon precursor to prepare carbons with hierarchical pores via thermal treatment at 650–850 °C. Carbon material with a surface area of 1975 $m^2\ g^{-1}$ and pore volume of 3.07 mL $g^{-1}$ was obtained by temperature treatment at 650 °C for 3 h. Furthermore, effects of various other temperatures and dwelling times (up to 4 h) on the physical properties of templated carbons were investigated to obtain pores in the range of 2–20 nm, among which 38–67% of the pores were in the range of 2–6 nm [33]. Ordered mesoporous carbon was prepared via carbonization treatment of FA polymer that was successfully produced inside the mesopores of MCM-48 by thermal treatment at 90 °C. The metallic Ni was used as a catalyst for the formation of the graphitic structure within the mesopores of MCM-48 at 1000 °C. Briefly, the cationic surfactant cetyltrimethylammonium bromide (CTAB; $CH_3(CH_2)_{15}N(CH_3)_3Br$) was used to prepare MCM-48, tetraethoxysilane ($Si(OEt)_4$ acted as a silica source, FA as the carbon source, while the oxalic acid was dissolved in FA. The NaOH pellets were added to a mixture of $Ni(NO_3)_2.6\ H_2O$ to prepare Ni catalyst. MCM-48 and [Ni]-MCM-48 possessed BET surface areas of 1337 and 1291 $m^2\ g^{-1}$, respectively while the nitrogen adsorption-desorption isotherms for both carbons were typical type-IV. For a particular temperature treatment of 600 °C, with or without the Ni catalyst, carbons with BET surface areas up to 2300 $m^2\ g^{-1}$ were prepared [34].

Aluminosilicate zeolite (HZSM-5) and mesoporous silica (SBA-15) based micro-mesoporous composite materials were prepared by mechanosynthesis and used as templates to prepare micro-mesoporous carbons, where palm oil cooking waste was carbon source. HZSM-5/SBA-15 composites in different mass ratios (25:75, 50:50 and 75:25) were infiltrated with palm oil by a two-step procedure involving grinding followed by stirring the suspension in an oil solution which was followed by the carbonization under inert atmosphere (Fig. 4). Thus produced carbons displayed isotherm profile similar to type V and very close to type IV described for the template materials, indicating an ordered porous structure [35].

Silica foams-based monolithic structures possessing a monodisperse macroscopic structure along with macropores can be prepared via pickering emulsions where solid particles are used as stabilizers. These

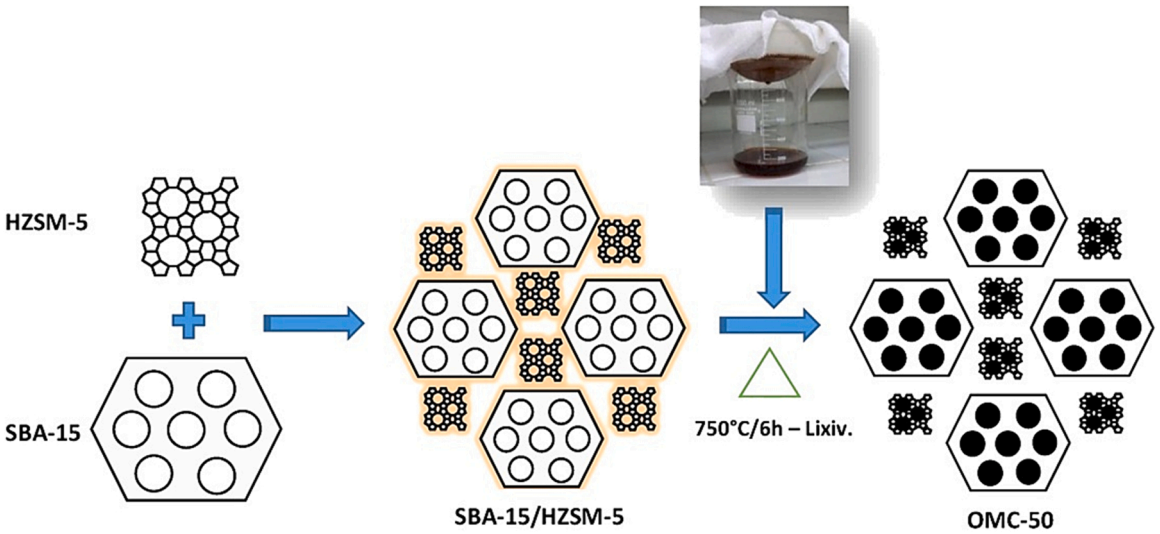


**Fig. 4.** Preparation of ordered micro-mesoporous carbon from palm oil cooking waste via nanocasting in HZSM-5/SBA-15 composite template. Reproduced with permission [35].

foams have been used as hard templates for phenolic resin for producing carbon monoliths with interconnected pores. In this regard, hexadecane, the surfactant cetyltrimethylammonium bromide (CTAB), TEOS, aerosil silica nanoparticles with diameter 12 nm, hydrofluoric acid and hydrochloric acid; (a resol-type formophenolic prepolymer in a hydro-alcoholic solution) have been used as precursors. Thus produced carbons possessed BET specific surface area between 700 and 900 $m^2\ g^{-1}$ and mesopore specific surface area between 200 and 500 $m^2\ g^{-}1$, macropore volume fraction of 45–70% with a narrow pore size distribution [36]. Aqueous slurry of SBA-15 with a polymer/$SiO_2$ mass ratio of 0.50–2.00 was used for the so-called nanoreplication of poly(furfuryl alcohol) onto silica surface to produce a series of ordered carbons [37].

SBA-15 was also used as sacrificial material for preparing ordered mesoporous carbon (OMC) via hard template method, followed by its removal using etching chemicals such as hydrofluoric acid (HF), sodium hydroxide (NaOH) and polyvinylidene fluoride (PVDF). Depending on the use of etching chemical a varying pore volume was achieved as follows HF (0.26 $cm^3\ g^{-1}$), NaOH (0.52 $cm^3\ g^{-1}$) and PVDF (0.11 $cm^3\ g^{-1}$) and the surface area between 224 $m^2\ g^{-1}$ to 643 $m^2\ g^{-1}$ [38]. Iron- and nitrogen-doped mesoporous carbon microspheres for electrocatalytic purposes was produced via in situ replication and polymerization strategy. Here, mesoporous ferroferric oxide ($Fe_3O_4$) microspheres are used as mesoporous structure-directing agent and source of $Fe^{3+}$ ions to be used as oxidation agent for the polymerization of pyrrole. The obtained carbon via the use of $Fe_3O_4$, pyrrole, CTAB used as precursors exhibited high BET surface area (674 $m^2\ g^{-1}$) with a total pore volume of 0.71 $cm^3\ g^{-1}$ [39].

In a recent work, Mashindi et al. [40] reported the use silica template for the synthesis of broken bowl-like hollow carbon spheres (BHCS – as shown in Fig. 5) as carbon support for platinum electrocatalysts for fuel cell applications. In this work, the authors first reacted nanosized $SiO_2$ spheres (~ 60 nm) and resorcinol-formaldehyde (RF) mixture in the presence of CTAB at room temperature for 24 h to form $SiO_2$ @RF. Upon etching with 10% hydrofluoric acid and annealing at 900 °C in argon, BHCS were obtained. Subsequently, the BHCS was doped with nitrogen (i.e., BNHCS) and then served as an excellent support for Pt nanoparticles. The developed fuel cell electrocatalysts exhibited small-sized Pt nanoparticles (3–5 nm) which are supported on BHCS with high BET surface area (755–782 $m^2\ g^{-1}$). The broken bowl-like morphology conferred excellent interconnectivity with Pt, thus allowing for durable electrocatalytic performance for oxygen reduction reaction (ORR).

Lately, carbons with hierarchical pores have been prepared by using silica nanoparticles as template and D-glucose as carbon precursor [41]. A varying size of silica nanoparticles of 12 nm and 8 nm were used for preparing $SGT_{12\ nm}$ and $SGT_{8\ nm}$ carbons and their performance was compared with rice husk-based carbon. This work shows that the capacitance is dependent on the porosity of carbon which can be tuned by adating the pores to the size of electrolyte ions. High surface area ($S_{BET}$ – $SGT_{12\ nm}$ = 1069 $m^2/g$ and $SGT_{8\ nm}$ = 1319 $m^2/g$) carbons possessed high fraction of mesopores compared to the RH carbon which possessed mainly micropores. The EDLCs assembled with mesoporous hierarchical carbons demonstrated lower capacitance than the RH-based carbon at room temperature. However, the presence of high mesoporous fraction in hierarhcial templated carbons facilitated the bulk electrolyte like behavior at low temperature which led to an excellent performance of EDLCs with $SGT_{12\ nm}$ and $SGT_{8\ nm}$ at − 40 C, while the EDLCs with RH

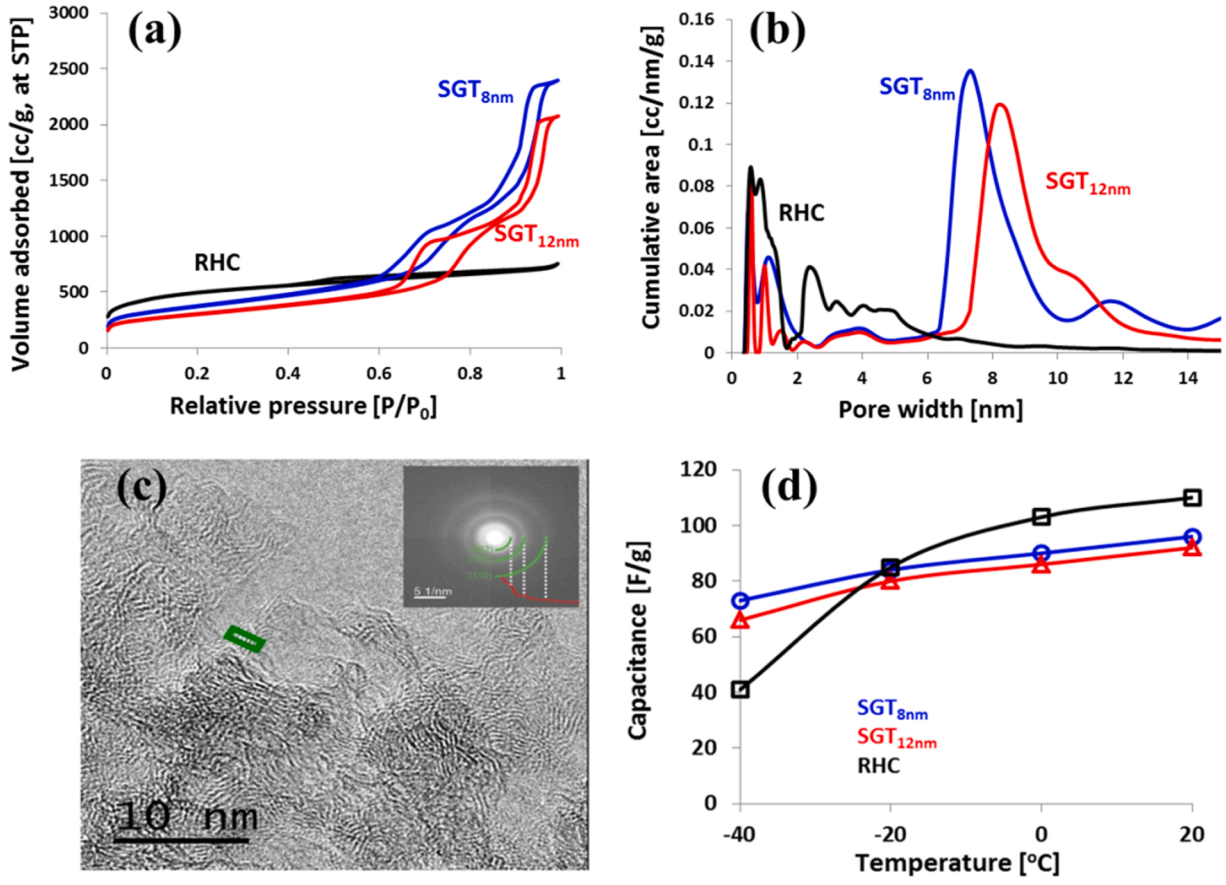


**Fig. 5.** Physicochemical and electrochemical characterization of templated carbon prepared from silica nanoparticles and D-glucose precursor (a) $N_2$ gas adsorption/desorption isotherms, (b) pore size distribution of $SGT_{12\ nm}$, $SGT_{8\ nm}$ (prepared via silica templates of sizes 12 nm and 8 nm) and RHC (rice husk-based carbon), (c) TEM image of $SGT_{12\ nm}$ and (d) capacitance versus operating temperature of electric double-layer capacitors (EDLCs) using these three carbons in ionic liquid-based electrolyte from 20 °C to −40 °C [41].

carbon showed very high ohmic losses at this temperature. It is assumed that the presence of large amount of micropores in RH-based carbon leads to the freezing of ionic liquid at low temperature. On the other hand, mixed ionic liquid electrolyte keeps bulk properties which is at the origin of better low temperature performance of mesoporous hierarchical carbons than a strictly microporous carbons in EDLCs [41].

### 2.2.2. Zeolites

Hierarchical zeolite templated carbons (ZTCs) were firstly prepared by using mesoporous zeolites as sacrificial scaffolds. Chemical vapor deposition was used to introduce the carbon precursor inside the pores. Sodium hydroxide, cetyltrimethylammonium bromide, ammonium nitrate, hydrofluoric acid, sodium bicarbonate, boric acid, ethylene and nitrogen were used as precursors. The salient features of these carbon include tailored microporosity and high degree of mesoporosity that allow to bridge the gap between classical ZTCs and CMK-like materials. Carbon materials possessing high surface area of 2140 $m^2$ $g^{-1}$ and mesopore volume of 0.85 $cm^3$ $g^{-1}$ were prepared with surfactant templated mesoporous zeolites [42]. Also, the Alcell lignin solutions were used as carbon precursor to prepare templated carbon materials with hierarchical pore structure by liquid phase impregnation of different zeolite templates. The effect of templating mixture (lignin/zeolite), carbonization temperature (500, 700 and 900 ºC) and of zeolite framework resultant carbons was analyzed in terms of structural and chemical properties. In this regard, the lignin to zeolite mass percentage was changed from 25% to 50%, the BET surface area and the total pore volume of the resulting carbon material increased; for example from 589 to 952 $m^2$ $g^{-1}$ for 50–700-Y carbon (total pore volume = 0.38 $cm^3$ $g^{-1}$) with respect to 25–700-Y carbon (total pore volume = 0.50 $cm^3$ $g^{-1}$), respectively [43].

High surface area carbons up to 3332 $m^2$ $g^{-1}$ and pore volume of 1.66 $cm^3$ $g^{-1}$ have been reported which were prepared by the use of zeolite 13X as a template. The synthesis was carried out by a two-step process combining liquid impregnation and chemical vapor deposition. The first step is the nanocasting of furfuryl alcohol into zeolite 13X followed by the CVD of ethylene at 700 °C. Overall, a small influence of heating rate was noted for all the prepared ZTCs prepared in this study [44]. In another work, to enhance the porosity of the diatomite-templated carbon and to increase its adsorption capacity for methylene blue, KOH activation was performed. Here, KOH not only worked as activation agent, but also as an etchant to remove the diatomite templates. Thus prepared diatomite-based carbons possessed macroporous carbon pillars and tubes, which were derived from the replication of the diatomite templates, and specific surface areas up to 988 $m^2$ $g^{-1}$ and pore volumes of 0.675 $cm^3$ $g^{-1}$ [45].

Certainly, external carbon layers formation onto zeolite structure hinders a faithful replication, and also significantly limits the adsorption and storage capability of the resultant ZTCs. Therefore, and as demonstrated in Fig. 6, acetylene CVD at a relatively mild temperature of 550 °C followed by a thermal treatment at 800 °C was used for selective deposition of carbons in the micropores of zeolites. As a result, high surface area zeolite replicated carbons with high BET surface area of ~2700 $m^2$ $g^{-1}$ and micropore volume (>1.10 $cm^3$ $g^{-1}$) were obtained without depositing nonporous external carbon layers [46]. Another new methods was used for the preparation of zeolite-templated carbons having large surface areas (~3000 $m^2$ $g^{-1}$) with ordered microporous structures were synthesized in a bubbling fluidized bed using CVD process on NaX zeolite with propylene used as a carbon source [47]. These carbons were then used for the construction of EDLCs in 1 M $H_2SO_4$ electrolyte exhibiting high specific capacitance.

## 2.3. Evaporation induced self-assembly (EISA)

Among the pioneer research on EISA-based synthesis was introduced by Galen Stucky group who prepared mesoporous metal oxides [48]. The process is based on controlling the formation of an inorganic network with nano-crystalline structure through voids of liquid-crystalline phase during slow solvent evaporation. The evaporation step is critical to the orientation, arrangement and ordering of the formed material. Both thermodynamic and kinetic factors govern the mechanism of synthesis similar to thin film formation [49]. EISA has been successfully employed for the synthesis of diverse carbon materials.

Coal-based nitrogen-doped ordered porous carbon is synthesized using EISA (see Fig. 7) as an efficient metal-free catalyst for carbon dioxide electrochemical reduction [50]. The study showed that pores shrinkage took place as the temperature was increased, where dicyandiamide acted as nitrogen source which are inserted within the carbon micropores. Hydrogen-rich gas production can be realized by catalytic steam reforming of biomass tars using Ni-based catalysts. Highly ordered carbon-coated mesoporous silica-supported Ni-based catalyst (Ni-$SiO_2$ @C) was synthesized using EISA and followed by calcination for hydrogen production [51]. The conversion efficiency of the Ni-$SiO_2$ @C to a biomass tar model, namely toluene, was as high as 99.9% at 550 °C. Electrodes in flexible electronics with porous structure are in high demand as they fulfill efficient electron and mass transfer conditions. Using water-EISA process, a dendritic-lamellar MXene/carbon nanotube/poly(vinylpyrrolidone) conductive electrode with high void

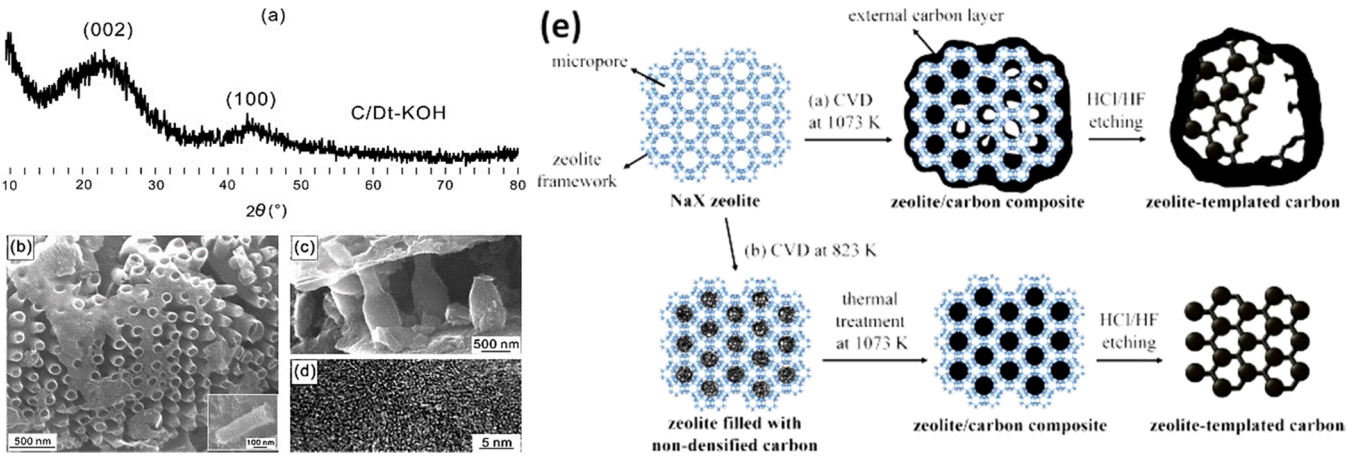


**Fig. 6.** (a) X-ray diffraction pattern of KOH etched carbon; (b) SEM images of carbon tubes of (the inset: a single carbon tube) and (c) carbons pillars; (d) TEM image of micropores on carbon walls [44], and (e) Schematic representation of carbon deposition process on the zeolite at different chemical vapor deposition and temperature conditions. (a) Direct acetylene CVD at 800 °C, and (b) acetylene CVD at 550 °C, followed by subsequent heat treatment at 800 °C under argon flow. Reproduced with permission [46].

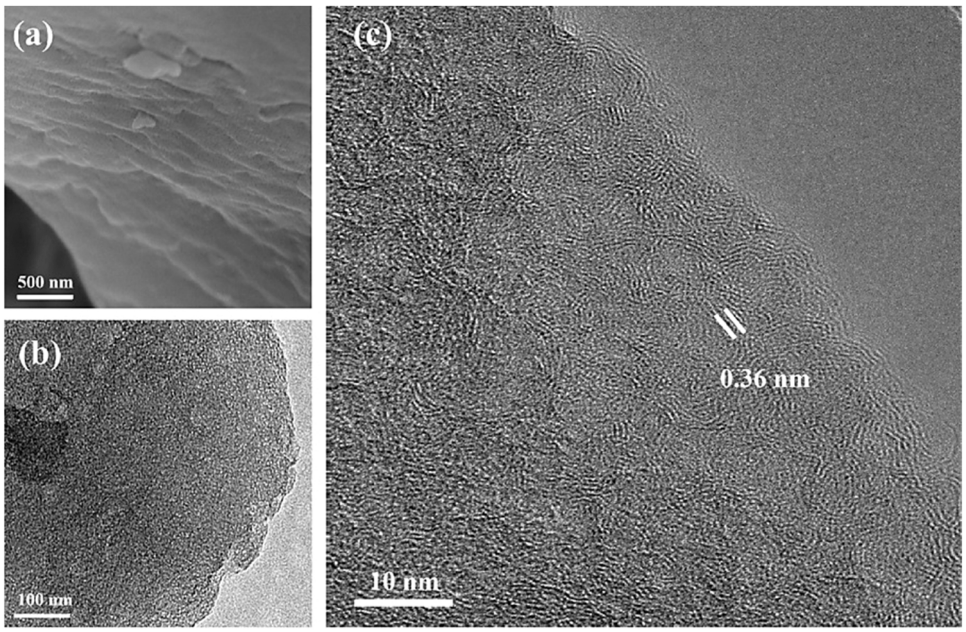


**Fig. 7.** Electron microscopy images of nitrogen-doped porous carbon with ordered structure. Reproduced with permission [50].

space and flexibility was prepared [52]. A voice recognition and pulse sensor was fabricated by printing this electrode on rubber substrate with possible applicability to two dimensional nanostructures. Single-wall carbon nanotubes (SWCNTs) were included in a composite structure of cellulose nano-crystal conducting films using EISA from water [53]. The morphology, thermal, electrical and dielectric film properties were function of the SWCNTs content. Highly ordered mesoprous carbon and doped with nitrogen was prepared using EISA process; pyrrole and carbamide were used as nitrogen sources [54]. The resulting 2D-hexagonal mesostructures had uniform pore size and high specific surface area allowed their employment as ultra-high capacitors with specific capacitance of 310 F $g^{-1}$ at a current density of 1.0 A $g^{-1}$ and high energy density of 17.8 Wh $kg^{-1}$ at a power density of 225 W $kg^{-1}$. EISA synthesis process and suspension polymerization were used to prepare sub-millimeter-sized hierarchically porous carbon spheres [55].

The porous carbon spheres were used for high efficiency removal of nuclear wastewater, namely U(VI), as high as 232.45 mg $g^{-1}$. Masson pine alkali lignin was used as carbon source to prepare ordered mesoporous carbon solid acid by EISA [56]. The solid acid was used as catalyst in the hydrolysis of bagasse cellulose with an index of crystallinity of 70%. High-speed electronic devices such as transistors are affected with the architect of the material used. In a recent work, aligned carbon nanotube traces were applied to a flexible poly(imide) substrate using high-resolution aerosol jet printing technique and EISA process [57]. It was reported that printed tracks in the range of 30–80 μm and conductive tracks (single CNT twin-line width) in the range of 600–1500 nm were obtained. Biocompatibility is essential in biological fields in particular when using materials for culturing and growing cells. Multiwalled carbon nanotube (MWCNT) rings were prepared in a Petri dish by EISA technique to form different shapes and morphologies [58]. The MWCNT rings were further employed to culture L929 cells in oriented cell growth protocol for the purpose of regulating cells in tissue repairing. The interfacial interaction of activated carbon (AC) with volatile organic compounds was improved by modifying AC-surface with nano-metal oxide particles using EISA technique [59]. The measurements and DFT calculations showed that AC/ZnO composites exhibited the best adsorption performance for acetone (415 mg $g^{-1}$) and methanol (481 mg $g^{-1}$). High specific area and pore volume of ordered mesoporous carbon (OMC) flakes were prepared using EISA technique [60]. The microwave absorption properties of OMC were improved by electroless plating its surface with Fe-particles and the specific surface area and pore volume of the flakes reached 1727 $m^2$ $g^{-1}$ and 2.05 $cm^3$ $g^{-1}$, respectively. While EISA process normally takes place at normal or room temperatures, some modification may take place by imposing heating to accelerate the rate of evaporation of the solvent used. Thus, highly ordered micro-mesoporous carbon was fabricated using heated-EISA with reverse micro-emulsion [61]. The method was used to prepare the mesoporous carbon in F127/MMA in a reverse micro-emulsion method and the resulting material exhibited excellent supercatacitor characteristics. Another variation to the original EISA method is the use of two solvents or more in the process. Thus, OMCs were synthesized using two solvents, low molecular weight resins as carbon source and tri-block co-polymers [62]. The tri-block co-polymers were used as template for EISA method used in the synthesis. The study showed that the mesophases formed were controlled by the ratio of copolymers used and the co-solvents ratio. EISA method could also be combined with other techniques for carbon materials preparation. For example, ordered mesoporous carbon film on graphite was synthesized by a combination of two steps: dip-coating and EISA [63]. The 2D hexagonal film was used as solid-phase micro-extraction coating with efficiencies higher than commercial PDMS fibers. Several factors affect the EISA process such as the temperature of the substrate. A recent study showed that the temperature of poly(imide) substrate and CNT concentration affect the evaporation dynamics and alignment in deposition pattern when using EISA method [64]. EISA was found applicable for the preparation of nano-composites made of graphitic carbon/iron carbide for sulfur-based batteries applications [65].

The cathode side of a battery made of this nano-composite exhibited reversible capacity exceeding 1300 mAh $g^{-1}$. The degree of order and alignment of nano-composites made of carbon-based materials and inorganic elements for lithium ion batteries applications were synthesized using EISA method [66]. The material, carbon-silica-titania, is employed as anode in Li-ion battery configuration with reversible capacity of 574 mAh $g^{-1}$. The high degree of order of the material results in improved electron transport through the arranged graphene layers and ease of electrolyte merge into the formed mesopores. The production of carbon-based materials from naturally occurring organic polymers such as lignin using EISA approach was reported [67]. In this study, “green” chemicals replaced the usually used pholo-glucinol and formaldehyde by lignin and glyxal with the ordered mesoporous carbon

obtained used as super-capacitor. The fabrication of transparent and conducting thin films over flexible substrates from highly ordered structure is of prime importance for electronic and solar energy industries. In this respect, MWCNTs were regularly patterned over large silicon and glass wafers [68]. The structure was administered over the substrates using EISA under wedge-shaped geometric confinement. The study showed that the film conductance increased with depositing time and a decrease in transparency was observed.

### 2.4. Microphase separation

Phase separation using permeable membranes has been established among the major assets in industry namely gas and oil, energy conversion and water treatment industries. The inclusion of carbon-based materials in membranes and their use in microphase separation have extensively been investigated. Highly ordered and vertically aligned carbon nanotubes were included within poly(urethane-urea) nanocomposite [69]. The resulting nano-composite exhibited good mechanical strength, toughness and thermal energy dissipation. For dye-sensitized solar cells, the development of alternative electrocatalyst to platinum is crucial to reduce the cost of energy production. A carbonization process of poly(butyl acrylate)-poly(acrylonitrile) block copolymer and Ru(III)-acetyl acetonate resulted in template-free mesoporous material [70]. Stabilization took place and a microphase separation occurred in the block copolymer; the poly(acrylonitrile) is transformed into N-doped semi-graphitic carbon. The material was used as counter electrode in a dye-sensitized solar cell and exhibited a power conversion efficiency of 11.42%. For the fabrication of composite materials involving carbon-based structure, the microphase separation between other components of the composite controls the porosity of the carbon component. Thus, ultra-microporous carbon with pore diameter 0.6 nm was obtained when microphase separation between pre-carbonized polymer networks takes place [71]. With specific surface area as high as 1551 $m^2\ g^{-1}$ the resulting material when used as electrode in capacitor setup the obtained specific capacitance was 268 $F\ g^{-1}$ at 0.5 $A\ g^{-1}$. Microphase separation between polymer networks reinforced with carbon-based material form an adhesive resin to bind to metallic substrates.

In a recent work, microphase interpenetrating polymer networks formed of diglycidyl ether of bisphenol epoxy resin and poly(di-cyclopentadiene) reinforced with carbon fiber had higher bond strengths with steel compared to the individual polymers [72]. In another study, a special ionic liquid was used to self-assemble poly(benzoxazine) to obtain a porous carbon through microphase separation process in the form of skin-tissue-bone-like structure [73]. Interestingly, the ionic liquid used, $C_{16}mimPF_6$, acted as heteroatom precursor to add a pseudocapacitance component through P doping to the porous carbon. The capacitance obtained was 209 $F\ g^{-1}$. In pseudocapacitors applications mass loading is critical in controlling charge transport, thus using regular carbon materials for supporting high mass results in slow electron conduction and ionic conduction. Combined processes of self-assembly and microphase-separation of block copolymers was realized to apply over porous carbon fibers partially filled with manganese dioxide with misopores size of 11.7 nm [74]. With mass loading of 7 mg $cm^{-2}$ of the prepared composite (with manganese oxide 50% of the total mass), the gravimetric and areal capacitances were 1148 $F\ g^{-1}$ and 3141 $mF\ cm^{-2}$, respectively. Carbon dots with variable hydrophilicity were mixed with blended polymers of poly(vinly-pyrrolidone) and poly(ether-sulfone) [75].

Carbon dots were used as dopants up to 10 wt% to the resulting membrane that resulted in variation in its microphase separation characteristics that affected the proton conductivity. With conductivity of 0.086 $S\ cm^{-1}$ the carbon dots doped polymer membrane was employed in a fuel cell test as a candidate for membrane electrolyte in high temperature proton exchange membrane applications. Carbon-based materials are good candidates for reinforcing polymer matrices that affects the rheological behavior of the resulting hybrids. It was recently reported that multi-walled carbon nanotubes and carbon fibers were compounded through a melting process with thermoplastic poly(urethane) [76]. The study showed multi-walled carbon exhibiting higher interaction with the polymer matrix compared to carbon fibers that was attributed to the formation of microphase separated domains within the hybrid material. Carbon black was used as a reinforce and promoter of microphase separation during the formation of poly(urethane) using di-isocyanate hard segment, castor oil soft segment, dimethylol-propionic acid hydrophilic component and tri-ethanolamine neutralizer [77]. Atomic force microscopy measurements proved the effect of hydrogen bond interactions on the extent of microphase separation in the polymer matrix. Bicontinuous structural battery electrolytes were prepared using thermally initiated polymerization induced phase separation with carbon fibers as electrodes and structural reinforcement [78]. The effect of UV-curing temperature for polymerization initiation affected the morphology, ionic conductance, mechanical and electrochemical performance of the material as electrodes in structural batteries. Carbon fibers have unique properties beside large surface area such as ionic and molecular interactions.

One preparation route is to blend poly(acrylonitrile) with additives resulting in poorly controlled porous carbon fibers. This is due to macrophase separation that took place after the pyrolysis step. Microphase separation for copolymer is the alternative route to prepare meso-porous carbon fibers with controlled pore size of 10 nm and micropores of 0.5 nm [79]. Nitrogen and oxygen served as dopants to the resulting carbon fibers when using polymers such as poly (acrylonitrile-block-methyl methacrylate). This increased the ionic transport with substantially high capacitance of 66 $mF\ cm^{-2}$. Nanofibers of poly(acrylonitrile) and poly(urethane) were generated by electrospinning with different viscosities with the inclusion of a variety of carbon nano-fillers [80]. The different carbon-based materials had different dimensions; these are carbon nanoparticles (0D), acid-functionalized MWCNTs (1D), hydroxyl-functionalized graphenes (2D) and hierarchical structures of MWCNTs embedded into graphene flakes (3D). The study showed direct impact of the type of carbon-based material on the topology and orientation of the polymer chains. Anisotropic hierarchical micro-domains were formed in the presence of 0D materials, microphase separation was observed on 1D nanofillers. For 2D functional surface produced highly folded nanoscale lamellae by molecular interactions with polymeric chains. In the case of $^1D$–$^2D$ hybrid fillers, networks created multifaceted structural hierarchies.

### 2.5. Soft-template, self-template and salt-template

#### 2.5.1. Soft-template

Soft-template method is used for producing mesoporous materials via arrangement of structure directing large molecules such as surfactants, assisted by the high temperature treatment. For example, mixture of phenolic resol and melamine was used as a carbon source while the F127 used as a soft template accompanied with silica particle emulsifier utilized to prepare pickering emulsion. Resulting mixture was polymerized and subsequently carbonized at 600 °C to prepare carbon monolith consisting of mesoporous carbon microspheres [81]. Nitrogen adsorption/desorption isotherm of the monolith shows a type-IV curve and a mesoporous structure shown by H1-type hysteresis loop. The BET specific surface area of 316 $m^2\ g^{-1}$ and pore volume of 0.27 $cm^3\ g^{-1}$ was achieved. The pore size distribution curve based on the BJH model is centered at 5.3 nm. According to the XRD result and the TEM data, the material shows a large domain regularity with a well-ordered mesostructure [82]. Carbon microspheres (CMSs) prepared via use of D-xylose as precursor under hydrothermal conditions and followed by carbonization, whereas F127 acted as soft template. Effect of temperature and stirring on the porosity of resulting carbons is schematically presented in Fig. 10. By using a particular stirring speed of 200 rpm, the synthesized mesoporous carbon microspheres exhibited a uniform size

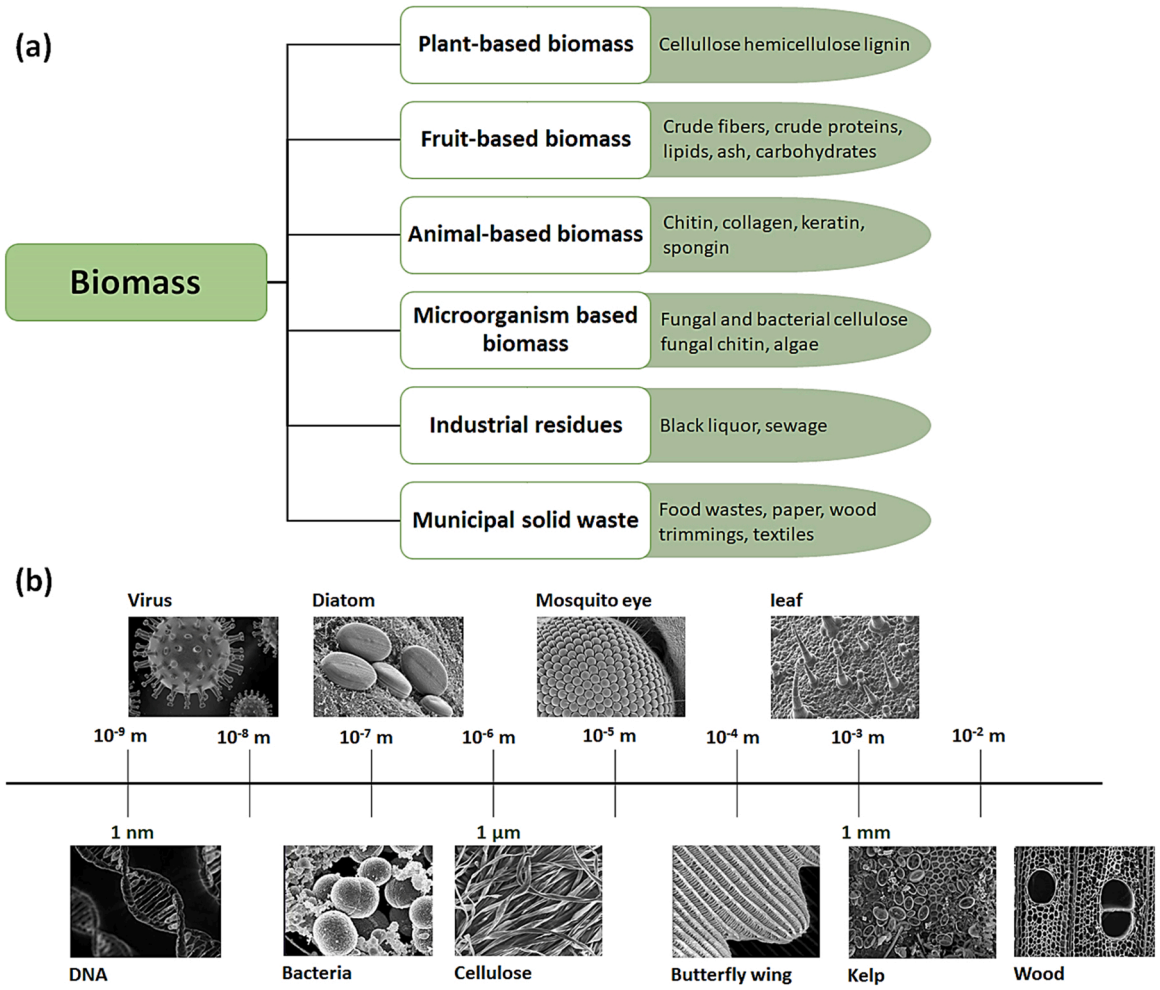


**Fig. 8.** Representation of biomass resources in nature (a) with an overview of the size of biomass placed on the length scale according to their critical dimensions (b).

distribution from 1 to 1.4 μm and surface area of 452 $m^2\ g^{-1}$ [83].

A brand new silica-based copolymer template is developed by co-condensation of TEOS and (3-methacryloxypropyl)-trimethoxysilane (MPS). The framework morphology and size of this template can be tailored by tuning the MPS concentration. Thus, the templated carbons with unimodal and bimodal mesoporosity as well as macroporous structure can be easily obtained by varying the preparation techniques. The pore size and BET surface area of these carbons can be tuned from 4.3 to 55.0 nm, and 779–1649 $m^2\ g^{-1}$, respectively [84] (Fig. 11).

Self-assembly of materials combined with pyrolysis technology proves to be an innovative template-like method for preparing sewage sludge-based mesoporous carbons (SSMCs) where the sewage sludge acts as precursor, while using three different flocculants including polyacrylamide (cationic), polyacrylamide (anionic) and chitosan as template (see Fig. 12). The flocculant plays roles of nucleation, pore formation and surface group modification. SSMCs prepared by template-like method have specific surface area in the range of 102–137 $m^2\ g^{-1}$ and pore volume between 0.149 and 0.183 $cm^3\ g^{-1}$. The phenol adsorption capacity of PAM-MC is relatively large (132.33 mg $g^{-1}$), and the mesoporous structure plays an important role in phenol adsorption, while the high content of amide group and p-p interactions assists in adsorption process [85].

### 2.5.2. *Self template*

Self-template method is used to incorporate elements such as nitrogen and phosphorus into the carbon backbone to enhance the chemical and electrochemical activity of desired templated carbons. Schematic in Fig. 13 demonstrates a graphitic carbon nitride (g-$C_3N_4$) based self-templating method to construct a phosphorus and nitrogen co-doped porous carbons. This material was then investigated for oxygen reduction catalytic performance. According to the experimental procedure, diaminonaphthalene (DAN) in ethanol was mixed with the g-$C_3N_4$ self-template to initiate the polymerization, and then phytic acid was added to the admixture. Afterwards, the composite material was pyrolyzed under nitrogen to obtain a series of nitrogen and phosphorus dual-doped carbon catalysts. The gas adsorption/desorption isotherms of all the prepared carbons were identified as type IV that is specific for mesoporous materials. The surface areas of these materials was between 236 and 838 $m^2\ g^{-1}$. Pore size distribution plots indicated that the dual-doped porous carbon materials possess mesopores centered at 6–10 nm. The synergistic effect of nitrogen and phosphorus doping could greatly improve the content of graphitic nitrogen, which is the reason of achieving high catalyst activity [86].

A feasible and attractive strategy has been proposed where template-assisted and self-activation processes occur due to the synergistic effect of dicyandiamide as nitrogen precursor and template and zinc gluconate as carbon/oxygen precursor as well as activating agent. The carbon material obtained via this route possessed nitrogen and oxygen co-doping along with mesoporous structure as demonstrated in Fig. 14. The presence of broad pore size distributions and nitrogen/oxygen functional groups on the carbon structure facilitate the $2e^-$ oxygen reduction for $H_2O_2$ generation along with •OH via electro-Fenton process. A high surface area of 831 $m^2\ g^{-1}$ and a nitrogen content of 3.7 wt % was achieved [87].

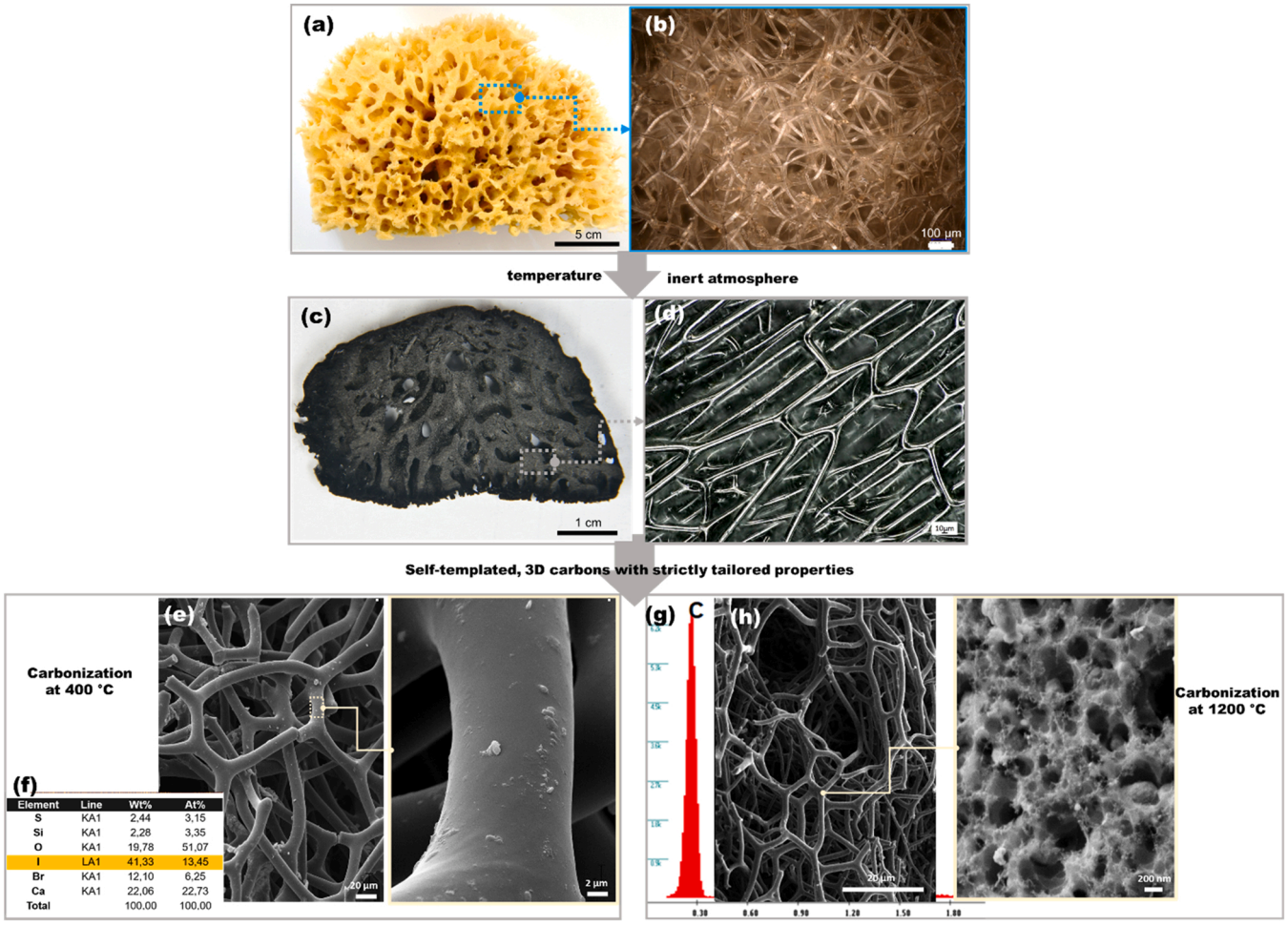


**Fig. 9.** Camera image of spongin-based scaffolds isolated from commercial sponge (A) and its carbonized form (C) with the optical microscopy image of the organization of the fibers (B and D, respectively); SEM images of the carbonized spongin-based scaffold at 400 °C (E) and 1200 °C (in different magnifications) with corresponding surface composition (F and G).

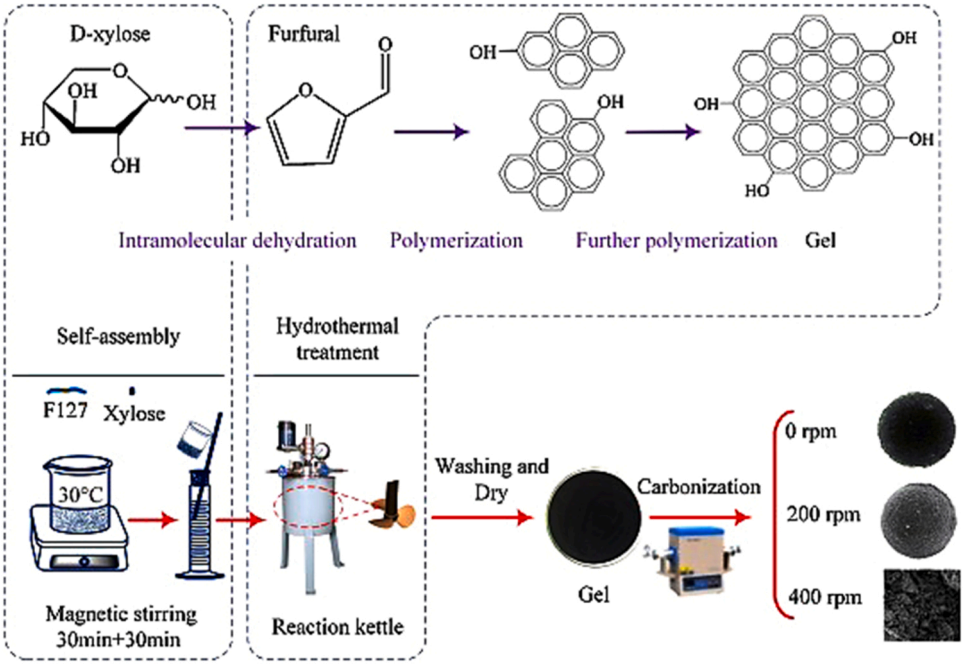


**Fig. 10.** Preparation process of highly dispersed mesoporous carbon microspheres and polymerization of precursors. Reproduced with permission [83].

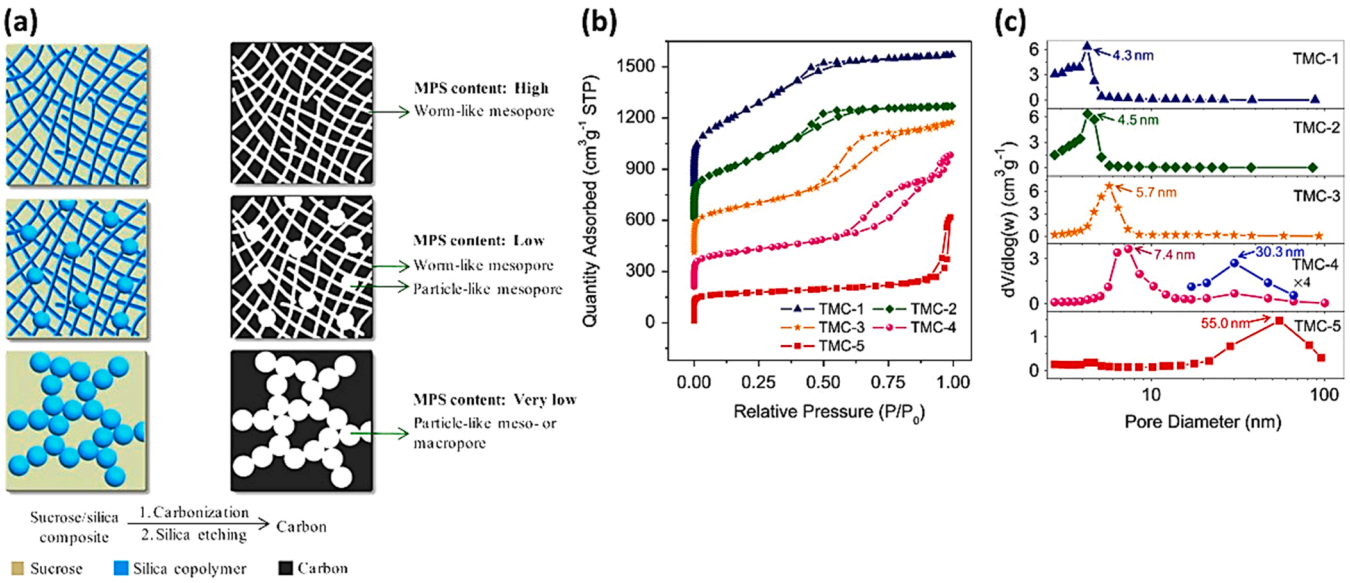


**Fig. 11.** (a) Schematic for the effect of (3-methacryloxypropyl)-trimethoxysilane content on the nanopore structure of as-prepared carbon materials, (b) $N_2$ adsorption/desorption isotherms and (c) BJH pore size distributions of templated mesoporous carbons (TMCs). Reproduced with permission [84].

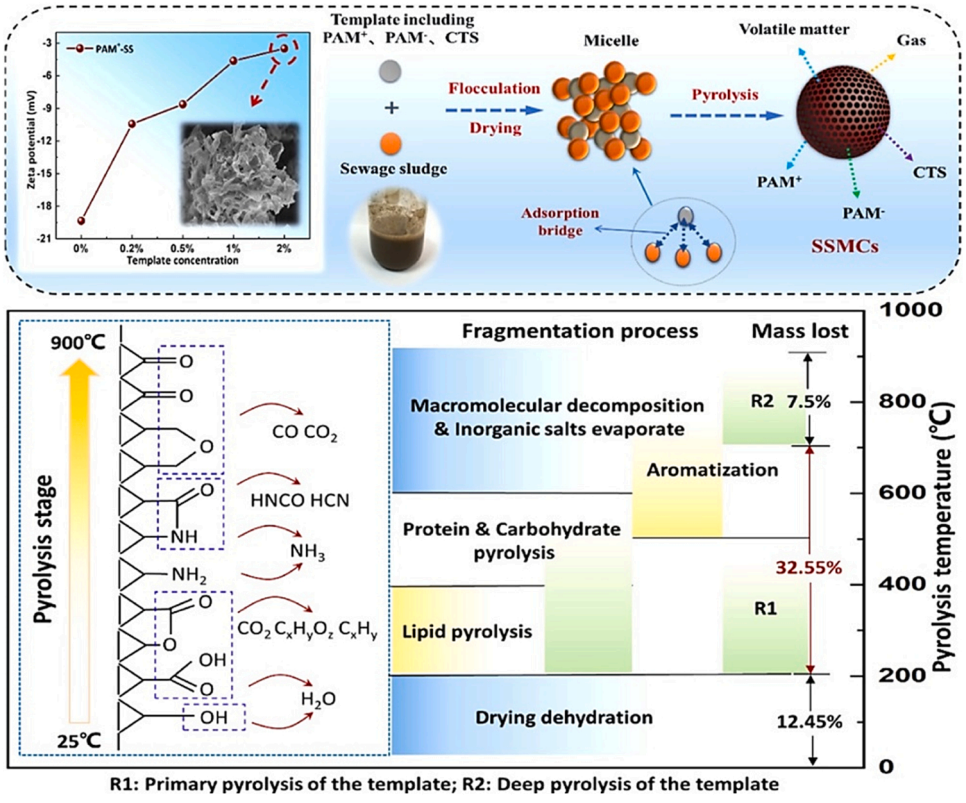


**Fig. 12.** Schematic diagram demonstrating the pyrolysis mechanism (various stages developed by varying temperature) and the preparation process of sewage sludge-based mesoporous carbons (SSMCs). Reproduced with permission [85].

An innovative strategy was reported where self-templating is carried out with phytic acid to prepared carbons with hierarchical porosity and nitrogen-phosphorus-iron tridoped (schematically shown in Fig. 15). These carbons were then used as catalysts with high efficiency, reliability and alternatives to platinum-based catalysts for oxygen reduction reaction. A high BET surface area up to 1216.3 $m^2\ g^{-1}$ and hierarchical pore size distribution was obtained. The larger surface areas of these carbons is attributed to the phytic acid due to its pore creation ability, which left a high fraction of micropores after decomposition during high-temperature annealing. As a result of well-organized nitrogen and phosphorus doping and the feasible structure of the carbon, an enhanced mass transfer ability and abundantly available active-sites ensure high performance in catalyzing oxygen reduction reaction [88].

### 2.5.3. *Salt templates*

In this template method, salt such as NaCl are used as template to

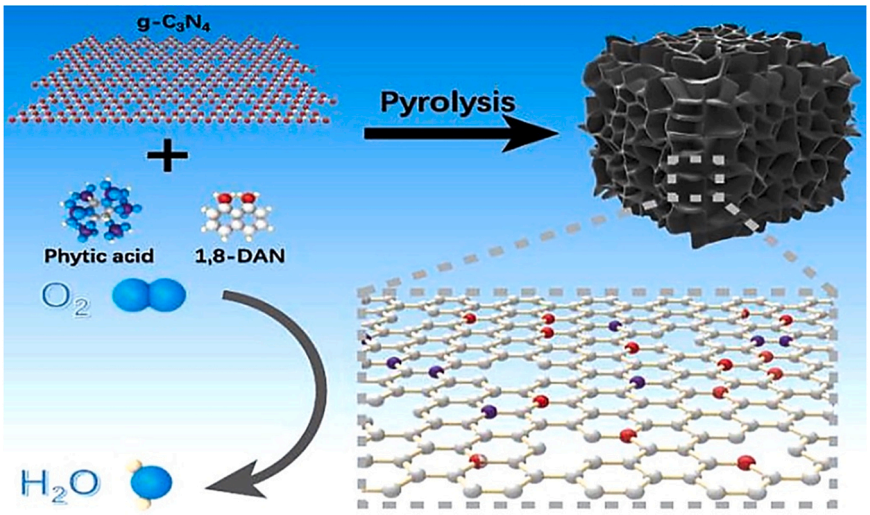


**Fig. 13.** Schematic illustration of the synthesis of nitrogen and phosphorus doped hierarchical porous carbons used as electrocatalysts. Reproduced with permission [86].

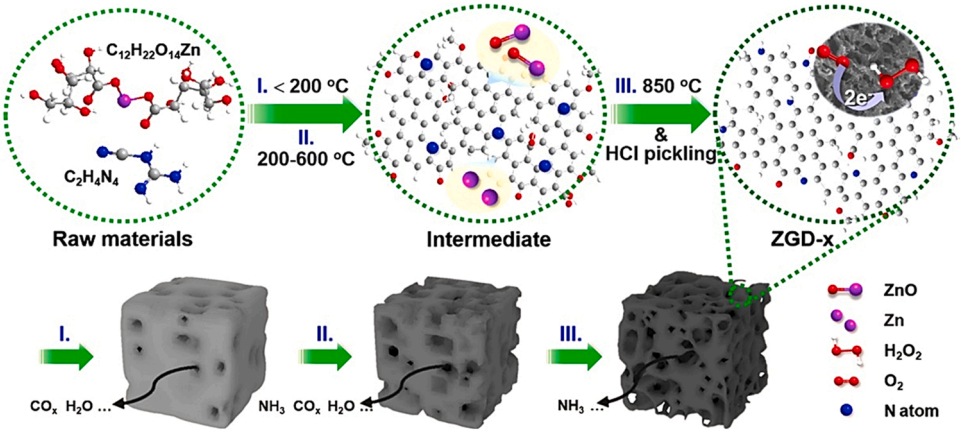


**Fig. 14.** Scheme for the formation mechanism of mesoporous nitrogen and oxygen co-doped carbon materials prepared by template-assisted self-activation method. Reproduced with permission [85].

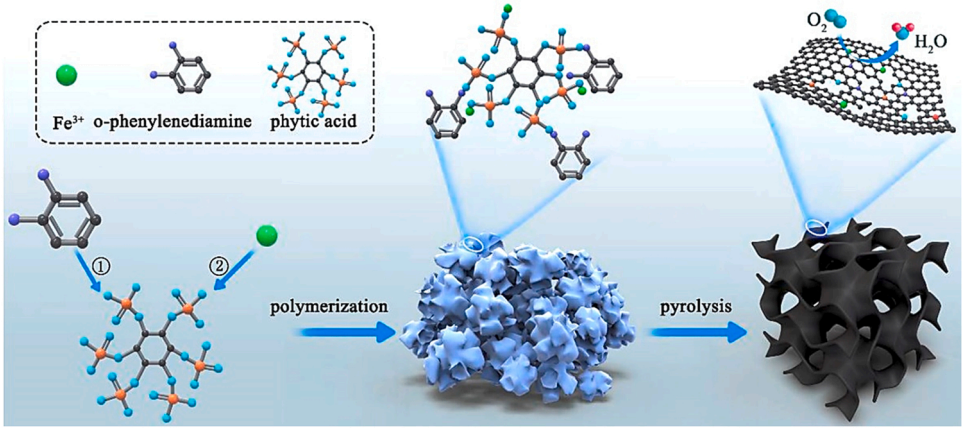


**Fig. 15.** Scheme of self-template strategy for the synthesis of nitrogen, phosphorus and iron doped three-dimensional nanoporous carbon materials. Reproduced with permission [88].

prepare porous composite carbons where phenolic resin and pitch act as carbon precursors. The main advantage is that the NaCl template inhibits the graphite crystallite growth during carbonization, and thereby small graphitic domains with expanded interlayer spacing are obtained, which is suitable for sodium storage. In addition, the presence of NaCl templates help to create abundant mesopores and macropores which

provide channels for fast sodium ion diffusion. Overall, the porous structure and the graphite crystalline structure can be precisely controlled by simply adjusting the mass ratio of NaCl. In this particular case, the pitch, phenolic resin, and NaCl (4 g, 8 g, and 12 g, respectively) were mixed via wet ball milling method in the ethanol for 12 h, followed by carbonization at 750 °C (illustrated in Fig. 16). The gas adsorption/desorption isotherms of resulting carbons exhibit the feature of Type II, that indicates the existence of mesopores and macropores. Depending on the initial fraction of NaCl the resulting surface area of carbon can reach up to 234 $m^2 g^{-1}$ [89].

Hierarchical pores together with nitrogen-doping in a carbon material possessing high surface area has been prepared by using sucrose as carbon precursors, and ethylenediamine tetraacetic acid disodium zinc salt ($EDTANa_2Zn$) as nitrogen source, activating agent and hard template. The presence of important characteristics in a single compound gives an advantage to this method for preparing novel carbon materials. The nano-ZnO and $Na_2CO_3$ particles that are produced during the heat treatment of $EDTANa_2Zn$/sucrose composites, are evenly dispersed in the nitrogen-doped carbon. This helps to create mesopores due to the hard templates characteristics of these particles. Furthermore, the nano-ZnO particles can help to etch carbon as an activation agent at high temperature (Fig. 17). Here, $EDTANa_2Zn$ salt ($C_{10}H_{12}N_2O_8Na_2Zn{\cdot}xH_2O$) and sucrose were used as the precursors and the obtained carbon possessed high surface area of 2160 $m^2 g^{-1}$ along with hierarchical porous architecture [90].

Ginkgo leaf derived nitrogen and sulfur codoped porous carbon nanosheets (PCNSs) using $CaCl_2$/KCl molten salt as activating/template agent. The $CaCl_2$/ KCl as a green and non-toxic template can regulate the pore structure and microstructure of carbon materials. Thus obtained carbon materials demonstrated specific surface area of 395 $m^2 g^{-1}$ and total pore volume of 0.24 $cm^3 g^{-1}$ [91]. This is an eco-friendly and one-pot method to produce hierarchical porous carbon materials that are co-doped with heteroatoms and even the production can be extended to large-scale without any toxic impact on the environment (scheme presented in Fig. 18). Furthermore, the potassium carbonate template can be recycled via a simple rinsing and re-precipitation process. The final product is nitrogen-doped porous carbon possessing a surface area of 2018 $m^2 g^{-1}$ and heteroatom dopants (14.8 wt% oxygen and 1.03 wt % nitrogen) [92].

Also, the nitrogen and sulfur co-doped hierarchical porous carbons were prepared with well-balanced pore characteristic by taking ginkgo leaf as carbon source and $KCl/K_2CO_3$ molten-salt as template/activation agent. The as-obtained carbons possess a well-developed interconnected sheet-like structure, accompanying with high N, S and O contents, conductive to abundant ions transport channels and exposure of more ions-accessible active sites [93]. Furthermore, porous nitrogen-doped carbons were prepared by chemical vapor deposition method and using nanoparticles as template which are produced by the decomposition of calcium tartrate in thermal shock conditions (see Fig. 19). The heat treatment was carried out from 650 °C to 900 °C with a step increase of 50 ℃ and acetonitrile vapors were supplied into reactor immediately after the template production. The carbon material prepared in this work exhibited a surface area of 866 $m^2 g^{-1}$ and total pore volume of 1.78 $cm^3 g^{-1}$ [94].

In another work, hierarchical porous carbons were synthesized from heavy residue of waste tire derived pyrolytic oil (TPO). As schematically presented in Fig. 20, magnesium acetate powder was adopted as a pore development agent which was mixed with heavy residue and tetrahydrofuran (THF) by grinding. The maximal value of BET specific surface area of resulting carbons was up to 1005 $m^2 g^{-1}$ [95].

A simple one-pot method was also used that harnesses the self-assembly of various water-soluble NaX salts (X: $Cl^-$, $CO_3^{2-}$, $SiO_3^{2-}$) as a structure-directing template to prepare hierarchical porous carbons. Particularly, calcination of the salts/glucose self-assembly followed by removing the three dimensional self-assembly of the salts via simple washing with water. In particular, NaCl, $Na_2CO_3$ and $Na_2SiO_3$ were used as templates, while the glucose as a carbon source. There is a direct influence of weight ratio of the salts on the pore size evolution. Here, the average mesopores size of carbon increased from 0, 4, 8–18 nm with increasing the weight ratio of $Na_2SiO_3$/NaCl from 0, 1.5%, 2.5–5%. The specific surface area of obtained was 588 $m^2 g^{-1}$ (pore volume = 1.5 $cm^3 g^{-1}$) up to 1088 $m^2 g^{-1}$ (pore volume = 1.3 $cm^3 g^{-1}$) [96]. The soluble salts NaCl and $Na_2SiO_3$ serve as hierarchical templates and support the formation of three dimensional glucose-urea (carbon precursor) complex. The precursor material is heat-treated to obtain nitrogen-doped carbon network characterized by mesoporous nanosheets. In another work where glucose, urea, sodium silicate and sodium chloride were used as the precursors, carbon with high BET surface area up to 692 $m^2 g^{-1}$ and nitrogen adsorption-desorption isotherms corresponding to the Type IV was obtained [97]. Biomass has been also used along with salt templates, for example, adenine is a cheap biomass and can give highly developed carbons when $NaCl/ZnCl_2$ are introduced as templates. Another important factor is the influence of ratio between the two salt on the pore structure. The eutectic mixture of salts leads to the generation of micro- and mesopores with high total pore volume of 3.0 $cm^3 g^{-1}$ and a very high surface area of 2900 $m^2 g^{-1}$ [98].

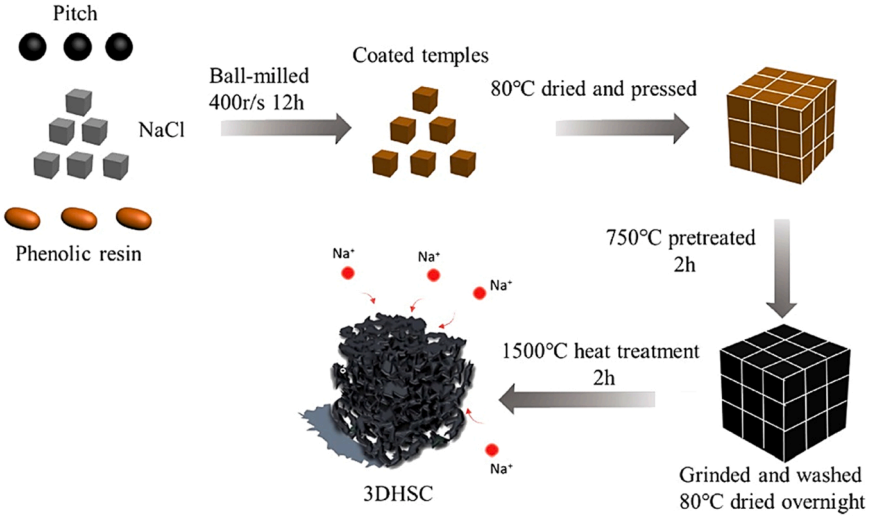


**Fig. 16.** Schematic of the synthesis process for three-dimensional porous hard-soft composite carbon based on NaCl template. Reproduced with permission [89].

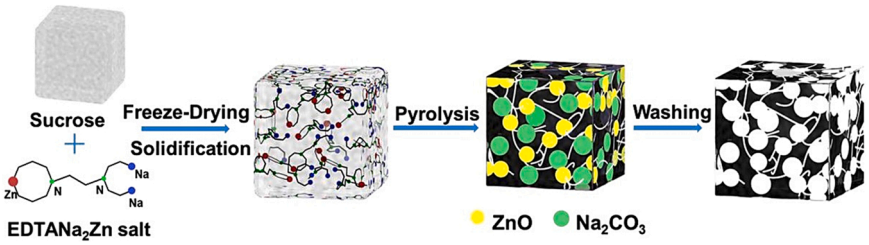


**Fig. 17.** Schematic diagram for the preparation of hierarchical carbons with nitrogen-doping from ethylenediamine tetraacetic acid disodium zinc salt (EDTANa2Zn) that simultaneously acts as hard template, activation agent and nitrogen source. Reproduced with permission [90].

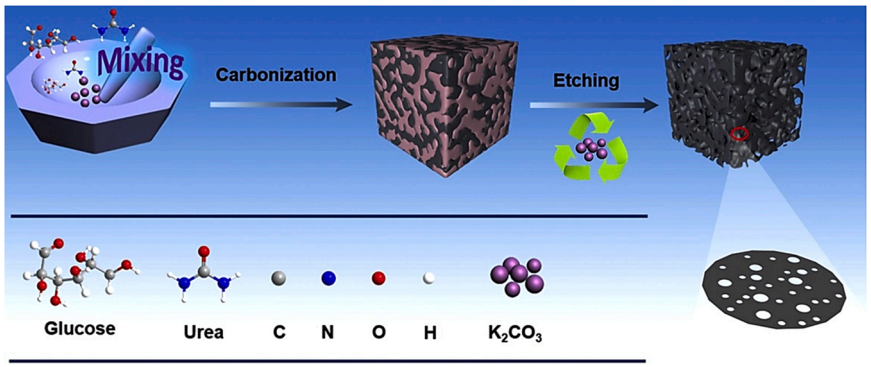


**Fig. 18.** Schematic diagram of the synthesis of hierarchically porous carbon via a recyclable, eco-friendly salt-templating method in a one-step pyrolysis where glucose and urea are carbon source. Reproduced with permission [92].

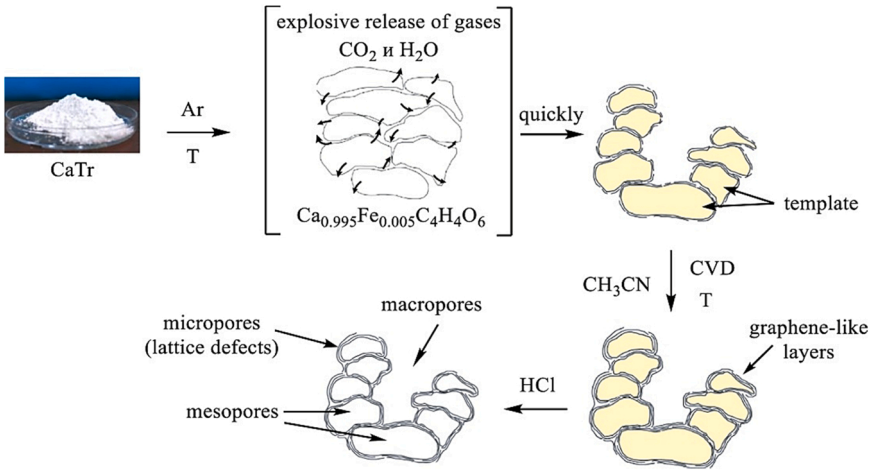


**Fig. 19.** Scheme for the preparation of nitrogen-doped porous carbons where decomposition of calcium tartrate between 650° to 900 °C produced template nanoparticles (TNPs) which were immediately used for the casting of acetonitrile (CH3CN) molecules as carbon source. Reproduced with permission [94].

### *2.6. Development of structured self-templated bio-carbons*

As described in the introduction, the preparation methods of structured carbons are generally complicated, time-consuming, and precursors are mostly expensive and derived from non-renewable sources [99,100]. Despite several advances in their design, the need to use the costly templates to avoid collapsing of carbon structure is still a huge and unsolved problem [101]. Likewise, template synthesis is often a tedious procedure, resulting in increased production costs and an overall carbon footprint. Additionally, the pollution and energy demand caused by the consumption of fossil fuels and other non-renewable sources have grown into a severe crisis that has a huge economic and sociological impact on societies. For this reason, it is essential to encourage scientists to develop and design crucial materials such as structured carbons from renewable and sustainable resources to minimize waste and environmental pollution. Consequently, seeking precursors that might be used in self-templated processes has become more attractive recently.

Therefore, the preparation of hierarchical carbons from various biomass and wastes has gained widespread attention [99,102–106]. Such materials are referred to in the scientific literature as 'bio-carbons.' The bio-carbons are obtained by converting the carbon-rich biomass or wastes into porous, carbon materials through artificial methods, including thermal, hydrothermal carbonization, or templated methods [107]. The bio-carbon term has a broad scope and consists of various materials biochar, hydrochar, activated carbons, among others; all of them are produced from biomass [108].

Important to emphasize is the fact that in comparison to classically structured carbons obtained in templated methods, the bio-carbons

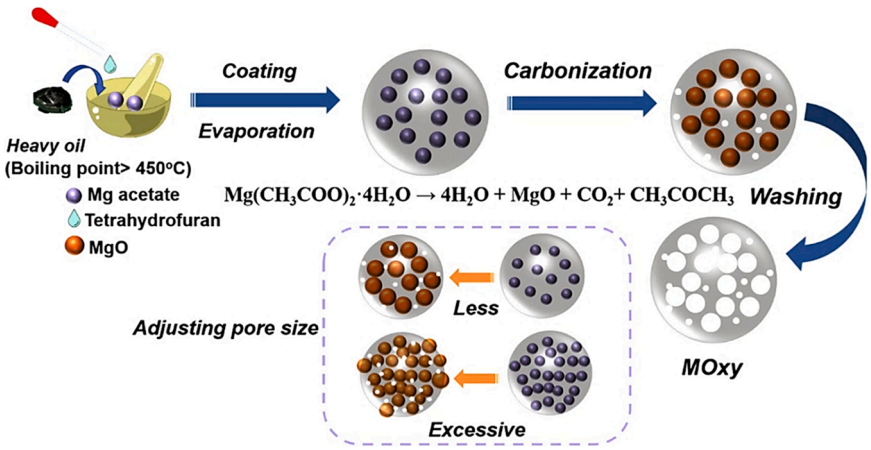


**Fig. 20.** Schematic illustration for synthesis of carbons with adjustable pore size via mixed magnesium acetate and waste tire derived pyrolytic oil. Reproduced with permission [95].

possess several benefits, including cost-effectiveness – the precursors are cheap and mainly derived from plant organs, animal wastes, food, and microorganisms. The structure of biomass precursor is preserved during carbonization under the protection of inner gas. Consequently, the vast majority of biomass precursors might be successfully used to prepare self-assembled structured bio-carbons avoiding costly templated procedures. Thus, the interconnected carbon structures with nanopores can be generated in situ.

Versatility – various biomass can be transformed into bio-carbon with a simple approach: purification, carbonization, and eventually activation. Moreover, different chemicals like – metal oxides – can be implemented during the preparation process to mold selected properties of received bio-carbons. Finally, bio-carbons are considered as environmentally friendly products. The fabrication of bio-carbons does not need to apply high-pressure conditions and harsh chemicals, as in the case of graphene or carbon nanotubes. Therefore, these materials are considered as energy-saving and environmentally friendly. Nonetheless, the application of cheap, renewable biomass or biowaste represents green chemistry in the formation of functional carbon materials [103, 104,109].

However, the key point in bio-carbons development is the selection of biomass precursors, which critically impacts the final properties. The microstructural characteristic, the elemental and chemical composition of the selected precursor affect the carbon yield, the microporosity, and the doping level of resulted bio-carbon material. Therefore, biomass can be assumed as a perfect source of heteroatom-doped carbons with a specified structure designed for various applications – which will be evaluated in this part in detail. Over the past decade, various biomaterials, including cellulose, lignin, hemicellulose, various peels, nutshells, egg white, mushrooms, algae, bacteria, hair, chitin, collagen, were utilized as a source of bio-carbons, among others [110–120]. These materials were proven to be useful in preparing self-templated bio--carbons. The sources of bio-carbons can be divided into several groups taking into consideration the origin and chemical nature of biomass, which are presented in Fig. 8.

On the other hand, a new biomaterial is currently gaining attention as a potential source of structured bio-carbon, and it is spongin. This halogenated scleroprotein builds the skeletons of some sponges from Demosponginae class, recognized as ‘bath sponges’ [121]. The chemical composition of spongin is still unknown. However, it can be compared to collagen and keratin, despite the presence of various halogens, which differs this material among collagen and keratin.

Nevertheless, searching for new biomass sources still plays a critical role in the economic aspect. In this case, even the superior properties of prepared bio-carbon are not enough to fulfill society’s needs. The perfect example is the biochar obtained from chicken eggshells [122]. Regardless of its superior properties, the low amount of eggshell membrane in the egg excludes utilizing this efficient material on a big scale. While the application of biomass to the formation of various bio-carbons is widely described [103,106,123,124], the utilization of biomass to prepare the ready-to-use structured carbon or as a bio-template or self-template still needs to be investigated. Therefore, in this section, we would like to emphasize the current works, which show the biomass utilized in self-assembly manner and bio-template to form interesting and useful composites for various applications (see Table 1).

Every biomass group is characterized by different chemical and elemental compositions, doping level, and structural properties. Therefore, a detailed investigation with understanding the structural-chemical relationship is crucial to finding satisfactory material for the specific application. However, interesting studies dealing with the nature of the familiar biomass sources were already published [103–105, 108].

The development of structured bio-carbons with strictly designed properties using a self-assembly approach is still a hot topic in material chemistry. However, such materials obtained from biomass are usually fragile, two-dimensional with tendencies to exhibit poor conductivity, agglomeration of materials, and poor electrochemical performance or need harsh preparation conditions and expensive additions to prepare structured bio-carbon. Therefore, seeking new precursors is still an important issue. Nevertheless, some precursors seem to have promising application possibilities. As is presented in Table 1, various biomass can be successfully applied as a self-template to obtain in-situ three-dimensional bio-carbons. Lignin is an essential biopolymer, considered one of the most biodegradable, renewable biomaterials derived from plants (except cellulose). Lignin is produced annually in the amount reaching approx. billions of tons - as the third most abundant biomaterial worldwide [141]. The possibility of application of the various form of lignin activated or not made the utilization of this biomaterial a crucial environmental issue [142]. The aromatic chemical structure, rich in phenolic functional groups and high carbon content of lignin, is similar in molecular structure to bitumen. Hence, converting lignin to porous, structured bio-carbon seems to be a practical approach.

Moreover, thanks to the similarities between the aromatic chemical structure of lignin and synthetic resin, this biomaterial seems to be a perfect carbon precursor in the soft-templated approach. The variety of cross-linking agents and solvents allows tailoring the structure of resulting bio-carbon, shape, and size of pores. For this reason, the template approach combined with carbonization and in-situ activation led to the development of hierarchical, porous bio-carbons with high surface area, tunable structure for application in energy storage devices, and water remediation [143,144]. On the other hand, it should be noted that the application of various chemicals during template synthesis is

**Table 1**
The preparation methodology with received structural parameters of biomass-derived structured bio-carbons produced from a different plant-, fruit-, microorganism- and animal-based precursor.

| Biomass precursor | Preparation method | Properties | Potential application | Ref. |
|---|---|---|---|---|
| Mycelium pellets | Bio-templating method: mycelium pellet as a template<br>Carbonization 750 °C<br>Activation with $ZnCl_2$<br>Nitrogen incorporation by addition of $NH_4Cl$ | A hierarchical porous structure composed of micropores and macropores preserved from precursor<br>Surface area 709.9 $m^2g^{-1}$<br>N doping level 7.7 at% | The electrode in supercapacitor with a specific capacitance of 237.2 $Fg^{-1}$ at 10 $mVs^{-1}$ | [125] |
| Yeast cells | Hydrothermal pre-carbonization<br>Pyrolysis at 850 °C<br>The hydrothermal approach used to prepare $mno_2$/carbon hollow structure | Preservation of regular elliptical sphere shape (width of 2 mm and a length of 2.5 mm) – the role of self-template<br>BET surface area before modification equalled 912 $m^2g^{-1}$ | The electrode in supercapacitors with a specific capacitance of 255 $Fg^{-1}$ at 1 $Ag^{-1}$ in 1 M $Na_2SO_4$ electrolyte voltage window 41.4 $Whkg^{-1}$ at a power density of 500 $Wkg^{-1}$ | [126] |
| Banana peel | Treatment with $Zn(NO_3)_2$<br>Mixing with 2-aminophenol and furfural solution<br>Polymerization at 120 °C<br>Carbonization at 1000 °C | Banana peel was used as a self-template and additional carbon source<br>Presence of macroporous cores with mesoporous and microporous channels<br>N doping at a level of 0.6 wt%<br>BET surface area 1650 $m^2g^{-1}$ | The electrode in supercapacitor with specific resistance 206 $Fg^{-1}$ at 1 $Ag^{-1}$ in KOH electrolyte | [127] |
| White straw | Cross-linking with citric acid and $NaH_2PO_4$<br>Freezing and freeze-drying<br>Carbonization (800 °C)<br>Activation in KOH | Hierarchical, open porous structure preserved from precursor; the role of self-template<br>Surface area 2560 $m^2g^{-1}$<br>Lack of additional contaminants with high carbon content 98.15% | The electrode in supercapacitor specific capacitance of 294 $Fg^{-1}$, (Rate performances of 200 $Fg^{-1}$ at 10 $Ag^{-1}$<br>Flexibility and low-temperature resistance) | [128] |
| *E. Coli* bacteria | Mixing with $fecl_3$ solution, and graphene<br>Freezing in liquid nitrogen<br>Carbonization (700 °C). | Bacteria cells were used as a template<br>Desirable specific surface area (181.6 $m^2g^{-1}$) with pore volume (0.74 $cm^3g^{-1}$)<br>The abundance of foreign atoms (N, P, S, Fe) | The electrode in supercapacitor with high specific capacitance 327 $Fg^{-1}$<br>Good stability | [129] |
| Rice straw | Homogenization with $KHCO_3$<br>Carbonization at 300 °C<br>Removal of residual potassium salt and silica by washing with 1 M HCl and 20% NaOH (w/w).<br>Activation with $KHCO_3$ and KOH | Dense, compact structure maintained after carbonization – a self-template role<br>Well distributed C, O and Si within the bio-template<br>Porous architecture with BET surface 1903 $m^2g^{-1}$ and pore volume 1.01 $cm^3g^{-1}$ | The electrode in the three-electrode system with a specific capacitance of 357 $Fg^{-1}$ (0.5 $Ag^{-1}$ in 1 M $H_2SO_4$) In two-electrode system 260 $Fg^{-1}$ (1 $Ag^{-1}$ in 1 M $Na_2SO_4$) | [130] |
| Poplar catkins | Pre-carbonization at 400 °C,<br>Activation with $ZnCl_2$.<br>Removal of metal oxide and salt with 2.0 M HCl solution and deionized water. | Maintenance of precursor structure – a self-template role<br>Surface area 1361.9 $m^2g^{-1}$ with pore size in the range of 0.5–1 nm<br>Tube wall thickness decreased from 1 μm 0.3 μm<br>Nitrogen content 2.9 wt% | $CO_2$ adsorbent: with a high adsorption capacity of 6.22 and 4.05 $mmolg^{-1}$ at 273 and 298 K, respectively, at 1 bar of $CO_2$. | [131] |
| Agaric | Preparation of agaric, manganese acetate, and sodium chloride composite<br>Molten-salt approach<br>Carbonization at 800 °C | Interconnected, monodispersed nanoparticles with relatively uniform size<br>BET surface area equalled 139.6 $m^2g^{-1}$<br>Tight coverage with MnO nanoparticles | An anode in lithium-ion battery:<br>reversible specific capacity 876 $mahg^{-1}$ at 0.1 $Ag^{-1}$,<br>rate capability (402 $mahg^{-1}$ at 2 $Ag^{-1}$)<br>promising cycle stability (783 $mahg^{-1}$ after 1000 cycles at 0.5 $Ag^{-1}$ with no capacity decay) | [132] |
| Bio-oil | Nano-MgO was used as a template in the hard-template approach<br>Dissolution of bio-oil in magnesium acetate (precursor of nano-MgO)<br>Carbonization at 800 °C<br>Washing with HCl | Hierarchical porous structure with a variety of O-containing functional groups<br>Surface area 1177.12 $m^2g^{-1}$ with total pore volume 0.98 $cm^3g^{-1}$<br>low yield of carbon 17.36% | Electrode in supercapacitor:<br>the capacitance of 344 $Fg^{-1}$ at 0.5 $Ag^{-1}$,<br>rate performance of 168 $Fg^{-1}$ at a heavy current density of 50 $Ag^{-1}$<br>cycling stability in 6 M KOH electrolyte solution | [133] |
| Lignocellulose fibers | The bio-templated method<br>Heterocoagulation of lignocellulose fibers with functionalized $TiO_2$ | Lignocellulose fibers utilized as a self-template<br>Fibers are tightly coated with $TiO_2$ nanoparticles<br>The particle size of the resulted composite dispersed showed a bimodal volume distribution | An electrode component in dye-sensitized solar cell achieving 6% of photo efficiency | [134] |
| Waste Coca Cola® | Hydrothermal carbonization of waste Coca Cola® with CTAB and ammonia at 200 °C<br>Chemical activation with KOH or $ZnCl_2$ | Formation of spherical bio-carbons<br>Bio-carbon activated with KOH exhibits high BET surface area 1405 $m^2g^{-1}$<br>$ZnCl_2$ activated bio-carbon has BET surface area 1994 $m^2g^{-1}$<br>Oxygen and nitrogen doping 12.5 and 10.1 wt% for KOH activated and 10.3 and 4.2 wt% for $ZnCl_2$ activated. | KOH activated spherical bio-carbon:<br>capability for $CO_2$ with 5.22 $mmolg^{-1}$ at 25 °C and 1 atm<br>$ZnCl_2$ activated spherical bio-carbon:<br>the specific capacitance of 352.7 $Fg^{-1}$ at a current density of 1 $Ag^{-1}$ in 6 M KOH electrolyte | [135] |
| Spongin of commercial sponge origin | Bleaching using NaOH and $KMnO_4$ and decalcification with HCl<br>Carbonization at 650 °C<br>Hydrothermal functionalization to produce $MnO_2$ carbon composite | Preservation of the fibrous structure of the precursor – a self-template role<br>Bimodal pore distribution with minimal pore size 13.11 nm up to 285.19 μm | Electrode:<br>low resistance<br>good stability of the material over more than 3000 charging/discharging | [136] |
| Spongin of commercial sponge origin | Decalcification with HCl<br>Desilication with 0.5% HF<br>Carbonization at 1200 °C<br>Electroplating with cobalt oxide(I) | Preservation of the hierarchical organization of precursor – a self-template role<br>The decrease in volume after carbonization (up to 70%).<br>Surface area 425 $m^2g^{-1}$<br>Mechanical strength - the compression 1.3 MPa at a density of 0.1119 | The catalyst in the reduction reaction of 4-nitrophenol to 4-aminophenol in marine environment and freshwater:<br>calculated rate constant equalled k = 0.03 $s^{-1}$ and 0.04 $s^{-1}$ for simulated seawater and deionized water, respectively | [137] |

(*continued on next page*)

**Table 1** (*continued*)

| Biomass precursor | Preparation method | Properties | Potential application | Ref. |
|---|---|---|---|---|
| *Luffa cylindrica* plant sponge | Carbonization at various temperatures (700–900 °C) in $NH_3$ atmosphere<br>Chemical activation using KOH | The natural structure of luffa sponge was preserved – a self-template role<br>Bio-carbons have densely packed and parallel channels of 4–10 mm in diameter and 0.3–1 mm in wall thickness | Specific capacitances at 1 $Ag^{-1}$ equalled 167, 196, and 249 $Fg^{-1}$ in $Na_2SO_4$, KOH, and $H_2SO_4$ solutions, respectively | [138] |
| Collagen | Soaking in the acidic solution of various metal salts ($Zr(SO_4)_2$, $Al_2(SO_4)_3$, $Fe_2(SO_4)_3$).<br>Heating in the air at 100 °C<br>Heating under vacuum at 800 °C | Preservation of fibrous collagen structure – a self-template role<br>Hierarchical morphology<br>Surface equalled 529 $m^2g^{-1}$ (collagen Fe(II), 566 $m^2g^{-1}$ (collagen Al(III)) and 1212 $m^2g^{-1}$ (collagen Zr(IV) with well-developed mesoporous structure. | | [139] |
| Sodium lignin sulfonate | Hard-template synthesis: silica as a template<br>Carbonization at 500 °C<br>Etching silica template using diluted HF<br>In-situ alkali activation. | Three-dimensional lignin-based interconnected hierarchical porous carbon<br>Surface area 2784 $m^2g^{-1}$) with large pore volumes 1.382 $cm^3g^{-1}$ | Strong adsorption affinity for sulfamethazine with the maximum mono-layer adsorption capacity of 869.6 $mgg^{-1}$ at 308 K | [140] |

not a sustainable solution due to the production of wastes and high experimental costs, which hinder mass production.

On the other hand, a new biomaterial is currently gaining attention as a potential source of self-constructed bio-carbon is spongin. This halogenated scleroprotein builds the skeletons of some sponges from Demosponginae class, recognized as 'bath sponges' [121]. The chemical composition of spongin is still unknown. However, it can be compared to collagen and keratin, despite the presence of various halogens, which differs this material among collagen and keratin. Recent studies revealed that spongin-based skeletons possess a high content of carbon, oxygen, hydrogen, and nitrogen [121]. Moreover, the presence of halogens and other elements such as sulfur, sodium, silicon, calcium, magnesium, and iron has been confirmed [121]. The low amount of Fe, Si – usually are incorporated into the skeletons during the sponge's growth [145–148]. Sodium, calcium, magnesium, and aluminum have been proved in other studies and may depend on the environment [81]. However, proper treatment prior to carbonization led to removing such elements from the structure. Despite their unique chemistry, the spongin-based skeletons are an interesting source of biomaterials also from the morphological point of view. The skeletons have a hierarchical, multi-level organization of fibers with thickness varying from few to several micrometers – typically 10–15 μm [146]. Those fibers are built from densely packed microfibrils and arranged within a preferential orientation – typically in concentric layers. The diameter of microfibrils has been measured to be approx. 10 μm [121]. The spongin-based skeletons are three-dimensional, reticular, possessing open-pores cellular structures with multi-junctional regions (Fig. 9).

On the macroscale, the structure of spongin-based scaffolds seems to be favorable compared to other biomaterials. The hierarchical arrangement of fibers that form a system of open channels, often hexagonal in shape, recalls the honeycomb-like structure commonly observed in nature (Fig. 9B, D).

Nevertheless, this proteinaceous, fibrous material shows promising properties to be used as a self-template to produce fibrous scaffolds. The application of spongin in the development of carbon-based materials is economically feasible, considering the sustainability aspect of advanced new materials. Spongin is a natural, renewable, and ready-to-use source that can be cultivated under marine farming conditions at a large scale worldwide. As was proved in the study described in Table 1, spongin preserves the hierarchical, fibrous structure of precursor even after carbonization at 1200 °C [136] (Fig. 9H). This biomaterial can be used as a self-template, without "chemical stabilization" with various cations. The 3D, fibrous, structured bio-carbon preparation can be achieved in a simple carbonization process. Another significant advantage of spongin is a production of a bio-carbon with extraordinary mechanical strength – which is unusual considering other fragile biochar. Spongin-based bio-carbon can be simply sawn into slices approx. 2 mm thick. This study hypothesized that, because of occurring collagen microfibrils, which are polymerized, and hydrated, the carbonization process led to the break of interfibrillar bonds, thus releasing nanofibril structures and forming a carbonaceous backbone during heating was observed. The heating result in the transformation of collagen-based spongin into a hexagonal carbon structure. Consequently, it was proved that spongin is a great biomaterial that can be used as a self-template to form advanced structured bio-carbons. Such results agree with the hypothesis that biomass precursors with well-organized structures can be successfully applied in the preparation of ordered porous carbons in a self-assembly approach [149].

Moreover, spongin is naturally rich in various heteroatoms, including nitrogen and sulfur, among others. Thus, the carbonization at proper temperature develops carbonaceous material naturally rich with particular heteroatoms and avoids expensive doping procedures (Fig. 9E). Consequently, the diversity of surface functional groups may facilitate further functionalization processes – as was already shown, electroplating and hydrothermal treatment are sufficient to prepare advanced composites [135,136]. Moreover, as was shown elsewhere [150], the tailoring of carbonization temperature results in the formation of carbonaceous material with different physicochemical properties, which can be adjusted depending on the designed application [146, 147,150].

### 2.7. Metal-organic frameworks

Carbon materials with hierarchical pore sizes were also prepared via a chemical vapor deposition method where zeolitic imidazolate framework (ZIF) acts as template impregnated with furfuryl alcohol. Carbon material is obtained after KOH activation and it has high surface area of 2400 $m^2\ g^{-1}$ and significantly high pore volume of 1.6 $cm^3\ g^{-1}$. Other features of this method included a high yield of highly microporous ZIF-templated carbons and the templated carbon is obtained directly after CVD treatment without the need to etch out ZIF framework. High pore volume and a micropores fraction up to 82% make these carbon quite attractive for various applications [151]. Nanoporous carbon materials were also prepared by using ZIF-7 as a precursor and glucose as an additional carbon source. These carbons showed high nitrogen content and surface area 783 $m^2\ g^{-1}$ with excellent electrocatalytic activity for oxygen reduction reaction [152]. Direct carbonization of zinc-based metal organic framework at 800 °C was realized to synthesize ordered porous carbons with a high surface area of 1523 $m^2\ g^{-1}$ (Fig. 21) [153].

### 2.8. Surface functionalization by electrochemical grafting

Surface functionalization is an important tool that results in modifying the reactivity of the material at the interface between the substrate

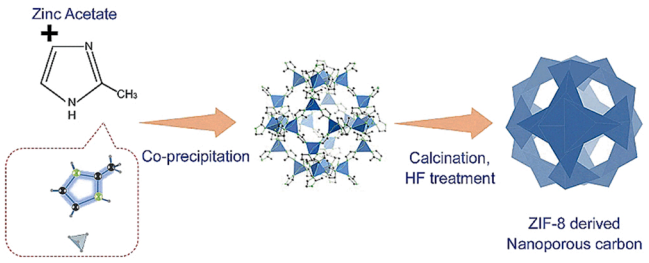


**Fig. 21.** Scheme of the carbon synthesis from metal organic framework based on zinc acetate. Reproduced with permission [153].

and the environment. Two approaches can be considered to accomplish this task: electrochemical and chemical grafting. The type of substrate dictates the type and extent of grafting and more rationally the chemistry of grafting that realizes the targeted surface functionalization.

One of the approaches recently presented was radio-frequency plasma treatment of carbon fiber fabric with nitrogen/hydrogen gas mixture [80]. The treatment resulted in the formation of –NHx and –N groups that allowed further grafting of conducting poly(aniline). Surface morphology and structural characteristics of the substrate showed distinct difference after grafting. The charge transfer resistance at the interface was minimized indicating the successful grafting process. Surface functionalization by covalent interaction to carbon surfaces with two different modifiers, diaryliodonium and aryldiazonium, were compared [154]. Aryldiazonium is considered one of the extensively studied modifiers for surface functionalization. However, diazonium precursors are unstable when grafted over carbon surfaces. The study showed that diaryliodonium precursors were more stable as an alternative to diazonium. Besides the various electrochemical techniques used to characterize and compare the grafted surfaces with the two precursors; Raman spectroscopy, scanning tunneling microscopy and X-ray photoelectron spectroscopy were further used to characterize the modified surfaces. The results indicated that iodonium precursors were more efficiently covalently bonded to the carbon substrate and higher surface coverage was realized compared to diazonium precursors. Electrochemical reduction of carbon dioxide to carbon monoxide is among the key reaction for renewable energy storage and chemical industry in general. This reaction was facilitated by the employment of a metal-free electrocatalyst of nitrogen-grafted over MWCNTs [155]. The surface modification was achieved by "exohedral chemical grafting" functionalization using aryl-diazonium salts with different nitrogen-containing precursors. The study showed that high carbon monoxide catalytic efficiency was obtained when using pyridine or 2, 6-dimethyl-pyridine. This was attributed to the fact that 2,6-$(Me)_2$Py and acridine frameworks realize an ideal balance between N-basicity for $CO_2$ activation/conversion to give the corresponding radical ion responsible for electron transfer and its stabilization by neighboring C-sites.

During the grafting process using diazonium precursors, a problem is developed at the interface due to the multilayer formation. In a recent study hydroxylamine monolayer formation was achieved over glassy carbon, as well as other surfaces, using phthalimide-protection and hydrazine-deprotection strategy [156]. Coverage over different substrates was 150–170, 40 and 100 pmol $cm^{-2}$ for glassy carbon, boron-doped diamond and gold surfaces, respectively. The study showed that this surface grafting facilitated the wiring of redox-active bio-molecules such as horseradish peroxidase enzyme to electrode surfaces. One strategy for surface grafting is to form a "pre-layer" via self-assembled molecular network that acts as template for further functionalization. A series of porous molecular networks was introduced to the surface by alkoxy-substituted dehydro-benzo [13] annulene derivatives at the liquid/graphite interface [157]. These molecules were connected to the surface through van der Waals interactions of the inter-digitated alkyl chains that altered the pore diameter and the pore-to-pore distance. This was followed by covalent electrochemical functionalization of template-graphite using an aryldiazonium salt. The orientation of the unit cells of the grafted aryldiazonium over the graphite substrate was found a function of the type of self-assembly molecular network template pre-formed over the surface. Sodium ion-based batteries are considered one of the promising solutions for high density energy storages that employ carbon electrodes.

Surface functionalization of the carbon electrodes is among the solutions to address poor reversible capacity and efficiency. In a recent review, the types of surface functionalization based on the structural changes in carbon materials were discussed [158]. Three categories for surface functionalization discussed are: heteroatom doping, grafting of functional groups, and the shielding of defects. The study revealed that heteroatom doping improved the electrochemical reactivity, the grafting of functional groups promoted the diffusion-controlled bulk process and surface-confined capacitive process, and the shielding of defects increased the efficiency and cyclic stability without sacrificing reversible capacity. Boron-doped nano-crystalline diamond constitutes good photo-electrode in dye-sensitized solar cells. In a recent study, the diamond surface photo-anode was stabilized by applying a monolayer of using 4-(trimethyl silyl) ethynyl benzene diazonium tetra-fluoroborate [159]. The successful formation of covalently bonded monolayers was confirmed by angular resolved X-ray photoelectron spectroscopy. Further functionalization of the surface involved the elimination of the trimethyl silyl groups and the resulting ethynyl functionalities were employed to immobilize organic donor-acceptor chromophores via Sonogashira cross-coupling reactions.

A direct goal of surface functionalization by electrochemical grafting is to improve the electrocatalytic activity of the modified surface. Thus, N,N,N′,N′-tetramethyl-p-phenylene diamine (TMPD) was coupled with 4-nitroaniline where the nitro functional group in the coupling product $N^2$,$N^2$,$N^5$,$N^5$-tetramethyl-4′-nitro-[1,1′-biphenyl]− 2,5-diamine (MNPD) was reduced electrochemically to the corresponding amino derivative (MAPD) [160]. Furthermore, the electro-generated MAPD was immobilized onto a nano-fibrillated mesoporous carbon modified glassy carbon electrode. Two electrochemical grafting routes followed: the first involved electrochemical reduction of MNPD in presence of sodium nitrite to form diazonium ions in situ; the second involved spontaneous adsorption in the absence of sodium nitrite. The electrocatalytic performance of the modified electrode was confirmed for its high reactivity in Michael addition reactions. In fuel cells the surface functionalization of nitrogen-containing species on carbon support controls the electrocatalytic activity and carbon-ionomer interaction of cell electrodes. Two approaches were suggested for grafting positively charged nitrogen-containing groups or negatively charged sulfonates groups onto three different carbon-based materials [161]. The study proved that the fuel cell performance was improved as the current density increase when interacting with para-phenylene diamine or ammonia and the performance decreased when functionalizing the surface with sulfonate groups. This was attributed to the reduced resistance of mass-transfer overpotential.

Lithium sulfonate groups were grafted to carbon surfaces and applied for the reduction of lithium polysulfide in the lithium-sulfur batteries [162]. Lithium sulfonate groups replaced the commonly used lithium nitrate and are attaced to the ordered mesoporous carbon CMK3 through three-step procedure. When CMK3 is functionalized by ethylene diamine or sulfonate groups and used as cathode in Li-S battery setup, the initial coulobmic efficiencies increased 75% compared to non-functionalized CMK3. Sub-monolayers were covalently grafted on glassy carbon substrates using Diels-Alder cyclo-addition with two soluble dienophiles, namely propargyl bromide and ethynyl ferrocene [163]. The grafting process took place under mild conditions by heating at 50 °C in toluene for few hours. The covalent bonds formed over the surface were ascertained by spectroscopic techniques including Fourier-transform infrared spectroscopy (FTIR), X-ray photoelectron spectroscopy (XPS), and electrochemical measurements using cyclic voltammetry. Untraditional

methods of grafting over surfaces such as ultra-sonication can be used for surface modification. Poly(N-isopropyl acrylamide) a thermo-sensitive polymer was grafted on carbon nano-fibers using ultrasonic source [164]. Switching the applied temperature to the surface led to a reversible alternation between hydrophilic/hydrophic characteristics of the material. The surface of a glassy carbon electrode was modified by the composite and was tested for response of clothianidin that was affected by the temperature of the medium. The cyclic voltammetric response showed higher current signal for clothianidin at 25 °C versus lower one at 40 °C. Acetylene black carbon was modified by covalent grafting of bis(1,10-phenanthroline)− 5-amino-1,10-phenanthroline iron (II) complex using diazonium chemical coupling reaction [165]. The resulting material was employed in $LiFeO_4$ cathodes in a battery setup. The delivered specific capacity was in the order of 60 mAh.g− 1 while the value was 25 mAh $g^{-1}$ for the unmodified electrode. Pyrolytic graphite electrodes were functionalized by ferrocene-alkyl monolayer and were tested in different electrolytes and solvents for charge storage capabilities [166]. The procedure for functionalization adapted electro-grafting of aryl-diazonium layers followed by de-protection to form an attached covalent monolayer, and finally a long chain alkyl ferrocene with ca. C11-chain was attached to the surface. The result of this stacking was to increase the charge density for supercapacitors applications.

Platinum nanoparticles encapsulated within amine-terminated sixth-generation poly(amido amine) dendrimers were used to functionalize the surface of single-walled nanotubes [167]. The structure was suggested for efficient field-effect transistor sensing applications. The surface of the modified carbon nanotubes were subsequently modified with glutamate oxidases for building a reliable FET-based sensor for glutamates. Hydrophilic, dense and compact thin film obtained over carbon electrodes were formed by grafting 4-diazopyridinium cations by in situ reduction [168]. An electroactive biofilm was applied over the formed film and it was verified by different techniques including contact angle, ellipsometry, atomic force microscopy and electrochemical measurements. High rate of electron exchange was observed at the interface suggesting its application in microbial fuel cells. Pyridine- and thiophene-based iodonium salts were successfully grafted over conducting surfaces such as glassy carbon replacing the conventionally used aryl diazonium salts [169]. Other suggested agents were used along the salts are iodo-substituted pyridine, thiophene, furan and pyrrole. The study showed that in the later are more stable than their diazonium analogs however the rate of grafting was relatively slower. In another study, SWCNTs were functionalized with ferrocene using ethylene glycol with variable chain lengths [170]. The modified surface was used for electro-enzymatic oxidation of a biomolecule namely nicotinamide adenine dinucleotide (NADH) with the help of grafted ferrocene derivatives for electron exchange mediation. The interfacial properties between carbon fibers and epoxy resin were improved using a grafting approach over carbon fibers surfaces using poly(urethane) with hyper-branching architect and functionalized with hydroxyl groups [171]. The grafting procedure was preceded by electrochemical oxidation of carbon fibers in nitric acid to form oxygen functional groups that was followed by grafting the hyper-branched poly(urethane) through the multi-OH groups and finally converting the functional groups to amino-groups.

## 3. Applications of templated porous carbons (TPCs)

The templated carbons possess this intrinsic advantage of exact controlled structures relative to the conventional nanocarbons. Moreover, the doping carried out via elemental physical insertion into the structure or chemical grafting of certain molecules enables them to achieve high charge storage capacity or electrochemical activity for a particular application.

### 3.1. Energy storage

The TPCs display exclusive properties of 1D, 2D, 3D, hierarchical structures, high porosity, high surface area and ease of heteroatom insertion that can be used in batteries, supercapacitor, fuel cell and sensors as well as other non-electrochemical sectors. For each of these applications, we highlight the strategies, type of template used, and discuss related physicochemical and electrochemical performance.

#### 3.1.1. Batteries

Batteries are the devices that store chemical energy and on demand convert it into electrical energy for use in different applications. Nanoporous templated carbons have been researched as anodes and cathodes in batteries applications [Table 2] as a result of the large surface areas and pore volumes, hierarchical pore structures, nanopores defects, etc. Du et al. used NiMo alloy template to prepare Mo single atom/cluster N-doped 3D nanoporous holey graphene with rich edges as bifunctional electrocatalysts [172]. The solid-state zinc-air battery fabricated from the obtained N and Mo co-doped nanoporous carbon material discharged and charged continuously for 88 h with high power density of 83 $mWcm^{-1}$. NaCl template was used to produce well distributed Co nanoparticles on a hierarchical nitrogen-doped porous carbon support with high accessible Co-Nx active sites. Such elemental composition is crucial for achieving high capacity and high power via facile electron transfer and improved electronic properties. Thus constructed all-solid-state zinc-air battery has a high specific power of 63 mW $cm^{-2}$ as well as excellent stability [173]. Kim et al. demonstrated that conductive carbon matrices with precisely designed pore structures synthesized using KCl template could be used to Na−Se and K−Se batteries that delivered 445 mAh $g^{-1}$ (400 cycles, 0.5 C) and 436 mAh $g^{-1}$ (120 cycles, 0.2 C) respectively [174]. The key issues of Li-S batteries (dissolution of polysulfide and volume expansion) were inhibited when the tetraethyl orthosilicate template synthesized mesoporous structured nanocarbon materials was used as positive electrode. The Li-S electrode has 1589 mAh $g^{-1}$ at 0.25 C (95% of the theoretical capacity, capacity retention: 87% at 2.5 C after 0.25 C activation) [175].

Nie te al [176]. used rice husks and silicon dioxide template to prepare hierarchical porous hard carbon having large specific surface areas and high pore volumes. The hard carbon anode for sodium-ion batteries gave a high capacity of 274 mAh $g^{-1}$ at 25 $mAg^{-1}$, 92.7% of retention capacity after 500 cycles.This suggests that the rational microstructure and texture design gives faster diffusion kinetic and reduced polarization. Qiu et al. [177] used self-template to design and synthesized hierarchical hollow hard carbon microstructure for sodium-ion batteries anode. The anode material has a specific capacity of 243.5 mAh $g^{-1}$ at 100 cycles and coulombic efficiency of almost 100%. This is because of the defective hexagonal lattice for $Na^+$ reversible binding-sites for and fast kinetic ion-transfer process. While Wang et al. [178] used MgO template to synthesize hierarchical pore configuration with abundant mesopores, good structural stability, and low oxygen content nanoporous carbon rods as sodium-ion batteries anode material. The anode has a discharge capacity (181 mAh $g^{-1}$ at specific current of 0.2 A $g^{-1}$) at 2000 cycles and 90% capacity retention. Hu et al. [179] used MgO template to produce an increased degree of graphitization, specific surface area and pore volume having hierarchical porous structured anode material. The Li-ion battery anode has an improved capacity (1495 mAh $g^{-1}$ at specific current of 0.1 A $g^{-1}$), cycle stability and high-rate capacity (391 mAh $g^{-1}$ at 10 A $g^{-1}$) for 1100 cycles.

Eutectic salt template approach has been reported to assisted in the preparation of hierarchical structured catalyst having increased catalytic active sites, surface area (1548.6 $m^2$ $g^{-1}$) and pore volume. The catalyst's oxygen reduction reaction activity has high half-wave potential (0.88 V), maximum power density (174 mW $cm^{-2}$, 263 mA $cm^{-2}$), specific capacity (753 mAh $g^{-1}$), long-term lifetime and rate capability [180]. The combination of doping and morphological regulation has

**Table 2**
Templates and properties of templated porous nano carbons for batteries.

| Template | Preferred properties | Ref. |
|---|---|---|
| NiMo | Nanoholes/edges on the nanoporous graphene | [172] |
| NaCl | Co nanoparticles on a hierarchical nitrogen-doped porous carbon | [173] |
| KCl | N, S-co-doped hierarchically porous carbon | [174] |
| Tetraethyl orthosilicate | Ordered channels for enhanced $Li^+$ transport | [175] |
| Silicon dioxide | Large specific surface areas, high pore volumes and hierarchical pore structures | [176] |
| Self-template | Hierarchical hollow 3D texture hard carbon | [177] |
| MgO | Hierarchical pore configuration | [178] |
| MgO | Increased degree of graphitization, specific surface area and pore volume | [179] |
| Molten salt ($NaCl/ZnCl_2$) | Hierarchical-structure, greater catalytic active sites, large surface area and pore volume | [180] |
| Zn based template | The N-doped 3D nanocarbon anode material has twisted-interconnected cuboidal hollow nanocages | [181] |
| Salt template KCl and $ZnCl_2$ | Nitrogen-phosphorus co-doped carbon material having an improved specific surface area | [182] |
| One-step dual template process: soft template (CTAB) and hard template (TEOS) | Interconnected-functionalized mesoporous carbon-nanospheres having micromesoporous volume and high-specific area | [183] |
| Sacrificial carbon nitride | Hollow-structured and highly dispersed binary FeCo-nitride-carbon material | [184] |
| Sacrificing template (ZIF-8) | High Si content and crystalized SiC inter-layer for enhanced high specific capacity | [186] |
| 3D mesoporous silica | Ordered porous structure and increased electronic conductivity | [187] |
| Ordered mesoporous silica and $ZnCl_2$ as hard- and salt template | Carbon materials doped with nitrogen having hierarchical pore network and a core-shell type particle with ordered-mesoporous carbon | [188] |
| Cobalt hydroxyl carbonate nanowires (Co-CH) | Large surface area and the good crystallinity, uniformly distributed CoxP nanoparticles in the carbon sheath | [189] |
| KCl | A unique microstructure that can absorb the large volumetric expansion and ease the inner stress | [190] |
| $Mg(OH)_2$ | The anode material with hierarchically porous structure and large surface area | [191] |
| $CaCO_3$ nanoparticles | Cross-linked porous carbon skeleton | [192] |
| In situ template (tetrathenyloxysilane) | Carbon with large surface specific area and total pore volume | [193] |
| NaCl | Nitrogen-rich hierarchically porous carbon | [194] |
| NaCl | Honeycomb-like, nitrogen-rich hierarchical carbon | [195] |
| Silica spheres | High sulfur content chemically incorporated into a carbon host, producing sulfur-grafted hollow carbon spheres (SHCS) | [196] |
| Silicate (zeolite) | High surface area and narrow pore size distribution | [197] |
| Nanoporous nickel | 3D bicontinuous naporous carbonaceous material, interconnected tubular pores and non-tubular pores | [198] |
| NaCl | 2D carbon nanosheets, nanoporous microstructure and high degree of mesoporosity | [199] |

been used to construct the advanced carbon material via Zn based template. The N-doped 3D nanocarbon anode material has twisted interconnected cuboid hollow nanocages and lots of nanopores defects across the shells. The anode material in Na-ion battery has high reversible capacities of 401.9 and 311.7 $mAhg^{-1}$ at 0.1 and 0.5 $Ag^{-1}$ respectively after 100 cycles,. And the anode material in Li-ion battery has capacities of 199.7 and 97.9 mAh $g^{-1}$ at 1.0 and 5.0 $Ag^{-1}$ respectively after 10,000 cycles [181].

Guo et al. [182] synthesized nitrogen–phosphorus co-doped porous carbon (NPPC) material using salt template KCl and $ZnCl_2$. Thanks to the presence of K and Zn atoms, the carbon materials exhibists uniform porous structutre decorated by the mesopores and macropores and a large specific surface area (589.97 $m^2g^{-1}$). The lithium-ion battery anode material has initial discharge capacity of 685 mAh $g^{-1}$ (at 0.1 A $g^{-1}$), reversible capacity of 715 $mAhg^{-1}$ after 50 cycles (coulomb efficiency 〉 97%) and 394.1 mAh $g^{-1}$ (2 $Ag^{-1}$) after 400 cycles. The large specific capacity and better cycling performance are not only caused by the porous carbon's larger electrode and electrolyte contact area, but also the porous carbon promoted smooth the diffusion of lithium ions and charge transfer. The capacity, rate and cycling performances are enhanced due to the increased active sites, stable interfaces for lithium storage and improved lithium-ion transport kinetics as a result of the doped nitrogen. The phosphorous-doped favored charge delocalization of carbon atoms thereby promoted the charge separation and improved conductivity. The Nitrogen and phosphorus co-doped caused an increase in the binding energy of carbon-carbon bond, thus boost the capacitive properties of materials. One-step dual template process (soft template (CTAB) and hard template (TEOS)) produced functionalized mesoporous carbon nanospheres having high BET surface area of 1875 $m^2$ $g^{-1}$ and micro-mesoporous volume of 4.75 $cm^3$ $g^{-1}$. The carbon-based cathode material has high sulfur content (90.4%) for long-life durability (3100 cycles). The MHCS/S@P composite cathode has discharge capacity of 780 mAh $g^{-1}$ (0.5 C), 572 mAh $g^{-1}$ at 100 cycles and 432 mAh $g^{-1}$ at 1100 cycles. The dissolution of polysulfides was effectively inhibited (0.054% capacity decay) [183]. Yan et al. [188] reported nitrogen-doped carbon material that has hierarchical pore architecture and a core-shell-type particle with ordered mesoporous carbon core and a polar microporous carbon shell. The doped material has large specific surface area of 1764 $m^2$ $g^{-1}$ and high pore volume exceeding 1.5 cm 3 $g^{-1}$ that can hold 72% sulfur. The Li-S battery cathode material has a high capacity (906 mAh $g^{-1}$.at 0.5 C) and 90% retention capacity at 250 cycles.

### 3.1.2. *Supercapacitors and pseudocapacitors*

Supercapacitors have been described as electrochemical devices that store energy by the electrostatic adsorption/desorption of ions or the charge storage associated with the pseudocapacitive reactions. It is commonly reported that supercapacitors has high power density and cycling stability, but has lower energy density relative to batteries and full cells. Therefore, efforts are tailored towards the search for materials that can simultaneously deliver high amounts of energy at high rates. For this purpose, rapid in-pore ionic movement is crucial along with high surface area as well as pseudocapacitive characteristics. The templated nanocarbons have attracted attention as the notable materials that can produce high energy and power densities supercapacitors [Table 3] because of their pore structure, high capacitance, rapid ion-transfer and uniform nanocavities [185]. Table 2 displays the characteristic examples.

Bottlebrush block copolymers and low-molecular-weight linear block copolymers were used as co-templates to synthesize bimodal porous-carbons having high surface area and the mesopores uniformly surrounding macropores. The supercapacitor's electrode has high gravimetric capacitance of 177 F $g^{-1}$ at 2 A $g^{-1}$ (areal capacitance 1420 mF $cm^{-2}$). Retention capacity of 92% at 10,000 cycles and 95% after voltage floating testing for 100 h [196]. The NaCl and NaOH used as dual template produced a honeycomb-like 3D network of interconnected

**Table 3**
Templates and properties of templated porous nano carbons for supercapacitors.

| Template | Preferred properties | Ref. |
|---|---|---|
| Co-templates (bottlebrush block copolymers and low-molecular-weight linear block copolymers) | Bimodal porous carbons having high surface area and the mesopores uniformly surrounding macropores | [200] |
| Dual template (NaCl and NaOH) | Honeycomb-like 3D network of interconnected carbon nanosheets having hierarchical pores with large specific surface area and high content of N element | [201] |
| MgO | High graphitic degree, high specific surface area and a large pore volume with hierarchical pores | [202] |
| Ceramic-carbon hybrid | High specific surface area and mesoporous structure | [194] |
| Nanocarbon | The nanoporous carbon materials has hierarchical micro- and mesoporosity, high specific surface area, pore volume and pore size distribution range of | [205] |
| $Mg(OH)_2$ | Flower-like material high surface area, rich mesoporosity with rich faradaic oxygen surface functional groups | [206] |
| $Mg(OH)_2$ | Nanosheet morphology, highly mesoporous, large surface area, high electro-active functionalities and homogenous distribution of elements | [207] |
| Soft template: hexadecylpyridinium chloride/poly-(acrylic acid) and hard template: in situ generated silica | High proportion of micropores and large surface area | [208] |
| Nanocarbon | High specific surface area, specific volume and porosity | [209] |
| Poly methyl methacrylate colloidal crystals and $SiO_2$ nanoparticle | High surface areas and well-defined pore structures | [210] |
| Silica nanoparticles | NC700 has high specific surface area and ultrahigh N content | [211] |
| Bottlebrush block copolymers | PC-2BET has high surface area and total pore volume | [212] |

carbon nanosheets having hierarchical porous structure and large specific surface area (~ 1438 $cm^3\ g^{-1}$) and high N content (~ 6%). The NPCA-650 electrode has high specific capacitance (264.3 F $g^{-1}$). The symmetric supercapacitor has high energy density (12.4 Wh $kg^{-1}$)and 98.6% capacity retention after 10,000 cycles [201]. Hu et al. reported MgO as template to synthesis high degree of graphitic character, high specific surface area and pore volume having hierarchical porous structure. The supercapacitor's electrode materials has high specific capacitance (287 F $g^{-1}$; 0.5 A $g^{-1}$), rate capacitance (196 F $g^{-1}$;100 A $g^{-1}$) and retention capacity retention of 95.4% (5 A $g^{-1}$ after 10,000 cycles) [179]. Bonsu et al. [203] used ecofriendly, cost effective and efficient sucrose templated microwave combustion method to synthesis induced symmetric 2D-mesoporous graphitic carbon spinel cobalt ferrite ($CoFe_2O_4$/2D-C). The large specific surface area (251.9 $m^2\ g^{-1}$) and mesoporous structure electrode delivered high specific capacitance (1318.1 F $g^{-1}$ at 2.5 $Ag^{-1}$) and energy density (77.3 Wh $kg^{-1}$) with outstanding capacity retention of 97.2% after 4000 cycles. Similarly, Swain et al. [204] adopted a simple synthesis method and commercially available inexpensive precursors to synthesize nanoporous carbon materials having hierarchical micro- and mesoporosity, high specific surface area (1400 $m^2\ g^{-1}$), pore volume (0.82 $cm^3\ g^{-1}$) and pore size distribution range of 1–4 nm. The fabricated supercapacitor exhibited an outstanding areal capacitance of 16 μF $cm^{-2}$ which corresponds to a high specific capacitance of 227 F $g^{-1}$ at the scan rate of 20 mV $s^{-1}$. In another work, Wei et al. [205] reported the environmentally friendly synthesis method where template induced self-oxidative polymerization of phenols was carried out to fabricate electrochemically active oxygen doped mesoporous carbon. The flower-like nanomaterial synthesized has large surface area (1303 $m^2\ g^{-1}$) and rich mesoporosity (over 80%) with rich faradaic oxygen functionalities (7.4 atom%). The electrode material in supercapacitor application gave a high energy density of 36.7 Wh $kg^{-1}$ at 1000 W $kg^{-1}$, 22.9 Wh $kg^{-1}$ at 18,800 W $kg^{-1}$ and retention capacity of 97.8% at 10,000 cycles. Also, Wei et al. [206] used $Mg(OH)_2$ template-assisted synthesis method for the fabrication of N,O-doped mesoporous carbon nanosheet from hydroxyquinoline-Zn complex. The synthesized material nanosheet is highly mesoporous and has large surface area of 816 $m^2\ g^{-1}$, electro-active functionalities (17.6 atom% of O and 4.4 atom% of N) and homogenous elemental distribution. Furthermore, the aqueous symmetric supercapacitor has energy densities of 30.6 at 2000 W $kg^{-1}$, 20.5 Wh $kg^{-1}$ at 39,620 W $kg^{-1}$, and retention capacitance of 96% after 10,000 cycles. One-pot dual-template is another strategy used by Xu et al. [207] to synthesis 3D hierarchical nanoporous carbon microspheres. High specific capacitance of 413 F $g^{-1}$ at 1 A $g^{-1}$ was observed. The AHNCMs-15-based symmetric supercapacitor has high energy density of 14.7 Wh $kg^{-1}$ at a power density of 250 $Wkg^{-1}$ and capacitance fading of 1.6% after 10,000 cycles at 2 A $g^{-1}$. The two-step synthesis of the nanoporous carbon hybrid from commercial nanocarbon template and a preceramic polymer reported by Swain et al. [208] delivered high specific capacitance of 333 F $g^{-1}$ with zero capacity decay after 1100 cycles due to the high specific surface area (1798 $m^2\ g^{-1}$), specific volume (1.2 $cm^3\ g^{-1}$) and porosity (1–4 nm) of the electrode material. The supercapacitor electrode (NC700) possessed high specific surface area (533 $m^2\ g^{-1}$) and ultrahigh nitrogen content (18.06 wt%) and showed high capacitance of 306 F $g^{-1}$ at 0.5 A $g^{-1}$ and 96.6% capacitance retention after 10,000 cycles at 3 A $g^{-1}$ [207], whereas PC-2BET has high surface area (573 $m^2\ g^{-1}$) and total pore volume (1.001 $cm^3\ g^{-1}$) delivered specific capacitance (254 F $g^{-1}$ at a current density of 2 A $g^{-1}$) [210].

### 3.1.3. Fuel cells

Fuel cells have been described as an ideal primary energy conversion device due to high energy density and are applied where an assured electrical supply is required for power generation, and distribution in uninterruptible way. Porous carbon materials are used for the fuel cell applications owing to their outstanding features of inertness, high mechanical stability, low cost, integrated carbon framework and high conductivity along with high surface area. Therefore, in this section, we outlined the templated nanoporous carbons applications in fuel cells in Table 4 and narrated the summaries below. Liu et al. [211] used impregnation-reduction method used to synthesize $Pd_xZn$/NPC catalyst via $Zn_4O$(1,4-benzenedicarboxylate)$_3$. The $Pd_2Zn$/NPC anode material has high specific surface area, pore volume, power density of 103.93 $mWcm^{-2}$ and test residual current density of 27.24 mA $cm^{-2}$ after 1000 s. The synthesis of 3D N- and O- codoped nanoporous carbon nanospheres (3D NOCS) by pyrolysis using nanosilica nanoparticle possess large amount of nanopores and high specific surface area. The direct methanol fuel cell's cathode electrocatalyst (3D NOCS-900) has power density of 20 $mWcm^{-2}$ at 15 °C [212].

**Table 4**
Templates and properties of templated porous nano carbons for fuel cells.

| Template | Preferred properties | Ref. |
|---|---|---|
| $Zn_4O$(1,4-benzenedicarboxylate)$_3$ | High specific surface area and pore volume | [211] |
| NanoSilica nanoparticle | Large amount of nanopores and specific surface area | [212] |
| HKUST-1 | Porous C-framework@ 700_C@Pt has ECSA of 109.52 $m^2 g_{Pt}^{-1}$ | [213] |
| sodium dodecyl sulfate | BET specific surface area of the carbon material is 180 $m^2 g^{-1}$ and total pore volume is 0.2 $cm^3 g^{-1}$ | [214] |

Wu et al. [213] reported the novel use of salt-recrystallization-fixing HKUST-1 template to synthesize porous and high-specific surface area carbon support material for proton exchange membrane fuel cells (PEMFCs). The PEMFC has maximum power density of 780 mW $cm^{-2}$ under the $H_2$/air test condition in ultra-low Pt loading (cathode 0.1 mg $cm^{-2}$). The nanoporous carbon material synthesized by sodium dodecyl sulfate surfactant templated sol-gel method has BET specific surface area of the carbon material is 180 $m^2$ $g^{-1}$ and total pore volume is 0.2 $cm^3$ $g^{-1}$ and the direct methanol fuel cells has Peak power density of 171 mW $cm^{-2}$ at 70 °C [214].

### 3.1.4. Sensors

Chemical sensor is "a small device that detects chemical interaction or process between the analyte gas and the sensor device, transforms chemical or biochemical information of a quantitative or qualitative type into an analytically useful signal". On the other hand, biosensor can be defined as a sensor that use biomolecule and/or structure to measure things with biological significance or bioactivity [215,216]. Biosensors measure biomolecules of concern and the chemical sensors measure chemical or molecular target. The biosensors are subsection of chemical sensors because the transduction methods (sensor platforms) are the same as those for chemical sensors [217]. It is of great importance that the sensors' materials should be highly sensitive and selective. Consequently, as discussed below (and outlined in Table 5) functionalized nanoporous materials have attracted great interest due to their high sensitivity and selectivity [218].

1D N-doped C/$TiO_2$ nanotube arrays has been synthesized using catalyst-free carbonization of polydopamine coating on $TiO_2$ NTAs template. The N-doped C/$TiO_2$ NTAs electrode has very high electrochemical activity because of its large surface area, high electron transfer pathway and high density of exposed edge plane sites. In case of Fe $(CN)_6^{3-/4-}$ redox couple, the heterogeneous charge transfer rate constants $k^0$ is greater than 0.5 cm/s. Determination of ascorbic acid, dopamine and uric acid at once, has been demonstrated with the linear ranges of 100–3000 μM, 5–50 μM and 0.1–150 μM respectively and detection limits (S/N = 3) of 1.8 μM, 0.015 μM and 0.11 μM, respectively [219]. Jia et al. [220] developed a simple approach of crystallinity, nanostructure engineering, and pyrolysis for the fabrication of well-defined Ni nanoparticle embedded on nanoporous carbon nanorods (Ni/NCNs) using 3D Ni-MOF template. The Ni/NCNs-500/GCE displays outstanding anti-interference, sensitivity and selectivity. Furthermore, it exhibits a wide linear range, low limit of detection, and fast response time due to the Ni/NCNs-500 high surface area and pore volume of 124.1 $m^2$ $g^{-1}$ and 0.2889 $cm^3$ $g^{-1}$ respectively.

Recently, Wang [221] used of EDA-assisted self-assembly between 3-aminophenol/formaldehyde resin and silica templates as a facile approach for the synthesis of N-doped mesoporous carbon spheres (MNCS/GCE). The MNCS/GCE has high sensitivity and good selectivity for the detection of ascorbic acid, dopamine and uric acid down to low detection limits (S/N = 3) of 5.39 μM, 0.17 μM and 0.34 μM, respectively. It also has good stability and great anti-interference towards some common compounds in body fluid. An OMC was synthesized by applying a soft template method [222]. The synthesized OMC has mesoporous structure, BET surface area 448.861 $m^2$ $g^{-1}$, large number of defect sites and high degree of graphitization. The OMC/GC electrode has detection limit of 0.186 μM (at S/N = 3) and a linear response over wide concentration ranges of aristolochic acids (0.6–10 μM and 10–50 μM), with sensitivities of − 1.77 and − 0.31 μA/μM, respectively. The electrode showed good selectivity, reproducibility, and stability [218]. Wang et al. [224] reported the fabrication of Co/$Co_3O_4$ nanoparticles (NPs) coupled with hollow nanoporous carbon polyhedrons Co/$Co_3O_4$ @HNCP) by the engineering of polydopamine@zeolitic imidazolate framework-67 (PDA@ZIF-67) template, pyrolysis and oxidation processes. The synthesized carbon material has ordered nanoporous structure, abundant active sites and favorable interface properties. The electrochemical results revealed that the electrode has low detection limit of 0.0083 μM (S/N = 3), a persistent anti-interference ability, and satisfactory stability. Chen et al. [225] use of ZIF-8 as self-template to synthesize (ZIF-8 @rGO) and (ZIF-8 C@rGO) by in-situ growth of ZIF-8 on graphite oxide (GO) and simultaneous carbonization/reduction. The material has high graphitization and surface area of about 983.6 $m^2g^{-1}$. The total pore volume is about 0.92 $cm^3$ $g^{-1}$. The ZIF-8 C@rGO based sensor has a wide linear range of 0.5–70 μM for both hydroquinone (HQ) and catechol (CC), with low detection limits of 0.073 and 0.076 μM for HQ and CC respectively. Sun et al. [226] fabrication of a simple and valuable molecularly imprinted electrochemical sensor by electropolymerizing molecularly imprinted polymer (MIP) layer on the nanoporous carbon (NC) modified electrode using calycosin as template. The sensor has excellent reproducibility, stability, selectivity and sensitivity due to the electrode material's large surface area and increased binding sites. Also, the sensor has linear range of $4.20 \times 10^{-7}$ to $1.29 \times 10^{-4}$ mol $L^{-1}$ with the detection limit of $8.5 \times 10^{-8}$ mol $L^{-1}$. The use of an easy, economic, and rapid process for the synthesis of free-standing, partially aligned Ag NP-impregnated porous carbon nanofibers using nanoporous CNFs was demonstrated by Mondal et al. [227]. The AgCNFs bioelectrode has high sensitivity (1.232 μAmg/$dL^{-1}cm^{-2}$) over a wide detection range (25–500 mg $dL^{-1}$), outstanding selectivity, good reproducibility, and faster response (10 s). The immobilization of Glucose oxidase (GOD) on a hierarchical nanoporous carbon with rich functional groups by carbonizing a biomass derivation extracted from green tree leaves on a nanostructured $CaCO_3$ template at high temperature produced sensor material with larger nanopores and high BET surface area. The quasi-reversible surface-controlled process sensor is highly sensitive and selective with an outstanding electrocatalytic activity and suppression of interferences [228]. Regiart et al. [230] reported the use of silica SBA-15 type to synthesize ordered mesoporous carbon (CMK-3/CH) electrochemical sensor electrode for the detection of triclosan in river water samples. The electrode material has high specific surface area (1125 $m^2$ $g^{-1}$), large pore volume (1.16 $cm^3$ $g^{-1}$), uniform mesostructure (4.4 nm). The CMK-3/CH sensor has excellent extraction selectivity, detection limit of 0.24 ng $mL^{-1}$ with wide linear range from 0.8 ng $mL^{-1}$ to 40 ng $mL^{-1}$.

**Table 5**
Templates and properties of templated porous nano carbons for electrochemical sensors.

| Template | Preferred properties | Ref. |
|---|---|---|
| $TiO_2$ NTAs | Large surface area, high electron transfer pathway and high density of exposed edge plane sites | [219] |
| 3D Ni-MOF | The Ni/NCNs-500 has high surface area and pore volume of 124.1 $m^2$ $g^{-1}$ and 0.2889 $cm^3$ $g^{-1}$ respectively | [220] |
| 3-aminophenol/ formaldehyde and silica | High nitrogen (8.21 at%) and surface areas (1149 $m^2$ $g^{-1}$) | [221] |
| Soft | Mesoporous structure, BET surface area 448.861 $m^2$ $g^{-1}$, large number of defect sites and high degree of graphitization | [222] |
| MgO | Macrostructure, high specific surface area and large pore sizes (100–200 nm) | [223] |
| PDA@ZIF-67 | Ordered nanoporous structure, abundant active sites and favorable interface properties | [224] |
| Self-templated ZIF-8 C | High graphitization and surface area of about 983.6 $m^2$ $g^{-1}$. The total pore volume is about 0.92 $cm^3$ $g^{-1}$ | [225] |
| Calycosin | Large surface area and increased binding sites | [226] |
| Nanoporous CNFs | High graphitization, total BET surface area and pore volume are 91.39 $m^2$ $g^{-1}$ and $6.49 \times 10^{-2}$ cc $g^{-1}$, respectively | [227] |
| Nanostructured $CaCO_3$ | Larger nanopores and high BET surface area | [228] |
| ZnO naoparticles | PC-30 samples possess larger surface area and higher pore volume | [229] |
| Silica SBA-15 type | High specific surface area (1125 $m^2$ $g^{-1}$), large pore volume (1.16 $cm^3$ $g^{-1}$), uniform mesopore structure (4.4 nm) | [230] |

#### 3.1.5. Hydrogen and carbon dioxide storage

The geometry optimizations and energy calculations on boron substitution on zeolite templated carbon vacancy, and the covering of sites with lithium, sodium, and calcium atoms were carried out. Herein it was revealed that boron substitution on zeolite templated carbon vacancy decorated with three sodium atoms can adsorb up to fifteen hydrogen molecules (5 hydrogen molecules per sodium atom), which gave a gravimetric storage capacity of 6.55% wt., which is sufficient for meeting Department of Energy's (DOE) gravimetric targets. In addition, the average binding energies and adsorption energies were calculated in the range 0.2298–0.2144 eV/$H_2$, which constitute desirable energies for hydrogen adsorption [231]. Silica gel templated carbons were produced at 650 ℃ and a dwelling time of 3 h where furfuryl alcohol acts as carbon precursor. This material demonstrated hydrogen uptake up to 0.16 wt% at adsorption temperature of − 100 ℃ [33]. KOH-activated ZIF templated carbons store up to 6.2 wt% $H_2$ at − 196 ℃ and pressure of 20 bar. In addition, the $CO_2$ uptake up to 2.4 mmol/g (at 25 ℃ and 1 bar) and exceptional storage density up to 4.5 μmol/$m^2$ was achieved [47]. As described in the Section 2.2.2 or this review, the zeolite template carbons were prepared using zeolite 13X as a hard template. These carbons demonstrated remarkable hydrogen uptake of 7.3 wt% at 20 bar and 77 K. This report also explores the mechanical stability of the ZTCs via compaction at up to 10 t (equivalent to 740 MPa) in which the compacted samples showed negligible changes and maintained high hydrogen storage capacity [43].

### 3.2. Catalysis

Carbon materials based catalysts which possess hierarchical pore structure are ideal for loading of heteroatom to lower the thermodynamic barrier, increase the adsorption properties and be employed as catasts for various chemical and electrochemical processes.

#### 3.2.1. Electrocatalysis

Iron-nitrogen-doped mesoporous carbon microspheres (Fe-NMCSs) obtained using mesoporous ferroferric oxide ($Fe_3O_4$) microspheres were employed as multifunctional template–mesoporous structure-directing agent [38]. These materials as electrocatalysts exhibited an onset potential of 1.027 V with a half-wave potential ($E_{1/2}$) of 0.86 V. These values are even better than for the commercial Pt/C catalyst. Nitrogen and phosphorus dual-doped carbon catalysts prepared through the graphitic carbon nitride (g-$C_3N_4$) self-templating method exhibited a high ORR performance. The dual-doping of nitrogen and phosphorus shows a synergistic effect that could greatly improve the content of graphic nitrogen and hence improve the overall catalyst activity. Specifically, for the potential values more relevant to ORR on non-noble metal catalysts (e.g., 1.23 V), while both catalysts show a rate determining step as the *OH to $H_2O$, the nitrogen-phosphorus co-doped carbon only show an uphill energy at 0.36 eV. This is in comparison to the 0.52 eV for the nitrogen doped catalysts, which means the nitrogen-phosphorus co-doped catalyst requires considerably less thermodynamic barrier than simply nitrogen doped catalysts [86]. In situ templates etching method using $Fe_2O_3$ nanoparticles and citric acid serving as a carbon source and etchant allowed to prepare 3D interconnected Fe-N doped hierarchical porous carbon materials which displayed excellent catalytic ORR performance with a positive half-wave potential (0.85 V), efficient four-electron reaction and excellent durability, which are superior to those of Pt/C (20 wt%) catalyst [24].

As described earlier in Section 2.5.2, a phytic acid-assisted self-templating strategy was implemented to fabricate nitrogen-phosphorus-iron tridoped carbon with a hierarchical pores which was then used as non-precious metal yet very efficient and stable for ORR. Sophisticated porous structure and well-designed multi-atoms co-doping condition impart final catalysts with enhanced mass transfer ability and abundantly available active-sites that ensures high catalytic performance for ORR. Here, the half wave potential of the optimal catalyst is 0.926 V (vs. RHE), which is 40 mV higher than the state-of-art platinum based catalyst and better than most reported ORR catalysts. When this catalyst was applied in a primary Zn–$O_2$ battery, it outperformed the commercial Pt/C catalyst whether on specific capacity or power density [88]. Ordered mesoporous carbon synthesized by hard template method using sacrificial silica template (SBA-15) was used to evaluate the electrocatalytic ORR activity which had an onset potential of 0.83 V vs RHE, current density of 3.3 mA $cm^{-2}$, Tafel slope of 83 mV $dec^{-1}$, and 2.4 electron transfer number per oxygen molecule. Eventually, a very low charge transfer resistance value $R_{ct}$ (16.6 Ω $cm^{-2}$) was observed for ORR in 0.1 M KOH medium [37]. Templated micro-mesoporous material obtained from adenine and a mixture of NaCl/$ZnCl_2$ displayed a high selectivity in oxygen reduction reaction toward the favored four electron process and showed an outstanding $E_{1/2}$ of ≈ 880 mV (vs RHE) [98].

#### 3.2.2. Homogeneous and heterogeneous catalysis

Highly ordered uniform porous carbons were synthesized by using removable colloidal silica crystalline templates and were used as a catalyst supporter for improved catalytic activity towards methanol oxidation in a fuel cell [232]. In this type of template, the acid catalyst sites were used for the polymerization of phenol and formaldehyde as a carbon precursor and the resulting material demonstrated a BET surface of 706 $m^2$ $g^{-1}$ and catalytic activity of 15% for methanol oxidation. Similarly, carbons with large pore were synthesized by using aggregates of polystyrene spheres in silica particles and then were employed for efficient methanol oxidation in fuel cell with improved performance owing to the high surface area and facile fuel and product diffusion properties [233]. As the surface functionalization of porous carbons is an effective strategy to enhance the catalytic acitivty [234], mesoporous carbons with functionalized active groups such as –$SO_3H$ for the esterification of oleic acid showed that the reactivity of the carbon-based catalysts is dependent on the total acidity, presenting a viable way for the biodiesel production [235]. Metal organic framework inspired catalysts were prepared by the ZnO nanoparticles trapped in the porous carbon followed by moderate oxidation treatment with the resulting catalyst exhibiting excellent activity for carbon dioxide cycloaddition reaction with epoxides [236]. Furthermore, ecofriendly preparation of nitrogen doped ordered carbons via self-template method has been proposed as effective catalysts for hydrogenation of nitroarenes and Knoevenagel condensation of aromatic aldehyde derivatives in aqueous solution [237]. MgO-templated carbons have been used for enzymatic oxidation of hydrogen and controlling the pore size has demonstrated great effect on catalytic activity [238]. It was shown that the pore size larger than the enzyme size favors high enzyme loading and improves the stability and activity for hydrogen oxidation. In another work, cobalt nitride-based porous hollow nanocages were successfully synthesized and used as heterogeneous catalyst for the reduction of 4-nitrophenol and methylene blue with a conversion ratio up to 90% [239].

#### 3.2.3. Photocatalysis

Adsorption of organic species is enhanced in the ordered pores of carbon, for this purpose, the performance (methylene blue degradation activity) of zeolite templated carbon and activated carbon was compared by preparing composite of each with $TiO_2$. The performance of templated material was found to be ~13 times higher than the simple activated carbon [240]. Various strategies have been explored to improve the performance graphitic carbon nitrides for the photocatalytic hydrogen production [241]. Among them, the soft templating appears to be quite attractive where a so-called worm-like structures mesoporous graphitic carbon nitride was produced via soft-templating of P123 surfactant with an overall quantum efficiency of 1.8% [242]. A metal free photocatalyst for hydrogen production by the in situ pyrolysis of Ni-based benzenedicarboxylic acid which demonstrated about 22 times higher activity as compared to pristine graphitic carbon nitride [243]. The high performance is attributed to the enhanced charge transfer and efficient separation of the photo-generated electrons

through the highly conductive carbon. In a novel strategy, activated carbon was used as template to synthesize sintered crystalline nanoparticles of Mesoporous $Ta_2O_5$ and $NaTaO_3$ which exhibited high photocatalytic activity for water splitting [244]. Certainly, the modification of synthetic routes and functionalization of graphitic carbon nitrides have been found as effective ways to improve their photocatalytic activity which involve the tuning of structure and surface properties [245–248].

### 3.3. Immobilized compounds and confinement effect (proteins, liquids and gases)

Adsorption of biomolecules on solid carbon support is generally considered an attractive area of active research in medicine, biotechnology and food processing. Porous carbons have been used to immobilize proteins, vitamins and enzymes [249–251]. Since the high pore volume and large surface of porous carbons favor such adsorption of large molecules, the tuning of these carbon parameters greatly influences the performance. In general, filteration method is used for immobilizing large molecules, however, recently magnetically separable mesoporous carbon have performed well due to the absence any complex formation [252]. In particular, the magnetic composites of mesoporous carbons have exhibited bimodal pore systems and large immobilization capacities for cytochrome c and lysozyme. Further, the well-known hard templating approach was used to synthesize mesoporous carbon spheres with controlled porous structure and particle size to improve the adsorption capacity of α-Chymotrypsin (Chy) in solution [253]. With these carbon materials, adsorption capacities of up to 1100 mg $g^{-1}$ were achieved compared to only 232 mg $g^{-1}$ for carbon aerogels and 147 mg $g^{-1}$ for SBA-15. Metal organic framework derived carbons were synthesized for the successful immobilization of acetylcholinesterase. In particular, the lanthanum containing MOF showed more active sites of multi-contents to increase the immobilization capability and facilitated the accessibility of electron transfer in order to shorten their diffusion length on the electrode surface [254]. Overall, the lanthanum based MOF demonstrated wide range of $1.0 \times 10^{-13}$–$5.0 \times 10^{-9}$ g $mL^{-1}$ and the low detection limit of $5.8 \times 10^{-14}$ g $mL^{-1}$. Templated carbons possessing pore in the range of 7.0–9.0 nm have been synthesized and the effects of confinement within the pores on the melting point depression of ionic liquids have been studied. It was found that the interactions between the ions and the pore walls constrained the molecular motions and resulted in a glass transition upon heating [255]. Such an interaction of pores with ionic liquid lead to the extension of liquid state at low temperatures. Confinement effects on water in zeolite templated carbons showed that the water freezes into a low-density amorphous ice with a glass transition at around − 123 °C [256]. Furthermore, this work proved the effectiveness of templated carbons to be ideal material for studying various properties of supercooled water.

### 3.4. Biomedical applications

Porous carbons possess unique ability to effectively adsorb organic compounds for longer time with nearly unmatched inertness. These properties helps to retain various compounds under challenging environments to minimize contamination issues [257,258].

#### 3.4.1. Drug delivery

A wide range of carbon materials with ordered structure have been used for drug delivery in targeted locations [259]. CMK-1 type mesoporous carbon nanoparticle which were synthesized by using template of MCM-48 type mesoporous silica nanoparticle were used for the delivery of chemicals with membrane impermeable characteristics inside of eukaryotic cells. The cellular biocompatibility of these carbons were found to be quite high with an inhibitory concentration ($IC_{50}$) in the range of 50 μg/mL per million cells [260]. Carbon nanospheres have been used as hard template along with cetyltrimethylammonium bromide (CTAB) as a soft template in combined facile soft–hard template route to prepare nanoporous materials for the biocompatibility and delivery of doxorubicin hydrochloride (DOX) and Cytochrome c (Cyt c) as the model drug and protein, respectively [261]. Similarly, structured nanoporous carbons and functionalized carbons with pores in the range of 3.5–4.0 nm have proved to be effective for drug delivery [262–264]. Pore structure was tailored in soft-templated carbons to study the effects on diffusion for the model drugs captopril, furosemide, and ranitidine hydrochloride and the diffusivity values were calculated as being of order $10^{-22}$-$10^{-24}$ $m^2$ $s^{-1}$ [265]. Nanoporous carbons with surface area around 1200 $m^2$ $g^{-1}$ derived from MOFs have been investigated for studying the loading capacity and release behavior of a chemotherapeutic drug cisplatin [266]. Furthermore, the use of inorganic compounds and metallic composites with carbons as composites have opened up new areas for studying targeted drug delivery related parameters [267,268].

#### 3.4.2. Entero- and hemosorbents

Enterosorbents include activated carbons or charcoals that can be included in diet as facile material to treat toxin. The presence of micropores in materials such as Enterosgel enables them to adsorb and retain small molecules within the micropores and larger toxins in the mesopores [269]. New material such as clay-based enterosorbents that can reduce toxin exposures when included in the diet. In a model investigation, toxin-sensitive living organism (*Hydra vulgaris*) was used to predict the efficacy and safety of newly developed sorbents [270]. Based on these new research directions, innovative templated methods possess great potential for the structuring of nanocarbons which would facilitates the administration and delivery at targeted location [271].

### 3.5. Environmental application

#### 3.5.1. Adsorbents

The phenol adsorption capacity of sewage sludge-based mesoporous carbons synthesized using anionic polyacrylamide ($PAM^-$) as flocculant is relatively large (~132 mg $g^{-1}$), and the mesoporous structure plays a certain role in phenol adsorption, while the high content of amide group and p-p interactions play a major role in the adsorption process [85]. Micro-mesoporous materials obtained by a mechanosynthetic strategy using palm oil cooking waste as carbon source incorporated into the SBA-15 hard template demonstrated adsorption capacity of methylene blue at around 40 mg $g^{-1}$ [35]. KOH-activated diatomite-templated carbons possessed larger methylene blue adsorption capacity (the maximum Langmuir adsorption capacity: 645.2 mg $g^{-1}$) than those of the original carbons and $CO_2$-activated carbons [44]. Hierarchical porous carbon prepared from heavy residue of waste tire derived pyrolytic oil and magnesium acetate powder exhibited best adsorption capacity (843.5 mg $g^{-1}$) at 298 K for methylene blue. Furthermore, the effect of pH and temperature on adsorption capacity of prepared porous carbon were also investigated [95].

#### 3.5.2. Wastewater treatment

Ordered mesoporous carbons have been produced by using template method possessing 2D hexagonal mesostructure with high surface areas, large pore volumes ranging from 0.51 to 2.16 $cm^3$ $g^{-1}$ and uniform pore sizes between 4.5 and 6.4 nm. Then these carbons were used for investigating the adsorption behavior of bulky basic dyes. It was found that the carbons with hierarchical porosity and surface area around 2600 $m^2$ $g^{-1}$ showed the highest retention of methylthionine chloride, fuchsin basic, rhodamine B, brilliant yellow, methyl orange, or Sudan G [272]. On the other hand, zeolite-templated carbon was found to be an excellent adsorbent for the removal of monoaromatic compounds such as phenol, 1,3-dichlorobenzene, and 1,3-dinitrobenzene [273], where the interconnected three-dimensional pore structure helps to retain these compounds for longer time. A mesoporous carbon was synthesized by

using alumina-templated strategy with a high surface area of ~1100 $m^2$ $g^{-1}$ to remove rhodamine B (RhB) and the obtained data showed high equilibrium adsorption amount of 374.3 mg $g^{-1}$ and fast adsorption rate for RhB at 317.8 mg $g^{-1}$ within 5 min [274]. Removal of cationic dyes and organic pollutants from aqueous solutions have been investigated by using carbons with hierarchical porosity where the pore structure of tuned size and surface play a key role for the efficient adsorption and retention of organic compounds [146,275]. The adsorption and removal of methylchlorophenoxypropionic acid (a well-known herbicide compound) has been studied in aqueous solution over MOF-polymer derived monoliths which showed a high adsorption capacity of 34.33 mg $g^{-1}$ and retained it for long time [276]. Graphitic carbon nitride (g-$C_3N_4$) hybrid aerogels have been prepared by using eco-friendly materials such as carboxymethyl cellulose, and β-cyclodextrin and it was used for the successful removal of Rhodamine B (Rh B) up to 97.99% in 90 min [277].

### 3.5.3. Food and beverages

Zeolitic imidazole framework (ZIF-67) has been used both as carbon source and a precursor for the synthesis of ordered mesoporous carbon for the extraction of flunitrazepam from beverage samples [278] and it showed an excellent stability after using for several cycles.

### 3.5.4. Miscellaneous

Nitrogen-oxygen co-doped mesoporous carbons obtained using self-activation strategy by synergistic effect of dicyandiamide and zinc gluconate were implemented to realize helical spring-like triboelectric nanogenerators (HS-TENGs). Considering the construction of self-powered electrochemical system with energy-efficient perspective, a series of flexible and shape-adaptive printed HS-TENGs were fabricated as electric supply (see Fig. 22). In such system, typical printed rectangular HSTENG possessed a short-circuit current of 700 μA, open-circuit voltage of 1500 V, transfer charge of 2.5 μC and high output power density of 2.1 W $m^{-2}$. Such integrated system delivered the accessible electro-Fenton degradation efficiencies of 98.2% and 97.3% for malachite green and methylene blue in 80 min with good reusability, satisfying the environmentally friendly electro-Fenton degradation system [87].

Templated carbon prepared via the catalyst-free method of producing 1D N-doped carbon coated $TiO_2$ nanotube arrays (N-doped C/$TiO_2$

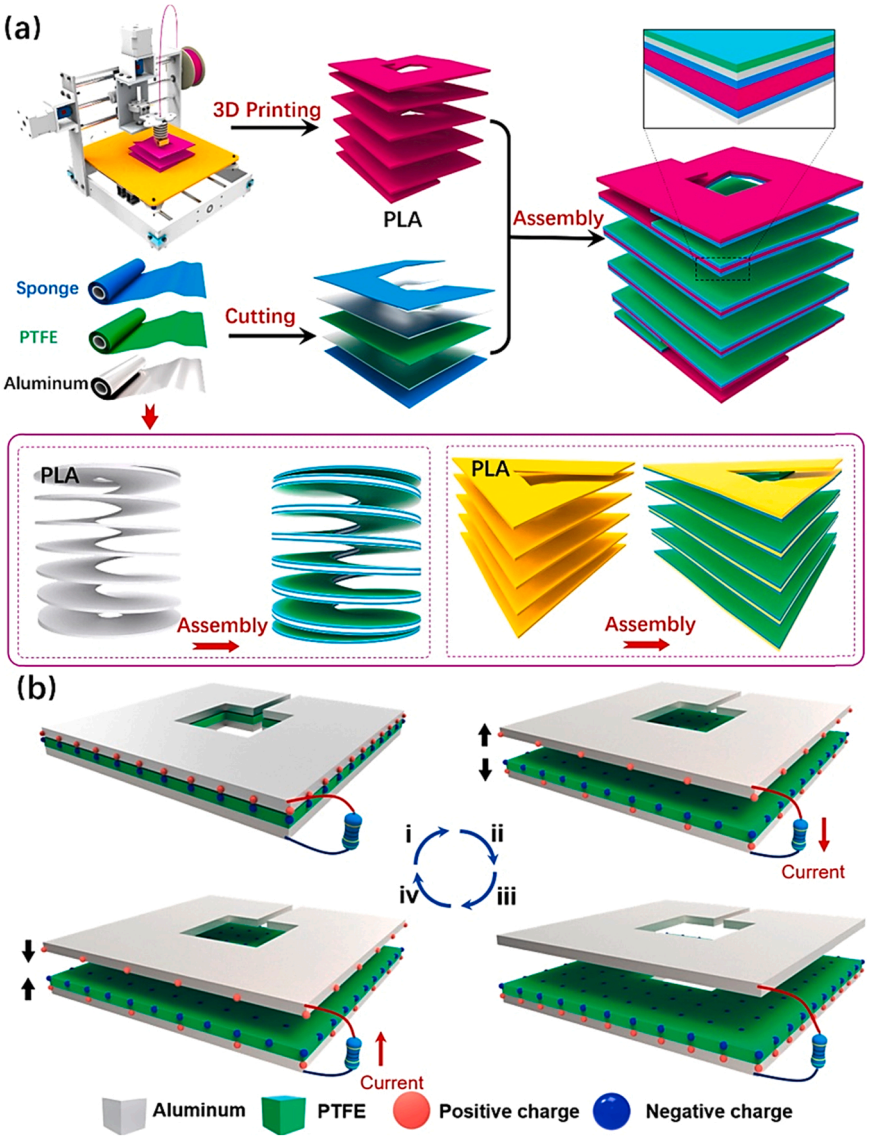


**Fig. 22.** The fabrication and assembly process of the printed helical spring-like triboelectric nanogenerators. The substrates are prepared by 3D printer where aluminum foils, PTFE films and sponges are cut into desired shapes and assembled on the substrate respectively, while the PTFE films and aluminum foils are placed face to face, (b) The charge transfer mechanism. Reproduced with permission [87].

NTAs) by template carbonization of polydopamine nanofilm coated anodized $TiO_2$ NTAs were implemented as electrochemical sensors. Herein the electrochemical sensors based on the N-doped C/$TiO_2$ NTAs electrode showed high electrochemical activity with the heterogeneous charge transfer rate constants $k^0$ greater than 0.5 cm/s for $Fe(CN)_6^{3-/4-}$ redox couple. It also showed the determination of ascorbic acid, dopamine and uric acid with the linear ranges of 100–3000 μM, 5–50 μM and 0.1–150 μM, respectively with detection limits (S/N = 3) of 1.8 μM, 0.015 μM and 0.11 μM, respectively [22].

## 4. Summary and future outlook

Templated porous carbons owing to their defined size and geometry of pores and surface properties, give excellent control and precision in many applications of science and technology including adsorption, wastewater treatment, energy storage, catalysis and biotechnology. There is still a quest for the development of new methodologies to synthesize low cost, eco-friendly and chemically inert TPCs with unique pore structure. In recent years, apart from classical one route procedure, new strategies coupling more than one preparation method have achieved a lot of research interest that also lead to the selection of easily available raw materials and energy saving synthetic processes. In particular, the use of waste materials as precursor would be ideal approach which compensate relatively high cost of template and adds ecofriendliness to the process. Furthermore, new trend towards biomaterials as precursor from marine and plant origin appear to be promising. It would be interesting to look into more localized functionalization of the templated carbons for the catalysis applications in order to firstly load a fixed amount of materials and then to distribute properly at defined reaction sites. In this regard, more research effort are required to investigate the diffusion properties and surface functional groups of these materials. In addition the selection of a specific template is very important which would give a first-hand information about the reactivity and transport behavior within the carbon pores. Some of the newly emerging fields such as templated carbons applications in photocatalysis need more research attention in order to explore different type of materials as well as behavior of carbons as effective carriers to provide efficient reaction sites. Enterosorbent and homosorbent is another important area where templated carbons could be applied and so far, not much literature is available. Recently, templated carbons applications in the field of sensors have seen a great increase and it would define the future applications in this direction which are expected to rise. One drawback with the use of hierarchical carbons in energy storage field is the low volumetric energy which can be overcome by a combination of various approaches. In this regard, the use of redox species impregnation (loading redox species into the desired pore volume) could be an effective method leading to the improvement of energy density, since the redox active materials such as bromine or iodine would fill the pores of templated carbons to be used as redox electrode in batteries and hybrid energy storage. Similarly, confinement of redox species in carbons of defined pores would also improve the energy density and cycle life of batteries. Further work is needed in designing of new carbons where proteins, ionic liquids, organo-aqueous mixtures and various medicines could be effectively adsorbed. In order to harness the great advantage of template carbons which is the ability to tune the pore diameter via controlled template thickness would result in larger payload capacities. Templated graphitic carbon nitride and carbon nanotubes are a rising trend in the field of materials science. The main advantage is that template synthesized nanotubes can be differentially functionalized on their inner and outer surfaces. This possibility of nanotubes modification is useful in drug extraction, antibody–antigen interactions and magnetization is discussed. Certainly, looking at the recent progress in carbons with hierarchical porosity, new materials with unique properties could be expected in near future which would galvanize the research in materials science and engineering and related fields.

## Declaration of Competing Interest

The authors declare no conflict of interest.

## Data Availability

The data will be made available upon reasonable request to the corresponding authors.

## Acknowledgments

Q.A. thanks The Austrian Research Promotion Agency (FFG) Austria for providing funds for the project number 39966764. V.P. acknowledges the funding from the Ministry of Education and Science of the Republic of Kazakhstan (Grant no. AP09259890). Q.A. and V.P. thank the Austrian Agency for International Cooperation in Education and Research (OeAD-GmbH) Austria for awarding mobility funds in EPU-Projekt Call 2019. This work was partially supported by Ministry of Education and Science Poland under the PUT research grant 0912/SBAD/2206 (S.Ż.). This work was also financed and prepared as part of a research project supported by the National Science Centre Poland, no. 2017/27/B/ST8/01506 (T.J.). A.B.H. and K.I.O. thank the South Africa's Research Chair Initiative, DSI/NRF/Wits SARChI Chair in Materials Electrochemistry and Energy Technologies (MEET) (Grant No. 132739), for supporting the prepararion of this study.

## References

[1] K.S.W. Sing, D.H. Everett, R.A.W. Haul, L. Moscou, R.A. Pierotti, J. Rouquerol, et al., Pure Appl. Chem. 57 (1985) 603.
[2] R.E. Franklin, Proc. R. Soc. Lond. Ser. A Math. Phys. Sci. 209 (1951) 196–218.
[3] H.F. Stoeckli, F. Kraehenbuehl, Carbon 22 (1984) 297–299.
[4] P.J.F. Harris, Int. Mater. Rev. 42 (1997) 206–218.
[5] M. Inagaki, M. Toyoda, Y. Soneda, S. Tsujimura, T. Morishita, Carbon 107 (2016) 448–473.
[6] T. Morishita, T. Tsumura, M. Toyoda, J. Przepiórski, A.W. Morawski, H. Konno, et al., Carbon 48 (2010) 2690–2707.
[7] T. Kyotani, Bull. Chem. Soc. Jpn. 79 (2006) 1322–1337.
[8] D.S. Su, G. Centi, J. Energy Chem. 22 (2013) 151–173.
[9] M. Inagaki, H. Orikasa, T. Morishita, RSC Adv. 1 (2011) 1620–1640.
[10] T. Kyotani, N. Sonobe, A. Tomita, Nature 331 (1988) 331–333.
[11] J.H. Knox, K.K. Unger, H. Mueller, J. Liq. Chromatogr. 6 (1983) 1–36.
[12] V. Malgras, J. Tang, J. Wang, J. Kim, N.L. Torad, S. Dutta, et al., J. Nanosci. Nanotechnol. 19 (2019) 3673–3685.
[13] L. Kong, M. Liu, Z. Diao, D. Chen, X. Chang, Y. Xiong, Sci. Rep. 6 (2016) 1–9.
[14] B. Sakintuna, Y. Yürüm, Ind. Eng. Chem. Res. 44 (2005) 2893–2902.
[15] N. Sonobe, T. Kyotani, A. Tomita, Carbon 26 (1988) 573–578.
[16] K. Putyera, T.J. Bandosz, J. Jagieo, J.A. Schwarz, Carbon 34 (1996) 1559–1567.
[17] N. Sonobe, T. Kyotani, A. Tomita, Carbon 29 (1991) 61–67.
[18] A.A. Zakhidov, R.H. Baughman, Z. Iqbal, C. Cui, I. Khayrullin, S.O. Dantas, et al., Science 282 (1998) 897–901.
[19] N. Diez, M. Sevilla, A.B. Fuertes, Carbon 178 (2021) 451–476.
[20] Q. Fang, W. Zhang, X. Chen, Y. Zhang, M. Hu, Chin. Chem. Lett. 31 (2020) 303–306.
[21] L. Wang, K. Qin, J. Li, N. Zhao, C. Shi, L. Ma, et al., Appl. Surf. Sci. 427 (2018) 598–604.
[22] J. Zheng, M. Zhang, T. Miao, J. Yang, J. Xu, N.S. Alharbi, et al., Mater. Chem. Front. 3 (2019) 224–232.
[23] H. Liu, Z. Feng, J. Wang, J. Diao, D. Su, New Carbon Mater. 31 (2016) 87–91.
[24] P. Tian, J. Zang, S. Song, S. Zhou, H. Gao, H. Xu, et al., J. Power Sources 448 (2020), 227443.
[25] K. Qin, J. Kang, J. Li, C. Shi, Y. Li, Z. Qiao, et al., ACS Nano 9 (2015) 481–487.
[26] K. Qin, E. Liu, J. Li, J. Kang, C. Shi, C. He, et al., Adv. Energy Mater. 6 (2016), 1600755.
[27] S. Drieschner, M. Weber, J. Wohlketzetter, J. Vieten, E. Makrygiannis, B. M. Blaschke, et al., 2D Mater. 3 (2016) 45013.
[28] K. Kraiwattanawong, Eur. Polym. J. 130 (2020), 109678.
[29] X. Zheng, X. Liu, X. Yang, A. Fu, Y. Li, Y.-G. Guo, et al., Colloids Surf. A Physicochem. Eng. Asp. 610 (2021), 125740.
[30] J.W. Yu, Y.-M. Choi, J. Jung, N.-H. You, D.S. Lee, J.-K. Lee, et al., Synth. Met. 211 (2016) 35–39.
[31] Q. Meng, K. Qin, L. Ma, C. He, E. Liu, F. He, et al., ACS Appl. Mater. Interfaces 9 (2017) 30832–30839.
[32] F. Barzegar, V. Pavlenko, M. Zahid, A. Bello, X. Xia, N. Manyala, et al., ACS Appl. Energy Mater. 4 (2021) 1763–1773.
[33] R.J. Konwar, M. De, J. Anal. Appl. Pyrolysis 107 (2014) 224–232.

[34] S. Inagaki, T. Nakao, T. Miki, N. Kuroda, Y. Kubota, Microporous Mesoporous Mater. 241 (2017) 123–131.
[35] R.A.L. Sobrinho, G.R.S. Andrade, L.P. Costa, M.J.B. de Souza, A.M.G.P. de Souza, I.F. Gimenez, J. Hazard. Mater. 362 (2019) 53–61.
[36] S. Ungureanu, M. Birot, H. Deleuze, V. Schmitt, N. Mano, R. Backov, Carbon 91 (2015) 311–320.
[37] P. Janus, R. Janus, B. Dudek, M. Drozdek, A. Silvestre-Albero, F. Rodríguez-Reinoso, et al., Microporous Mesoporous Mater. 299 (2020), 110118.
[38] V. Duraisamy, K. Selvakumar, R. Krishnan, S.M.S. Kumar, ChemistrySelect 4 (2019) 2463–2474.
[39] F. Meng, Z. Wang, H. Zhong, J. Wang, J. Yan, X. Zhang, Adv. Mater. 28 (2016) 7948–7955.
[40] V. Mashindi, P. Mente, N. Mpofu, T.N. Phaahlamohlaka, O. Makgae, A. I. Kirkland, et al., J. Appl. Electrochem. (2021) 1–18.
[41] V. Pavlenko, S. Kalybekkyzy, D. Knez, Q. Abbas, Z. Mansurov, Bakenov Zh, et al., Ionics (2021), https://doi.org/10.1007/s11581-021-04354-w.
[42] T. Aumond, J. Rousseau, Y. Pouilloux, L. Pinard, A. Sachse, Carbon Trends 2 (2021), 100014.
[43] M.J. Valero-Romero, E.M. Márquez-Franco, J. Bedia, J. Rodríguez-Mirasol, T. Cordero, Microporous Mesoporous Mater. 196 (2014) 68–78.
[44] E. Masika, R. Mokaya, Prog. Nat. Sci. Mater. Int. 23 (2013) 308–316.
[45] D. Liu, W. Yuan, L. Deng, W. Yu, H. Sun, P. Yuan, J. Colloid Interface Sci. 424 (2014) 22–26.
[46] S. Choi, H. Kim, S. Lee, Y. Wang, C. Ercan, R. Othman, et al., Chem. Eng. J. 280 (2015) 597–605.
[47] H.C. Kwon, S. Choi, Y. Wang, R. Othman, M. Choi, Microporous Mesoporous Mater. 307 (2020), 110481.
[48] P. Yang, D. Zhao, D.I. Margolese, B.F. Chmelka, G.D. Stucky, Nature 396 (1998) 152–155.
[49] D. Grosso, C. Boissière, M. Faustini, Thin film deposition techniques. The Sol-Gel Handbook: Synthesis, Characterization, and Applications, 3 Volume Set, 2015, p. 3.
[50] W. Liu, J. Qi, P. Bai, W. Zhang, L. Xu, Appl. Catal. B Environ. 272 (2020), 118974.
[51] H. Xu, Z. Shen, G. Chen, C. Yin, Y. Liu, Z. Ge, et al., Fuel 275 (2020), 118036.
[52] M. Chen, X. Hu, K. Li, J. Sun, Z. Liu, B. An, et al., Carbon 164 (2020) 111–120.
[53] A.A. Dehesa, F. Luzi, D. Puglia, E. Lizundia, I. Armentano, L. Torre, J. Phys. Chem. C 124 (2020) 14901–14910.
[54] X. Xin, Z. Wang, R. Jia, C. Gao, L. Sui, H. Dong, et al., J. Alloy. Compd. 822 (2020), 153627.
[55] Z. Dong, Z. Zhang, R. Zhou, Y. Dong, Y. Dai, X. Cao, et al., Chem. Eng. J. 386 (2020), 123944.
[56] S. Wang, L. Zhang, G. Sima, Y. Cui, L. Gan, Chem. Phys. Lett. 736 (2019), 136808.
[57] G.L. Goh, S. Agarwala, W.Y. Yeong, ACS Appl. Mater. Interfaces 11 (2019) 43719–43730.
[58] H. Li, L. Zhao, W. Zhu, X. Qu, C. Wang, R. Liu, et al., ACS Omega 4 (2019) 16209–16216.
[59] K. Zhou, W. Ma, Z. Zeng, X. Ma, X. Xu, Y. Guo, et al., Chem. Eng. J. 372 (2019) 1122–1133.
[60] G. Shen, B. Mei, H. Wu, B. Zhao, J. Ren, X. Fang, et al., J. Mater. Sci. Mater. Electron. 30 (2019) 15321–15330.
[61] X. Hou, X. Huang, S. Li, W. Li, S. Luan, W. Li, et al., ACS Sustain. Chem. Eng. 7 (2019) 13845–13855.
[62] P. Li, X. Ma, Y. Zhao, J. Tan, F. Liu, K. Zhu, J. Porous Mater. 26 (2019) 1131–1135.
[63] B. Liu, Y. Hao, L. Wang, M. Li, H. Jiang, Anal. Methods 11 (2019) 3741–3749.
[64] G.L. Goh, N. Saengchairat, S. Agarwala, W.Y. Yeong, T. Tran, Nanoscale 11 (2019) 10603–10614.
[65] H. Wei, E.F. Rodriguez, A.S. Best, A.F. Hollenkamp, D. Chen, R.A. Caruso, ACS Appl. Mater. Interfaces 11 (2019) 13194–13204.
[66] J. Kim, D. Kim, J.H. Ryu, S. Yoon, J. Ind. Eng. Chem. 71 (2019) 93–98.
[67] S. Herou, M.C. Ribadeneyra, R. Madhu, V. Araullo-Peters, A. Jensen, P. Schlee, et al., Green Chem. 21 (2019) 550–559.
[68] X. Li, J. Shao, X. Zhu, H. Wei, Mod. Phys. Lett. B 32 (2018), 1850360.
[69] Y.R. Sliozberg, J.L. Gair Jr., A.J. Hsieh, Polymer 193 (2020), 122339.
[70] M. Aftabuzzaman, C.K. Kim, H. Zhou, H.K. Kim, Nanoscale 12 (2020) 1602–1616.
[71] Y. Ma, J. Gao, X. Chen, L. Kong, ChemElectroChem 7 (2020) 476–485.
[72] M. Liu, B.J. Rohde, R. Krishnamoorti, M.L. Robertson, M. Dawood, Polym. Eng. Sci. 60 (2020) 104–112.
[73] D. Yan, D.-C. Guo, A.-H. Lu, X.-L. Dong, W.-C. Li, J. Colloid Interface Sci. 557 (2019) 519–527.
[74] T. Liu, Z. Zhou, Y. Guo, D. Guo, G. Liu, Nat. Commun. 10 (2019) 1–10.
[75] Y. Dai, J. Wang, P. Tao, R. He, J. Colloid Interface Sci. 553 (2019) 503–511.
[76] I.S. Jouibari, V. Haddadi-Asl, A. Esmaeili, S. Shahsavari, F. Mohammadzadeh, M. Gholami, et al., Iran. Polym. J. 28 (2019) 801–811.
[77] J.-W. Li, W.-C. Tsen, C.-H. Tsou, M.-C. Suen, C.-W. Chiu, Polymers 11 (2019) 1333.
[78] L.M. Schneider, N. Ihrner, D. Zenkert, M. Johansson, ACS Appl. Energy Mater. 2 (2019) 4362–4369.
[79] Z. Zhou, T. Liu, A.U. Khan, G. Liu, Sci. Adv. 5 (2019) eaau6852.
[80] T. Ceregatti, L. Kunicki, S.R. Biaggio, L.C. Fontana, C. Dalmolin, Plasma Process. Polym. 17 (2020), 1900166.
[81] B. Mayzel, J. Aizenberg, M. Ilan, PLoS One 9 (2014), https://doi.org/10.1371/journal.pone.0095775.
[82] D. Liu, L. Zhang, P. Lv, Microporous Mesoporous Mater. 297 (2020), 110056.
[83] J. Su, C. Fang, M. Yang, Y. Cheng, Z. Wang, Z. Huang, et al., J. Mater. Sci. Technol. 38 (2020) 183–188.
[84] Z. Li, L. Li, H. Zhu, H. Liao, H. Zhang, Mater. Lett. 172 (2016) 179–183.
[85] W. Xin, X. Li, Y. Song, J. Clean. Prod. 282 (2021), 124458.
[86] Z. Xing, R. Jin, X. Chen, B. Chen, J. Zhou, B. Tian, et al., Chem. Eng. J. 410 (2021), 128015.
[87] M. Tian, Y. Zhu, Y. Chen, X. Liu, Y. Yang, S. Gao, Nano Energy 83 (2021), 105825.
[88] J. Deng, S. Chen, Q. Zhou, Y. Nie, J. Li, R. Wu, et al., J. Power Sources 451 (2020), 227808.
[89] D. Qiu, T. Cao, J. Zhang, S.-W. Zhang, D. Zheng, H. Wu, et al., J. Energy Chem. 31 (2019) 101–106.
[90] L. Wang, Q. Zhu, J. Zhao, Y. Guan, J. Liu, Z. An, et al., Microporous Mesoporous Mater. 279 (2019) 439–445.
[91] W. Zhang, M. Lin, R. Cheng, L. Li, Y. Sun, S. Ran, et al., Diam. Relat. Mater. 113 (2021), 108278.
[92] C. Ma, J. Gong, S. Zhao, X. Liu, X. Mu, Y. Wang, et al., Green Energy Environ. (2020).
[93] H. Tian, Q. Fang, R. Cheng, L. Li, W. Zhang, S. Ran, et al., Colloids Surf. A Physicochem. Eng. Asp. 614 (2021), 126172.
[94] A.D. Nishchakova, M.A. Grebenkina, E.V. Shlyakhova, Y.V. Shubin, K. A. Kovalenko, I.P. Asanov, et al., J. Alloy. Compd. 858 (2021), 158259.
[95] Y. Zhang, G. Ji, C. Li, X. Wang, A. Li, Chem. Eng. J. 390 (2020), 124398.
[96] S. Zhu, J. Li, C. He, N. Zhao, E. Liu, C. Shi, et al., J. Mater. Chem. A 3 (2015) 22266–22273.
[97] S. Zhu, J. Li, L. Ma, L. Guo, Q. Li, C. He, et al., ACS Appl. Mater. Interfaces 8 (2016) 11720–11728.
[98] J. Pampel, T. Fellinger, Adv. Energy Mater. 6 (2016), 1502389.
[99] X.-L. Zhou, H. Zhang, L.-M. Shao, F. Lü, P.-J. He, Waste Biomass Valoriz. 12 (2021) 1699–1724.
[100] Y. Xu, Z. Yang, G. Zhang, P. Zhao, J. Clean. Prod. 264 (2020), 121645.
[101] W. Zhang, Z.-Y. Wu, H.-L. Jiang, S.-H. Yu, J. Am. Chem. Soc. 136 (2014) 14385–14388.
[102] W. Yang, S. Chen, Ind. Eng. Chem. Res. 59 (2020) 6391–6404.
[103] Y. Liu, J. Chen, B. Cui, P. Yin, C. Zhang, C 4 (2018) 53.
[104] Z. Bi, Q. Kong, Y. Cao, G. Sun, F. Su, X. Wei, et al., J. Mater. Chem. A 7 (2019) 16028–16045.
[105] J. Bedia, M. Peñas-Garzón, A. Gómez-Avilés, J.J. Rodriguez, C. Belver, C 4 (2018) 63.
[106] M. Wang, S. Wang, H. Yang, W. Ku, S. Yang, Z. Liu, et al., Front. Chem. 8 (2020) 116.
[107] C. Baskar, S. Baskar, R.S. Dhillon, Biomass Conversion: The Interface of Biotechnology, Chemistry and Materials Science, Springer Science & Business Media, 2012.
[108] W.-J. Liu, H. Jiang, H.-Q. Yu, Chem. Rev. 115 (2015) 12251–12285.
[109] K. Lawrence, C.L. Baker, T.D. James, S.D. Bull, R. Lawrence, J.M. Mitchels, et al., Chem. Asian J. 9 (2014) 1226–1241.
[110] X. Xu, J. Zhou, D.H. Nagaraju, L. Jiang, V.R. Marinov, G. Lubineau, et al., Adv. Funct. Mater. 25 (2015) 3193–3202.
[111] A.C. Fingolo, J. Bettini, M. da Silva Cavalcante, M.P. Pereira, C.C.B. Bufon, M. Santhiago, et al., ACS Sustain. Chem. Eng. 8 (2020) 7002–7010.
[112] K.Y. Perez-Salcedo, S. Ruan, J. Su, X. Shi, A.M. Kannan, B. Escobar, J. Porous Mater. 27 (2020) 959–969.
[113] M. Picard, S. Thakur, M. Misra, D.F. Mielewski, A.K. Mohanty, Sci. Rep. 10 (2020) 1–14.
[114] Z. Al-Kaabi, R. Pradhan, N. Thevathasan, A. Gordon, Y.W. Chiang, P. Arku, et al., J. Environ. Chem. Eng. 8 (2020), 103520.
[115] L. Cao, Z.-W. Kang, Q. Ding, X. Zhang, H. Lin, M. Lin, et al., Sci. Total Environ. 723 (2020), 138008.
[116] S. Cao, J. Song, H. Li, K. Wang, Y. Li, Y. Li, et al., Waste Manag. 105 (2020) 531–539.
[117] Z. Li, C. Reimer, M. Picard, A.K. Mohanty, M. Misra, Front. Mater. 7 (2020) 3.
[118] L. Lan, J. Li, Q. Feng, L. Zhang, Q. Fu, X. Zhu, et al., Int. J. Hydrog. Energy 45 (2020) 3833–3839.
[119] Y. Zhong, Q. Li, R. Liu, ChemistrySelect 5 (2020) 1029–1036.
[120] Y. Wang, R. Liu, Y. Tian, Z. Sun, Z. Huang, X. Wu, et al., Chem. Eng. J. 384 (2020), 123263.
[121] T. Jesionowski, M. Norman, S. Żółtowska-Aksamitowska, I. Petrenko, Y. Joseph, H. Ehrlich, Mar. Drugs 16 (2018) 88.
[122] Z. Li, L. Zhang, B.S. Amirkhiz, X. Tan, Z. Xu, H. Wang, et al., Adv. Energy Mater. 2 (2012) 431–437.
[123] O.C. Altinci, M. Demir, Energy Fuels 34 (2020) 7658–7665.
[124] Z. Li, D. Guo, Y. Liu, H. Wang, L. Wang, Chem. Eng. J. 397 (2020), 125418.
[125] J. Hao, Y. Huang, C. He, W. Xu, L. Yuan, D. Shu, et al., Sci. Rep. 8 (2018) 1–9.
[126] W. Du, X. Wang, J. Zhan, X. Sun, L. Kang, F. Jiang, et al., Electrochim. Acta 296 (2019) 907–915.
[127] Y. Lv, L. Gan, M. Liu, W. Xiong, Z. Xu, D. Zhu, et al., J. Power Sources 209 (2012) 152–157.
[128] W. Du, Z. Zhang, L. Du, X. Fan, Z. Shen, X. Ren, et al., J. Alloy. Compd. 797 (2019) 1031–1040.
[129] H. Sun, L. Cao, L. Lu, Energy Environ. Sci. 5 (2012) 6206–6213.
[130] Z. Chen, H. Zhuo, Y. Hu, L. Zhong, X. Peng, S. Jing, et al., ACS Sustain. Chem. Eng. 6 (2018) 7138–7150.
[131] B. Chang, W. Shi, H. Yin, S. Zhang, B. Yang, Chem. Eng. J. 358 (2019) 1507–1518.
[132] H. Zhang, Z. Zhang, J. Luo, X. Qi, J. Yu, J. Cai, et al., ChemSusChem 12 (2019) 283–290.
[133] J. Li, R. Xiao, M. Li, H. Zhang, S. Wu, C. Xia, Fuel Process. Technol. 192 (2019) 239–249.

[134] Z. Gonzalez, J. Yus, Y. Bravo, A.J. Sanchez-Herencia, A. Rodríguez, J. Dewalque, et al., Cellulose 27 (2020) 7543–7559.
[135] Y. Boyjoo, Y. Cheng, H. Zhong, H. Tian, J. Pan, V.K. Pareek, et al., Carbon 116 (2017) 490–499.
[136] T. Szatkowski, K. Kopczyński, M. Motylenko, H. Borrmann, B. Mania, M. Graś, et al., Nano Res. 11 (2018) 4199–4214.
[137] I. Petrenko, A.P. Summers, P. Simon, S. Żółtowska-Aksamitowska, M. Motylenko, C. Schimpf, et al., Sci. Adv. 5 (2019) eaax2805.
[138] J. Li, Z. Ren, Y. Ren, L. Zhao, S. Wang, J. Yu, RSC Adv. 4 (2014) 35789–35796.
[139] D. Deng, X. Liao, B. Shi, ChemSusChem 1 (2008) 298–301.
[140] Z. Chang, J. Dai, A. Xie, J. He, R. Zhang, S. Tian, et al., Ind. Eng. Chem. Res. 56 (2017) 9367–9375.
[141] J. Xi, H. Li, J. Xi, S. Tan, J. Zheng, Z. Tan, Environ. Sci. Pollut. Res. 27 (2020) 20675–20684.
[142] T.J. Szalaty, Ł. Klapiszewski, T. Jesionowski, J. Mol. Liq. 301 (2020), 112417.
[143] H. Li, D. Yuan, C. Tang, S. Wang, J. Sun, Z. Li, et al., Carbon 100 (2016) 151–157.
[144] M. Zhang, A.D. Igalavithana, L. Xu, B. Sarkar, D. Hou, M. Zhang, et al., Crit. Rev. Environ. Sci. Technol. (2020) 1–34.
[145] M. Norman, S. Żółtowska-Aksamitowska, A. Zgoła-Grześkowiak, H. Ehrlich, T. Jesionowski, J. Hazard. Mater. 347 (2018) 78–88, https://doi.org/10.1016/j.jhazmat.2017.12.055.
[146] S. Żółtowska, J.F. Miñambres, A. Piasecki, F. Mertens, T. Jesionowski, J. Environ. Chem. Eng. 9 (2021), https://doi.org/10.1016/j.jece.2021.105631.
[147] S. Żółtowska, Z. Bielan, J. Zembrzuska, K. Siwińska-Ciesielczyk, A. Piasecki, A. Zielińska-Jurek, T. Jesionowski, Sci. Total Environ. 794 (2021), 148692, https://doi.org/10.1016/j.scitotenv.2021.148692.
[148] M. Norman, J. Zdarta, P. Bartczak, A. Piasecki, I. Petrenko, H. Ehrlich, T. Jesionowski, Open Chem. 14 (2016) 243–254, https://doi.org/10.1515/chem-2016-0025.
[149] D. Deng, X. Liao, B. Shi, ChemSusChem 1 (2008) 298–301.
[150] S. Żółtowska, I. Koltsov, K. Alejski, H. Ehrlich, M. Ciałkowski, T. Jesionowski, Polym. Test. (2021) 97.
[151] A. Almasoudi, R.A. Mokaya, Microporous Mesoporous Mater. 195 (2014) 258–265.
[152] P. Zhang, F. Sun, Z. Xiang, Z. Shen, J. Yun, D. Cao, Energy Environ. Sci. 7 (2014) 442–450.
[153] R.R. Salunkhe, Y. Kamachi, N.L. Torad, S.M. Hwang, Z. Sun, S.X. Dou, et al., J. Mater. Chem. A 2 (2014) 19848–19854.
[154] R. Steeno, M.C. Rodriguez González, S. Eyley, W. Thielemans, K.S. Mali, S. De Feyter, Chem. Mater. 32 (2020) 5246–5255.
[155] G. Tuci, J. Filippi, A. Rossin, L. Luconi, C. Pham-Huu, D. Yakhvarov, et al., Energies 13 (2020) 2703.
[156] N.D. Yates, M.R. Dowsett, P. Bentley, J.A. Dickenson-Fogg, A. Pratt, C.F. Blanford, et al., Langmuir 36 (2019) 5654–5664.
[157] K. Tahara, Y. Kubo, S. Hashimoto, T. Ishikawa, H. Kaneko, A. Brown, et al., J. Am. Chem. Soc. 142 (2020) 7699–7708.
[158] Q. Lin, J. Zhang, W. Lv, J. Ma, Y. He, F. Kang, et al., Small 16 (2020), 1902603.
[159] J. Raymakers, A. Artemenko, F. Verstraeten, H. Krysova, J. Cermák, S.S. Nicley, et al., Electrochim. Acta 337 (2020), 135762.
[160] M.T. Ghafari, F. Varmaghani, B. Karimi, V. Khakyzadeh, Analyst 145 (2020) 596–606.
[161] Z. Fang, M.S. Lee, J.Y. Kim, J.H. Kim, T.F. Fuller, J. Electrochem. Soc. 167 (2020) 64506.
[162] S.J. Fretz, U. Pal, G.M.A. Girard, P.C. Howlett, A.E.C. Palmqvist, Adv. Funct. Mater. 30 (2020), 2002485.
[163] W.N. Al Dine, A. Mehdi, I. BouMalham, Z. Herro, A. Vioux, N. Brun, et al., ACS Omega 4 (2019) 20540–20546.
[164] B. Mutharani, P. Ranganathan, S.-M. Chen, R.S. Kannan, Ultrason. Sonochem. 56 (2019) 200–212.
[165] H. Saneifar, N. Delaporte, G. Shul, D. Belanger, Mater. Chem. Phys. 235 (2019), 121739.
[166] Y. Aceta, Y. Leroux, P. Hapiot, ChemElectroChem 6 (2019) 1704–1710.
[167] C.-S. Lee, Y. Ju, J. Kim, T.H. Kim, Sens. Actuators B Chem. 275 (2018) 367–372.
[168] H. Smida, E. Lebègue, J.-F. Bergamini, F. Barrière, C. Lagrost, Bioelectrochemistry 120 (2018) 157–165.
[169] A. Sommerfeldt, S.U. Pedersen, K. Daasbjerg, Electrochim. Acta 261 (2018) 356–364.
[170] N. Allali, V. Urbanova, M. Etienne, X. Devaux, M. Mallet, B. Vigolo, et al., Beilstein J. Nanotechnol. 9 (2018) 2750–2762.
[171] M. Andideh, M. Esfandeh, Carbon 123 (2017) 233–242.
[172] P. Du, K. Hu, J. Lyu, H. Li, X. Lin, G. Xie, et al., Appl. Catal. B Environ. 276 (2020), 119172.
[173] N. Shang, S. Li, X. Zhou, S. Gao, Y. Gao, C. Wang, et al., Appl. Surf. Sci. 537 (2021), 147818.
[174] J.K. Kim, Y.C. Kang, ACS Nano 14 (2020) 13203–13216.
[175] Y.-Q. Wang, Y.-S. Zhao, X.-X. Yang, M.-X. Ren, B.-Y. Lei, W.-J. Meng, et al., Int. J. Hydrog. Energy 45 (2020) 32654–32663.
[176] W. Nie, X. Liu, Q. Xiao, L. Li, G. Chen, D. Li, et al., ChemElectroChem 7 (2020) 631–641.
[177] T. Qiu, W. Hong, L. Li, Y. Zhang, P. Cai, C. Liu, et al., J. Energy Chem. 51 (2020) 293–302.
[178] K. Wang, J. Qian, F. Sun, Z. Tian, J. Gao, G. Zhao, Fuel 281 (2020), 118782.
[179] J. Hu, Z. Xu, X. Li, S. Liang, Y. Chen, L. Lyu, et al., J. Power Sources 462 (2020), 228098.
[180] J.-J. Cai, Q.-Y. Zhou, X.-F. Gong, B. Liu, Y.-L. Zhang, Y.-K. Dai, et al., Carbon 167 (2020) 75–84.
[181] T. Sun, G. Liu, L. Du, Y. Bu, B. Tian, Mater. Today Energy 16 (2020), 100395.
[182] Y. Guo, Y. Meng, Y. Du, M. Duan, Y. Li, F. Zhu, Ionics 27 (2021) 97–105.
[183] J. Hou, X. Tu, X. Wu, M. Shen, X. Wang, C. Wang, et al., Chem. Eng. J. 401 (2020), 126141.
[184] Y. Wang, G. Zhang, M. Ma, Y. Wang, Y. Zhang, X. Sun, et al., Electrochim. Acta 341 (2020), 136066.
[185] H. Nishihara, T. Kyotani, Adv. Mater. 24 (2012) 4473–4498.
[186] Z. Zhang, H. Li, Appl. Surf. Sci. 514 (2020), 145920.
[187] S. Kim, W. Cha, K. Ramadass, G. Singh, I.Y. Kim, A. Vinu, Chem. Asian J. 15 (2020) 1863–1868.
[188] R. Yan, M. Oschatz, F. Wu, Carbon 161 (2020) 162–168.
[189] Y. Liu, X. Que, X. Wu, Q. Yuan, H. Wang, J. Wu, et al., Mater. Today Chem. 17 (2020), 100284.
[190] X.-D. He, Z.-H. Liu, J.-Y. Liao, X. Ding, Q. Hu, L.-N. Xiao, et al., J. Mater. Chem. A 7 (2019) 9629–9637.
[191] X. Miao, D. Sun, X. Zhou, Z. Lei, Chem. Eng. J. 364 (2019) 208–216.
[192] B. Xing, C. Zhang, Q. Liu, C. Zhang, G. Huang, H. Guo, et al., J. Alloy. Compd. 795 (2019) 91–102.
[193] Y. Lu, Q. Zhang, S. Lei, X. Cui, S. Deng, Y. Yang, ACS Appl. Energy Mater. 2 (2019) 5591–5599.
[194] C. Zheng, X. Hu, X. Sun, S.J. Yoo, X. Li, Electrochim. Acta 306 (2019) 339–349.
[195] X. Hu, X. Sun, S.J. Yoo, B. Evanko, F. Fan, S. Cai, et al., Nano Energy 56 (2019) 828–839.
[196] J. Ding, H. Zhang, H. Zhou, J. Feng, X. Zheng, C. Zhong, et al., Adv. Mater. 31 (2019), 1900429.
[197] R.J.-C. Dubey, J. Nussli, L. Piveteau, K.V. Kravchyk, M.D. Rossell, M. Campanini, et al., ACS Appl. Mater. Interfaces 11 (2019) 17686–17696.
[198] L.Q. Lu, N. Schriever, J.T.M. De Hosson, Y.T. Pei, J. Mater. Chem. A 6 (2018) 11405–11415.
[199] V. Etacheri, C.N. Hong, J. Tang, V.G. Pol, ACS Appl. Mater. Interfaces 10 (2018) 4652–4661.
[200] H.-F. Fei, W. Li, S. Nuguri, H.-J. Yu, B.M. Yavitt, W. Fan, et al., Chem. Mater. 32 (2020) 6055–6061.
[201] P. Li, H. Xie, Y. Liu, J. Wang, X. Wang, Y. Xie, et al., Electrochim. Acta 353 (2020), 136514.
[202] E.P. Yambou, B. Gorska, V. Pavlenko, F. Beguin, Electrochim. Acta 350 (2020), 136416.
[203] J.O. Bonsu, A.B. Appiagyei, J.I. Han, Mater. Res. Bull. 133 (2021), 111053.
[204] I.P. Swain, S.K. Behera, Microporous Mesoporous Mater. 303 (2020), 110290.
[205] W. Wei, L. Wan, C. Du, Y. Zhang, J. Chen, M. Xie, Microporous Mesoporous Mater. 307 (2020), 110510.
[206] W. Wei, W. Liu, Z. Chen, R. Xiao, Y. Zhang, C. Du, et al., Appl. Surf. Sci. 509 (2020), 144921.
[207] J. Xu, G. Du, L. Xie, K. Yuan, Y. Zhu, L. Xu, et al., ACS Sustain. Chem. Eng. 8 (2020) 8024–8036.
[208] I.P. Swain, S. Pati, S.K. Behera, Chem. Commun. 55 (2019) 8631–8634.
[209] D. Guo, J. Qian, R. Xin, Z. Zhang, W. Jiang, G. Hu, et al., J. Colloid Interface Sci. 538 (2019) 199–208.
[210] H.-F. Fei, W. Li, A. Bhardwaj, S. Nuguri, A. Ribbe, J.J. Watkins, J. Am. Chem. Soc. 141 (2019) 17006–17014.
[211] J. Liu, L. Yi, X. Wang, Q. Zhao, Y. Zhang, J. Gao, et al., Int. J. Hydrog. Energy 40 (2015) 7301–7307.
[212] Y. Liu, T. Zhang, X. Dai, Q. Tan, Y. Chen, Y. Liu, et al., ACS Appl. Nano Mater. 3 (2020) 5139–5148.
[213] M. Wu, Y. Xing, L. Zeng, W. Guo, M. Pan, Int. J. Energy Res. 45 (2021) 2334–2342.
[214] V. Parthiban, S. Akula, A.K. Sahu, J. Membr. Sci. 541 (2017) 127–136.
[215] B.-R. Adhikari, M. Govindhan, A. Chen, Sensors 15 (2015) 22490–22508.
[216] B. Shah, T. Lafleur, A. Chen, Faraday Discuss. 164 (2013) 135–146.
[217] J.R. Stetter, W.R. Penrose, S. Yao, J. Electrochem. Soc. 150 (2003) S11.
[218] M.R. Benzigar, S.N. Talapaneni, S. Joseph, K. Ramadass, G. Singh, J. Scaranto, et al., Chem. Soc. Rev. 47 (2018) 2680–2721.
[219] J. Wang, Y. Zeng, L. Wan, J. Zhao, J. Yang, J. Hu, et al., Appl. Surf. Sci. 509 (2020), 145301.
[220] H. Jia, N. Shang, Y. Feng, H. Ye, J. Zhao, H. Wang, et al., J. Colloid Interface Sci. 583 (2021) 310–320.
[221] Y. Wang, Q. Dai, L. Yang, Y. Liu, C. Yu, C. Yao, et al., J. Electroanal. Chem. 873 (2020), 114462.
[222] Y. Wang, M. Qiao, Y. Baikeli, X. Mamat, L. Li, X. Hu, et al., J. Hazard. Mater. 385 (2020), 121550.
[223] S. Tsujimura, S. Takeuchi, Electrochim. Acta 343 (2020), 136110.
[224] K. Wang, C. Wu, F. Wang, N. Jing, G. Jiang, ACS Sustain. Chem. Eng. 7 (2019) 18582–18592.
[225] H. Chen, X. Wu, C. Lao, Y. Li, Q. Yuan, W. Gan, J. Electroanal. Chem. 835 (2019) 254–261.
[226] B. Sun, C. Wang, J. Cai, D. Li, W. Li, X. Gou, et al., J. Electrochem. Soc. 166 (2019) H187.
[227] K. Mondal, M.A. Ali, C. Singh, G. Sumana, B.D. Malhotra, A. Sharma, Sens. Actuators B Chem. 246 (2017) 202–214.
[228] X. Zhong, W. Yuan, Y. Kang, J. Xie, F. Hu, C.M. Li, ChemElectroChem 3 (2016) 144–151.
[229] Q. Cheng, L. Ji, K. Wu, W. Zhang, Sci. Rep. 6 (2016) 1–8.
[230] M. Regiart, J.L. Magallanes, D. Barrera, J. Villarroel-Rocha, K. Sapag, J. Raba, et al., Sens. Actuators B Chem. 232 (2016) 765–772.
[231] F.J. Isidro-Ortega, J.H. Pacheco-Sánchez, A. González-Ruíz, R. Alejo, Int. J. Hydrog. Energy 45 (2020) 19505–19515.

[232] J.-S. Yu, S. Kang, S.B. Yoon, G. Chai, J. Am. Chem. Soc. 124 (2002) 9382–9383.
[233] G.S. Chai, I.S. Shin, J. Yu, Adv. Mater. 16 (2004) 2057–2061.
[234] J.L. Figueiredo, J. Mater. Chem. A 1 (2013) 9351–9364.
[235] J. Janaun, N. Ellis, Appl. Catal. A Gen. 394 (2011) 25–31.
[236] M. Ding, S. Chen, X. Liu, L. Sun, J. Lu, H. Jiang, ChemSusChem 10 (2017) 1898–1903.
[237] X. Hu, Y. Long, M. Fan, M. Yuan, H. Zhao, J. Ma, et al., Appl. Catal. B Environ. 244 (2019) 25–35.
[238] I. Mazurenko, R. Clément, D. Byrne-Kodjabachian, A. De Poulpiquet, S. Tsujimura, E. Lojou, J. Electroanal. Chem. 812 (2018) 221–226.
[239] J. Sheng, L. Wang, L. Deng, M. Zhang, H. He, K. Zeng, et al., ACS Appl. Mater. Interfaces 10 (2018) 7191–7200.
[240] W. Donphai, T. Kamegawa, M. Chareonpanich, K. Nueangnoraj, H. Nishihara, T. Kyotani, et al., Phys. Chem. Chem. Phys. 16 (2014) 25004–25007.
[241] X. Kong, X. Liu, Y. Zheng, P.K. Chu, Y. Zhang, S. Wu, Mater. Sci. Eng. R Rep. 145 (2021), 100610.
[242] H. Yan, Chem. Commun. 48 (2012) 3430–3432.
[243] M. Li, S. Song, C. Su, L. Li, Z. Yan, X. Cao, Catal. Sci. Technol. 9 (2019) 3828–3835.
[244] T. Grewe, H. Tüysüz, ChemNanoMat 2 (2016) 273–280.
[245] Y. Shen, X. Guo, X. Bo, Y. Wang, X. Guo, M. Xie, et al., Appl. Surf. Sci. 396 (2017) 933–938.
[246] L. Luo, J. Ma, H. Zhu, J. Tang, Nanoscale 12 (2020) 7339–7346.
[247] G.P. Mane, S.N. Talapaneni, K.S. Lakhi, H. Ilbeygi, U. Ravon, K. Al-Bahily, et al., Angew. Chem. Int. Ed. 56 (2017) 8481–8485.
[248] Z. Yang, Y. Zhang, Z. Schnepp, J. Mater. Chem. A 3 (2015) 14081–14092.
[249] A. Vinu, K.Z. Hossian, P. Srinivasu, M. Miyahara, S. Anandan, N. Gokulakrishnan, et al., J. Mater. Chem. 17 (2007) 1819–1825.
[250] D. Lee, J. Lee, J. Kim, J. Kim, Na.H. Bin, B. Kim, et al., Adv. Mater. 17 (2005) 2828–2833.
[251] A. Vinu, C. Streb, V. Murugesan, M. Hartmann, J. Phys. Chem. B 107 (2003) 8297–8299.
[252] Z. Wang, X. Liu, M. Lv, J. Meng, Carbon 48 (2010) 3182–3189.
[253] J. Wang, Q. Chen, X. Liu, W. Qiao, D. Long, L. Ling, Mater. Chem. Phys. 129 (2011) 1035–1041.
[254] S. Dong, L. Peng, W. Wei, T. Huang, ACS Appl. Mater. Interfaces 10 (2018) 14665–14672.
[255] F. Béguin, V. Pavlenko, P. Przygocki, M. Pawlyta, P. Ratajczak, Carbon 169 (2020) 501–511.
[256] H. Kyakuno, K. Matsuda, Y. Nakai, T. Fukuoka, Y. Maniwa, H. Nishihara, et al., Chem. Phys. Lett. 571 (2013) 54–60.
[257] M. Michel, B. Buszewski, Adsorption 15 (2009) 193–202.
[258] J.M.D. Tascón, Novel Carbon Adsorbents, Elsevier, 2012.
[259] J.L. Perry, C.R. Martin, J.D. Stewart, Chem. Eur. J. 17 (2011) 6296–6302.
[260] T.-W. Kim, P.-W. Chung, I.I. Slowing, M. Tsunoda, E.S. Yeung, V.S.-Y. Lin, Nano Lett. 8 (2008) 3724–3727.
[261] H. Zhang, H. Xu, M. Wu, Y. Zhong, D. Wang, Z. Jiao, J. Mater. Chem. B 3 (2015) 6480–6489.
[262] X. Huang, S. Wu, X. Du, Carbon 101 (2016) 135–142.
[263] S. Kapri, S. Maiti, S. Bhattacharyya, Carbon 100 (2016) 223–235.
[264] A. Rammohan, L. Tayal, A. Kumar, S. Sivakumar, A. Sharma, RSC Adv. 3 (2013) 2008–2016.
[265] D. Saha, K.E. Warren, A.K. Naskar, Carbon 71 (2014) 47–57.
[266] N.L. Torad, Y. Li, S. Ishihara, K. Ariga, Y. Kamachi, H.-Y. Lian, et al., Chem. Lett. 43 (2014) 717–719.
[267] S. Zhu, D. Zhang, Z. Chen, Y. Zhang, J. Mater. Chem. 19 (2009) 7710–7715.
[268] X. Yuan, W. Xing, S.-P. Zhuo, Z. Han, G. Wang, X. Gao, et al., Microporous Mesoporous Mater. 117 (2009) 678–684.
[269] C.A. Howell, S.V. Mikhalovsky, E.N. Markaryan, A.V. Khovanov, Sci. Rep. 9 (2019) 1–10.
[270] M. Wang, S.E. Hearon, T.D. Phillips, J. Environ. Sci. Health Part B 54 (2019) 514–524.
[271] H. Hillebrenner, F. Buyukserin, J.D. Stewart, C.R. Martin, Template Synthesized Nanotubes for Biomedical Delivery Applications, 2006.
[272] X. Zhuang, Y. Wan, C. Feng, Y. Shen, D. Zhao, Chem. Mater. 21 (2009) 706–716.
[273] L. Ji, F. Liu, Z. Xu, S. Zheng, D. Zhu, Environ. Sci. Technol. 43 (2009) 7870–7876.
[274] X. Wang, S. Chen, J. Sun, D. Zhang, Z. Yan, X. Xu, et al., Microporous Mesoporous Mater. 318 (2021), 110993.
[275] S. Karaca, A. Gürses, M. Açıkyıldız, M. Ejder, Microporous Mesoporous Mater. 115 (2008) 376–382.
[276] Q. Fu, L. Wen, L. Zhang, X. Chen, D. Pun, A. Ahmed, et al., ACS Appl. Mater. Interfaces 9 (2017) 33979–33988.
[277] H. Qi, X. Ji, C. Shi, R. Ma, Z. Huang, M. Guo, et al., J. Colloid Interface Sci. 556 (2019) 366–375.
[278] Q. Wu, S. Cheng, H. Chen, C. Wang, Food Anal. Methods 10 (2017) 2772–2780.

**Dr. V. Pavlenko** obtained his master of science degree from Al-Farabi Kazakh National University, Almaty city, the Republic of Kazakhstan; Faculty of Chemistry and Chemical Technology, Department of Chemical Physics and Material Sciences in 2009–2010. He then completed the doctoral thesis in Nanomaterials and Nanotechnology at Al-Farabi Kazakh National University, Almaty city, the Republic of Kazakhstan; Faculty of Chemistry and Chemical Technology, Department of Chemical Physics and Material Sciences in 2011–2014. Dr. Pavlenko is current an Associate Professor at the Al-Farabi Kazakh National University, Faculty of Chemistry and Chemical Technology. His duties involve development and implementation of educational – methodical complexes of the following courses: "Physical and chemical basis of catalyst preparation", "Technology of heterolytic and homolytic oil refining processes", "Designing of oil refining and petrochemical enterprises", etc. He has been Post-Doctoral Fellow at Poznan University of Technology, Institute of Chemistry and Technical Electrochemistry (Poland) in 2017 – 2019. He also was visiting scientist at Graz University of Technology, Institute for Chemistry and Technology of Materials (Graz, Austria) in the summer of 2021. Description of duties: Research on development of advanced energy storage systems, in particular the electrochemical supercapacitors operating due to application of new physical principle (nanoconfinement effect). Experimental and analytical works related to electrochemistry, gas adsorption, thermal analysis, temperature programmed desorption, chemical synthesis, along with the design of novel hierarchical porous carbon materials for high energy electrochemical capacitors.

**S. Khosravi H is** currently working on research pertaining to electro/ion conductive, semiconductor solid-state materials such as a metal oxide semiconductor (MOS) and ferroelectric ceramic as perovskite and protective for green energy applications, as well as electrochemical capacitors for modern batteries. In particular, he has been working on the synthesis and characterization of electrically conductive and ferroelectric solid materials for Li-battery and PEMFCs applications, as well as the development and electrochemical characterization of different semiconductor and multifunctional electroceramics and other materials that serve as a conducting host for electrochemically active elements in electrochemical energy storage. His research focuses on the synthesis and characterization of solid-state electronics materials, as well as multifunctional high electrochemical resistivity with high conductivity for high energy density hybrid/all-solid-state metal batteries and PEMFCs applications. Additionally, the development of metal-oxide-semiconductor such as BaTiO3, BaTiNbO3, BaLaTiO3 as perovskite materials, TiSiNbFeC as a MOS and, solid-state decoration for the design of separator membranes and PEMFCs, and preparation of protective conductive materials using solid-state chemistry technique are among his research interests. His research accomplishments at TU Graz has resulted in seven publications and one invention.

**S. Żółtowska** Master of Science: Organic Technology from Poznan University of Technology in 2015. She is currently a PhD student at the faculty of Chemical Technology, Poznan University of Technology. Besides she served as Expert scientist at the Czech University of Life Sciences in Prague in 2021. She is winner of Etiuda 7 Scholarship for research work at the TU Bergakademie Freiberg as well as obtained DAAD Scholarship for short term research at TU Bergakademie Freiberg. She has been author or coauthor of 26 research articles and her work has been cited for 472 times.

**Dr. A. Haruna** MSc (Chem.) University of Lagos, June 2004, PhD (Chem.) University of the Witwatersrand, Oct. 2020. Where he is currently a Postdoctoral Research Fellow. Electrochemical Energy Storage, Materials Science and Electrochemistry; Inorganic chemistry synthesis (especially microwave irradiation). My current research activities are on the RD&I of electrochemical energy storage (i.e., lithium-/sodium-ion batteries, lithium-sulfur and zinc-air batteries). Dr. Haruna has published research articles and review papers in high impact journals and presented his work at international prestigious scientific conferences.

**Professor M. Zahid** completed his PhD at the Institute of Physical and Theoretical Chemistry, Graz University of Technology, Graz/Austria in 2011 under the supervision of Prof. Dr. Günter Grampp with a topic of "Synthesis and photophysical characterization of new aromatic cyano-compounds". He Joined the University of Agriculture Faisalabad, Pakistan in 2011 as assistant professor and expanded his research interest in the field of materials science (semiconductor nanoparticles, nanocomposites, etc.) and their application in energy materials and environment. Now, I have been working with advanced materials such as graphene, graphene oxide, graphitic carbon nitride and their nanocomposites (magnetic nanocomposites, polymer composites, bio-composites, etc.). The graphene and its composites (especially semiconductor oxides-based) have been successfully used for the adsorption enhanced photocatalytic degradation of pollutants in wastewater under solar as well as simulated UV light. Prof. Zahid is involved as a reviewer for the several peer reviewed journals of high repute published by leading publishers. These include Environmental Science and Pollution Research, Water Science and Technology, Journal of Cleaner Production, Catalysts, International Journal of Industrial Chemistry, Journal of Environmental Management, Materials Research Express, Chemosphere, Environmental Progress & Sustainable Energy, Journal of Materials Research and Technology, Nanotechnology, Processes and several others. He supervised 03 PhD students, 10 MSc and 74 MPhil. research students as a supervisor and 04 PhD and more than 50 MPhil students as a member of the supervisory committee. He has published 86 research articles and review papers in peer-reviewed journals.

**Professor Z. Mansurov** is renowned scientist in the field of chemical combustion and interfacial processes. He is expert of developing novel nanocomposites based catalyst materials. He has been awarded with State Prize of the Republic of Kazakhstan in field of Science & Technology for the cycle of works "Fundamental research of chemical basis of combustion processes", K. I. Satpayev State Prize (the first) for the best scientific researches in natural sciences – discovery, as well as Medal of the Higher School Academy of Sciences of the Russian Federation "For services for the Higher School". He has also been awarded with UNESCO Medal for contributions to the development of nanoscience and nanotechnologies in 2018.

**Z. Supiyeva** is a PhD student at Al-Farabi Kazakh National University, Almaty city, the Republic of Kazakhstan; Faculty of Chemistry and Chemical Technology, Department of Chemical Physics and Material Sciences since 2017. Her topic of research is Nanomaterials and Nanotechnologies in the field of Chemical Sciences. She did his master of science in 2015 from Al-Farabi Kazakh National University, Almaty city, the Republic of Kazakhstan; Faculty of Chemistry and Chemical Technology, Department of analytical, colloidal chemistry and technology of rare elements on the topic of Chemical technology of inorganic compounds. Zhazira Supiyeva also serves as Senior Lecturer at Al-Farabi Kazakh National University, Faculty of Chemistry and Chemical Technology since 2020. Previously she was Research Fellow at the Laboratory of Carbon nanomaterials Institute of Combustion Problems of the Committee of Science of the Ministry of Education and Science of the Republic of Kazakhstan from 2016 to 2020. Her area of expertize include the study of electrochemical processes occurring on new carbon materials applicable in supercapacitors, development of scientific technological and innovative support of industries using electrochemical methods of extraction, analysis and production of new substances and materials.

**Prof. A. Galal** earned his BSc and MSc degrees in Chemistry from Cairo University, Egypt. He obtained MSc and PhD degrees from the University Of Cincinnati, OH, USA. He joined the chemistry department of Cairo University as assistant professor in 1992 where he is currently a full professor. Professor Galal worked at several universities where he assumed Professor visit-ship including: Ulm, Erlangen, Ilmenau, and Free Universities (Germany); Cincinnati and Texas A&M Universities (USA); University of Liverpool (UK); Polytechnic University of Turin (Italy); United Arab Emirates and Kuwait Universities. Professor Galal served as member of Strategic Planning and Technical Support Centre, a member of Board of Research for the Ministry of Higher Education & Scientific Research (Egypt); Development and Innovation Program, a Program funded by the European Union of the Ministry of Higher Education of Egypt. Professor Galal also served as Dean of Faculty of Science, Cairo University and as Interim Head of Center of Hazardous and Environmental Mitigation of the University. Professor Galal earned several honors: Graduate Fellowship Award, Quantum Chemical Corporation (USA); Fellowship award of the "Alexander von Humboldt Stiftung," Germany. He also acted as member in National Committee on New and Advanced Materials, the committee of Basic Sciences both of the Academy of Science and Technology of Egypt. Professor Galal was the Egyptian delegate to: International Science Technology and Innovation Centre for South-south Cooperation under the Auspices of UNESCO, (Malaysia); The inauguration of the Euro-Mediterranean University (EMUNI) (Slovenia); The RussNano Forum (Russia); COMEST meeting on Ethics of Science and Technology under the Auspices of UNESCO (Qatar). Professor Galal is a member of the Advisory Board for International Institute for Multifunctional Materials for Energy Conversion (IIMEC), Texas A&M University (USA). Professor Galal earned State and University of Cairo University Prizes; Appreciation and Excellence in Research in the area of Advanced Materials for Technological Applications. He authored and co-authored 210 research papers in international renowned journals and delivered over 70 lectures in international conferences and institutes. His research covers a wide spectrum of interests including surface tailoring with nano-structured materials for energy conversion, storage and sensing applications. Synthesis and modification of carbon based nano-structures with emphasis on graphene and carbon nanotubes, and perovskites.

**K.I. Ozoemena** is Research Professor and South African Research Chair Initiative (SARChI) Chair (Tier 1) in *Materials Electrochemistry and Energy Technologies* (MEET) at the University of the Witwatersrand (Wits), South Africa. Prior to joining Wits in 2017, he had worked at the South Africa's premier research council, the Council for Scientific and Industrial Research (CSIR) as Chief Scientist and Research Group Leader (2009–2017) in Electrochemical Energy Technologies. His current research interests are mostly focussed on Materials Science and Electrochemistry; from synthetic inorganic chemistry and electrochemical sensing to electrocatalysis and electrochemical energy storage and conversion systems (notably, advanced batteries, supercapacitors, fuel cells, and electrolyzers) and electrochemical sensors. He holds a PhD (Chemistry) degree from Rhodes University (2003). He has been recognized severally for his research and innovation activities, including: i) South Africa's National Research Foundation (NRF) top-rated scientist; ii) Finalist (*'Lifetime Award'*) 2018/2019 South Africa's National Science and Technology Forum (NSTF)-South32 Awards; and iii) listed amongst the "World Top 2% Scientists". He serves on the Editorial Board of several journals, including *Electrochemistry Communications* (Elsevier), *Current Opinion in Electrochemistry* (Elsevier), *Scientific Reports* (Springer-Nature), Journal of Electrochemistry (China), and *Materials Today Communications* (Elsevier). He is also an Associate Editor of *Electrocatalysis* (Springer Nature), and Chief Editor, *International Journal of Electrochemistry* (Hindawi-Wiley). In addition, he has served as Guest Editor for several journals including *Electrochimica Acta* (Elsevier), *Electrochemistry Communications* (Elsevier), *Current Opinion in Electrochemistry* (Elsevier), and *Electroanalysis* (Wiley). Prof Ozoemena has published over 210 peer-reviewed publications, 11 Book chapters, 3 edited books, and 10 patents (including 2 USA granted patents in high-energy cathode materials for lithium-ion batteries), with H-Index of 54 and over 8000 citations. As at 2021, he has successfully supervised to completion several graduate researchers (23 PhD, 22 MSc/MTech, and 9 Postdoctoral Fellows).

**Dr. Q. Abbas** passed his master in science (MSc, Applied Chemistry) from the University of Engineering & Technology, Lahore, Pakistan in 2002–2005. He then continued his PhD studies in corrosion science and electrochemistry under a fully funded scholarship between 2008 and 2011 at the institute of Inorganic Chemistry, Graz University of Technology, Austria. Qamar Abbas took up a post-doctoral fellowship under an EU funded Welcome Project in 2011 – 2015 and then full time faculty position in 2016 at the Institute of Chemistry and Technical Electrochemistry (ICTE), Poznan University of Technology, Poznan, Poland. He is currently a visiting researcher under prestigious Lise Meitner Fellowship at the Institute for Chemistry and Technology of Materials (ICTM), Graz University of Technology, Graz, Austria. His areas of research are hybrid supercapacitors, electric double-layer capacitors, battery electrodes, pseudocapacitive materials, nanoporous materials, carbon materials, and eco-friendly energy storage based on iodine electrochemistry. Qamar Abbas has published over 40 peer reviewed articles and review papers with a total citation over 1700 and h-index 17.

**Professor T. Jesionowski** currently serves as Rector of the Poznan University of Technology (PUT), the Chair of the Conference of Rectors of Polish Technical Universities, member of the Board of the Conference of Rectors of Academic Schools in Poland. Since 2020 member of Polish Academy of Science. He also serves as the head of the Chemical Technology Department. In period of 2016–2020 vice-rector for LLL & International Education, and from 2008 to 2016, he was deputy-dean of the Faculty of Chemical Technology at PUT. Prof. Teofil Jesionowski received the title of professor of chemical sciences in 2013. His research interests include the synthesis, characterization and applications of advanced functional materials, functional fillers and polymer composites; activators of rubber compounds, (bio)additives and eco-friendly fillers; biomineralisation – inspired syntheses and Extreme Biomimetics; biocomposites and biomaterials; removal of wastewater pollutants via adsorption, photocatalysis or precipitation methods; pigment composites; enzyme immobilization; colloid chemistry and surface modification; hybrid systems, biopolymers and biosensors. He has published over 450 publications indexed by Thomson Reuters JCR. He is also a co-creator of over 45 patents and patent applications. His publications received over 10,100 citations (h index = 46). He is the co-author of chapters in numerous monographs, published in renowned publishing houses (Springer, Wiley, InTech, etc.); and a scholarship holder of the Foundation for Polish Science. He is also a member of editorial boards of scientific journals: Dyes and Pigments – Elsevier, Physicochemical Problems of Mineral Processing. Nowadays serves as Section Editor in Chief Molecules journal (MDPI) as well as Materials (MDPI) and member of editorial board/associate editor of Scientific Reports (Nature Publishing Group).